博士論文

CVD growth of super-small diameter single-walled carbon nanotubes

(超小径単層カーボンナノチューブの CVD 合成)

侯　博

Table of contents

Abstract

Single-walled carbon nanotubes (SWNTs), which have a unique one-dimensional structure of a rolled-up graphene sheet, are widely used for applications in many fields due to its outstanding optical, electronic, thermal and mechanical properties. Depending on the chirality of the SWNTs, SWNTs can be either metallic or semiconducting. One-dimensional structure of semiconducting SWNTs exhibits electronic quantum confinement effects, and the bandgap increases with the reducing diameter. The potential tenability diameter is expected to strengthen their applicability to solar cells with controllable band gap. Therefore, growth of smaller diameter SWNTs with higher band gap is a challenge both for application and in the fundamental point of view. In this work, super-small diameter SWNTs have been grown by extending the condition for chemical vapor deposition (CVD) from high temperature and high pressure to low temperature and low pressure. Also, the influences of the carbon feedstock and the catalyst on the growth rate and the properties of SWNTs have been also investigated.

Super-small diameter SWNTs are grown by alcohol-catalyst chemical vapor deposition (ACCVD) method using USY-zeolite supported catalysts. In the conventional ACCVD process, usually, high-quality SWNTs can be grown around 800 ^{o}C and 1.3 kPa. Through the investigations of the influence of temperature and pressure on the formation of SWNTs in this work, the relationship between the effect of temperature and that of pressure was clarified: SWNTs can grow at lower temperature when applied with lower pressure, which was also supported by the kinetic model on the formation of SWNTs. The temperature range for high-quality SWNTs could be extended down to 430 ^{o}C in combination with very low partial pressure of ethanol down to 0.02 Pa. Extended-temperature range study opened a new operational window for efficient growth of small diameter SWNTs. During the experimental investigation with decreased temperature, super-small diameter SWNTs (0.8 nm > d_t > 0.5 nm) were obtained around 500 ^{o}C and 5 Pa. Previously, SWNTs with diameters smaller than (6,5) (~0.8 nm) have been known to be very difficult to grow except in a special zeolite pore or inside an outer nanotube. Super-small diameter SWNTs were rarely directly grown in reported works. By the low

temperature growth with the conventional Fe-Co catalysts, we could extend the small diameter limit; ratio of smaller diameter tubes could be increased with low temperature CVD with optimum low pressure. Resonant Raman with five-color laser lines, absorption and Photoluminescence excitation spectroscopy (PL) are used to characterize and measure the abundance of small diameter nanotubes, and chirality of small diameter SWNTs were assigned as (6,4), (5,4), (8,0), (5,3), (6,1) etc..

On the other hand, in the expanded condition, SWNTs grown at high temperature and low pressure demonstrated relatively broad diameter distribution, which is similar to those grown by HiPCo method. It is a powerful way that small diameter SWNTs or broad diameter distribution SWNTs can be grown only by adjusting CVD experimental conditions without any specific catalysts or treatment. And obtained growth boundaries at too low temperature and too low pressure are promising for understanding the mechanism of SWNTs growth in Fe-Co ACCVD.

The influences of the feedstock (carbon source) and the catalyst on the formation of SWNTs were also observed. In the CVD synthesis of SWNTs, several processes limit growth rate and formation of SWNTs. In the gas phase, the feedstock compound experiences thermal decomposition before reaching the catalysts, gas- phase decomposition products are adsorbed and dissociate on the surface of catalyst, then the carbon atoms diffuse bulk or surface, and finally carbon atoms participate the growth of SWNTs. Different feedstock and catalysts behave differently during all these processes. Therefore, the effect of the feedstock and catalysts were also studied, especially for the low-temperature and low-pressure CVD synthesis of small diameter SWNTs.

Gas-phase thermal decomposition of ethanol, dimethyl ether (DME) and acetonitrile were simulated using the chemical kinetic model under various SWNT growth conditions. Time-profiles of species concentrations were demonstrated at various temperature and pressure. FT-IR spectroscopy was used to measure the concentrations of the products of DME and ethanol decomposition. FT-IR experimental results at various conditions were found to be in good agreement with the corresponding simulations. The simulation results indicated following: (i) Decomposition of ethanol affected the growth rate of SWNTs. (ii)

However, cleaner SWNTs can be obtained at light decomposition condition of ethanol. (iii) For the condition of low-temperature and low-pressure CVD, the feedstock compound, ethanol, DME or acetonitrile directly arrives at the surface of catalysts almost without gas-phase decomposition.

Fe-Co catalyst was mainly used in this work, this effective catalyst assisted the exploration of CVD condition and super-small diameter SWNTs could be grown on it. In addition, Cu-Co and W-Co were also used to obtain specific SWNTs. By using Cu-Co catalysts, diameter distribution became narrower. The (6,5) SWNTs became predominant at 500 ^{o}C. On the other hand, the (12,6) chirality became predominant when the fraction of W was increased in the catalyst of W-Co. Growth of super-small diameter SWNTs and the narrower chirality distribution suggest the promising future works for application and fundamental understanding of CVD growth of SWNTs.

Chapter 1

Introduction

1.1 Carbon allotropic family

Carbon is the 15th most abundant element in Earth crust and is the main element of organic compounds. Carbon is inevitable for living bodies. Schematics of the carbon family are shown in figure 1-1. The well-known forms of carbon, diamond and graphite, have absolutely different physical and chemical properties due to the difference in geometric structure with different band structures.

Carbon nanomaterials, in some aspect, represent the initiation of nanotechnology in the 1980s. The discovery of fullerenes in 1985 is a hieroglyphic example [1]. So called cluster based fullerenes were recognized as zero dimensional nanomaterials which played critical role in plenty of leading-edge applications such as organic photovoltaic (OPV) and drug delivery systems (DDS). Following the discovery of one dimensional carbon nanotubes (CNTs) in 1991 [2, 3], CNTs attracted focus in various application fields, which will be described in other sections of this chapter. This thesis will focus on the single-walled carbon nanotubes (SWNTs) which is one of the major types of CNTs. Interestingly, the emergence of the carbon nanomaterials followed a way in the increase of the dimension. A two dimensional carbon material “graphene” was extracted from bulk graphite [4]. It boosted the experimental study of graphene as well as the theoretical study, which is now not at all hypothetical.

Zero- to two-dimensional, carbon nanomaterials attract both academia and industry. It is a prototypical example of successful technological innovation which received much attention and is already used in many applications with quantity production. The development is continued on a variety of hybrid materials or composite nano-carbons. Our knowledge on the carbon material is growing, for example, nanohorns [5], carbon dots [6], nanowalls [7], nanobuds [8], with the development of physics, chemistry and material sciences.

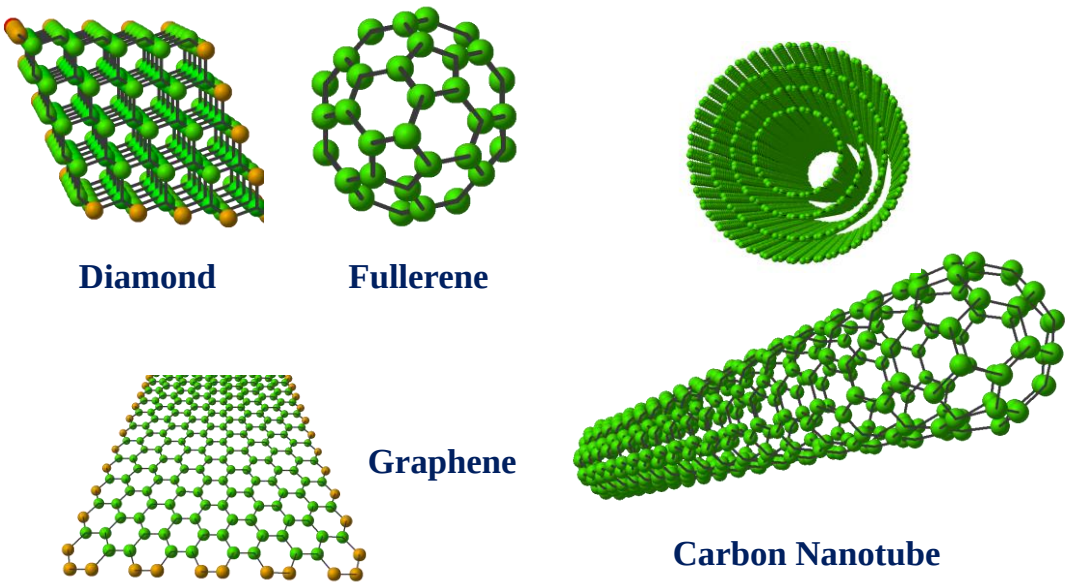

Figure 1-1 Structures of carbon allotropes

Reproduced with permission from Prof. Shigeo Maruyama's Carbon Nanotube Site

http://www.photon.t.u-tokyo.ac.jp

1.2 Geometry and electronic structure of SWNTs

1.2.1 Geometry of SWNTs

SWNTs can be defined as a single atomic layer graphene sheet rolled up into a seamless cylinder. The different way of rolling up results in the different geometric structure of SWNTs. The structure defined as chiral angle, the hexagon helix around the nanotube axis, which can be labeled in terms of the graphene lattice vectors. Figure 1- 2 (a) shows the graphene honeycomb lattice, the vectors $\mathbf{a_1}$ and $\mathbf{a_2}$ with 120° for hexagonal lattice in a unit cell are expressed as

$$\mathbf{a_1} = \left(\frac{\sqrt{3}}{2}, \frac{1}{2}\right) a_{C-C}, \mathbf{a_2} = \left(\frac{\sqrt{3}}{2}, -\frac{1}{2}\right) a_{C-C} \quad (1\text{-}1)$$

In the Cartesian *x*-*y* coordinate,

$$a \equiv |\mathbf{a_1}| = |\mathbf{a_2}| = 1.42 \times \sqrt{3} = 2.46\text{Å} \quad (1\text{-}2)$$

Where 1.42 Å is the bond length of carbon atom $a_{\text{C-C}}$ in graphene, and a is the unit length. So a_1 and a_2 also can be expressed by this unit length a as:

$$\mathbf{a_1} = \left(\frac{\sqrt{3}}{2}, \frac{1}{2}\right) a, \mathbf{a_2} = \left(\frac{\sqrt{3}}{2}, -\frac{1}{2}\right) a \quad (1\text{-}3)$$

The chiral vector $\boldsymbol{C}_\mathbf{h}$ expressed by these two vectors $\mathbf{a_1}$ and $\mathbf{a_2}$, which define the way a graphene sheet rolling up, considered as

$$\boldsymbol{C}_\mathbf{h} = n\mathbf{a_1} + m\mathbf{a_2} \equiv (n, m) \quad (1\text{-}4)$$

The integers (*n*, *m*) called chirality that denote the number of unit vectors $\mathbf{a_1}$ and $\mathbf{a_2}$ in the hexagonal honeycomb lattice contained in chiral vector $\boldsymbol{C_h}$. Usually, $n \geqq m$ is the way to express the chirality of a SWNT.

Peripheral length of a nanotube is the length of chiral vector $\boldsymbol{C}_\mathbf{h}$,

$$\boldsymbol{C_h} = \sqrt{3} a_{C-C} \sqrt{n^2 + nm + m^2} \quad (1\text{-}5)$$

So the diameter dt of a nanotube can be written in terms of the integers (n, m) as

$$d_t = \frac{C_h}{\pi} = \frac{\sqrt{3}a_{cc}(m^2+mn+n^2)^{\frac{1}{2}}}{\pi} \quad (1\text{-}6)$$

As shown in Figure 1- 2 (a), the angle between the chiral vector $\boldsymbol{C_h}$ and $\mathbf{a}_2$ (zigzag direction) is the chiral angle. The chiral angle θ is expressed as

$$\theta = \tan^{-1}\left[\frac{\sqrt{3}m}{m+2n}\right] \quad (1\text{-}7)$$

The other lattice unit vector which is perpendicular to the chiral vector $\mathbf{C}_h$ in the unit cell is translational vector **T**:

$$\mathbf{T} = t_1\mathbf{a_1} + t_2\mathbf{a_2} \equiv (t_1, t_2) \quad (1\text{-}8)$$

(t_1, t_2) can be expressed by (n, m) as

$$t_1 = \frac{2m+n}{d_R}, \quad t_2 = -\frac{2n+m}{d_R} \quad (1\text{-}9)$$

The length of T is the shortest repeat distance along the SWNT axis direction and is expressed as

$$T = \frac{\sqrt{3}C_h}{d_R} = 3a_{C-C}\sqrt{n^2+nm+m^2}/\boldsymbol{d_R} \quad (1\text{-}10)$$

Here

$$\boldsymbol{d_R} = \begin{cases} d & \text{if n}-\text{m is not a multiple of 3d} \\ 3d & \text{if n}-\text{m is a multiple of 3d} \end{cases} \quad (1\text{-}11)$$

where d is the highest common divisor of (n, m). The number of the hexagons contained in one unit cell of SWNT in a real lattice is given as

(a)

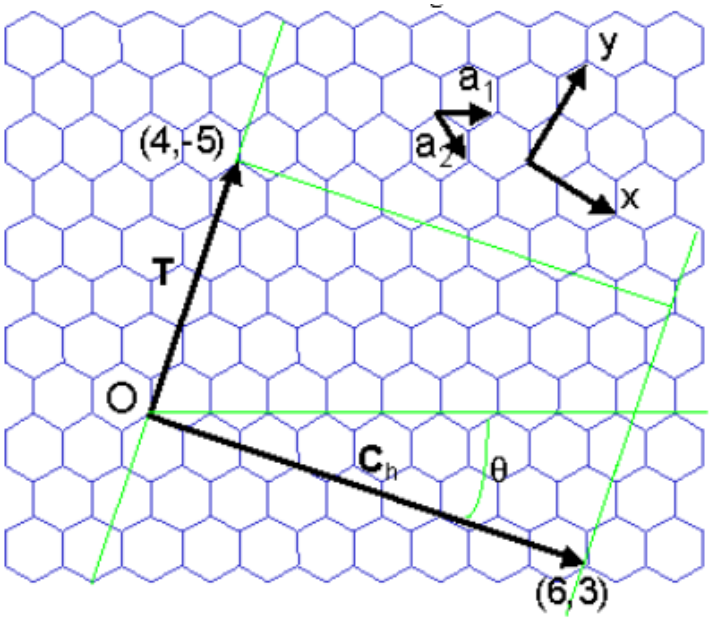

(b)

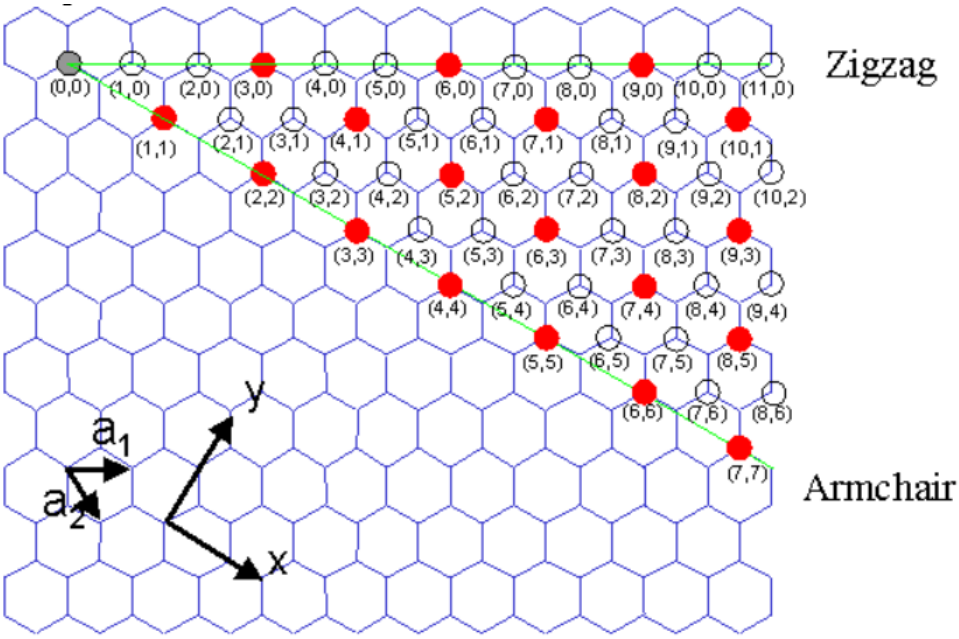

Figure 1-2 (a) Chiral vector translational vector in the graphene lattice for (6,3) SWNT; (b) chirality indices of SWNTs. a red solid point and a black open circle represents metallic nanotubes and semiconductor nanotubes, respectively. Types of Zigzag, armchair and are also marked. Images with permission from http://www.photon.t.u-tokyo.ac.jp/~maruyama/kataura/chirality.html

$$N = \frac{|C_h \times T|}{|a_1 \times a_2|} = \frac{2(m^2+mn+n^2)}{d_R} \quad (1\text{-}12)$$

Chirality indices was shown in figure 1-2 (b), When $2n+m=3q$ (q is integer), or $(n-m)/3$=integer, it can be sorted as metallic SWNT [9]. For an armchair SWNT, $d_t = \frac{3n}{\pi} a_{C-C}$, θ equals to 30°, T= $\sqrt{3}a_{C-C}$, and N= $2n$; a zigzag SWNT, $d_t = \frac{\sqrt{3}n}{\pi} a_{C-C}$, θ is 0°, T= $3a_{C-C}$, and N=$2n$; and for a chiral tubes θ is between 0° and 30°.

1.2.2 Electronic structure of SWNTs

Electronic structure of SWNTs can be considered from similar electronic structure of graphene. π-band in $2p_z$ orbit of graphene mainly arouse the electronic properties. Corresponding to real lattice vector in figure 1-2 (a), figure 1-3 (a) shows reciprocal lattice vector, in this reciprocal lattice, the basic vectors $\mathbf{b_1}$ and $\mathbf{b_2}$ with 120° in the reciprocal lattice are expressed as

$$\mathbf{b_1} = \left(\frac{2\pi}{\sqrt{3}a}, \frac{2\pi}{a}\right), \mathbf{b_1} = \left(\frac{2\pi}{\sqrt{3}a}, -\frac{2\pi}{a}\right) \quad (1\text{-}13)$$

Chiral vector $\boldsymbol{C_h}$ and translational vector $\mathbf{T}$ are transformed into $\mathbf{K_2}$ and $\mathbf{K_1}$, the relationship can be descripted as:

$$\boldsymbol{C_h} \cdot \mathbf{K_2} = 2\pi,\ \mathbf{T} \cdot \boldsymbol{K_2} = 0,\ \boldsymbol{C_h} \cdot \boldsymbol{K_1} = 0,\ \mathbf{T} \cdot \mathbf{K_1} = 2\pi \quad (1\text{-}14)$$

Reciprocal lattice vector $\mathbf{K_2}$ in the direction of circumference is expressed as:

$$\mathbf{K_2} = [(2m+n)\mathbf{b_2} + (2n+m)\mathbf{b_1}]/Nd_R;$$

$$|\mathbf{K_2}| = 2\pi/C_h = 2/d_t \quad (1\text{-}15)$$

Reciprocal lattice vector $\mathbf{K_1}$ along nanotube axis is expressed as:

$$\mathbf{K_1} = (m\mathbf{b_1} - n\mathbf{b_2})/N;$$

$$|\mathbf{K_1}| = 2\pi/|T| \quad (1\text{-}16)$$

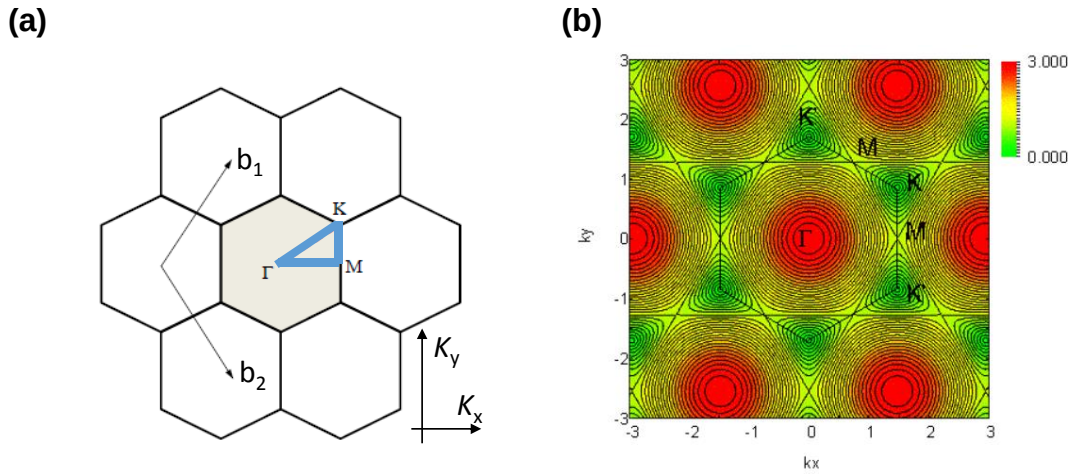

Figure 1-3 (a) The Brillouin zone of SWNTs in the reciprocal lattice; (b) the counter map of dispersion energy simplified by symmetry of conduction and valence bands. Images with permission from http://www.photon.t.u-tokyo.ac.jp/~maruyama/kataura/discussions.html

The center area of hexagon in Figure 1- 3 (a) is the Brillouin zone. In the Brillouin zone of graphene, the three high symmetry points, Γ, K and M of denote the center, the corner, and the center of the edge of a hexagon ring, respectively. From tight-binding approximation, 2D energy dispersion of π-band and π*-band between two carbon atoms in graphene are shown as:

$$E_{g2D}^{\pm}(\mathbf{k}) = \frac{\varepsilon_{2p} \pm \gamma_0 w(\mathbf{k})}{1 \mp s w(\mathbf{k})} \tag{1-17}$$

$$w(\mathbf{k}) = \sqrt{1 + 4\cos\frac{\sqrt{3}k_x a}{2}\cos\frac{k_y a}{2} + 4\cos^2\frac{k_y a}{2}} \tag{1-18}$$

Here, s=0.129, interaction energy of carbon-carbon γ_0 =2.9 eV, ε_{2p}=0. For calculating the energy difference between conduction and valence band, this 2D energy dispersion is simplified by symmetry of conduction and valence bands, as shown as:

$$E_{g2D} = \gamma_0 w(\mathbf{k}) = \gamma_0 \sqrt{1 + 4\cos\frac{\sqrt{3}k_x a}{2}\cos\frac{k_y a}{2} + 4\cos^2\frac{k_y a}{2}} \quad (1\text{-}19)$$

The counter map of this dispersion energy is shown in figure 1-3 (b).

From the influence of the wave function around the circumference of an SWNT, there are N lines parallel to the *z*-direction separated in the first BZ of an SWNT, called cutting lines.

The cutting lines N are resulted from wave function $\mu\mathbf{K}_2$ (μ=1-*N*/2,……, *N*/2). When the cutting lines come across the K point, then the SWNTs is metallic; if not, the SWNTs is semiconducting, which is due to each N line according to different π-band.

Using tight-binding approximation, electronic density of states (DOS), present Van Hove singularities (vHS), as shown in figure 1-4, semiconducting (6,4). At the Fermi energy the energy gap between vHS can be defined as E_{ii}^{S} for semiconducting SWNTs and E_{ii}^{M} for metallic SWNTs. When the energy of the incident light is equal to the energy gap between vHS, the absorption of photon energy occurs, which is also the basic usage for Kataura-plot (E_{ii} vs. dt) [10-12].

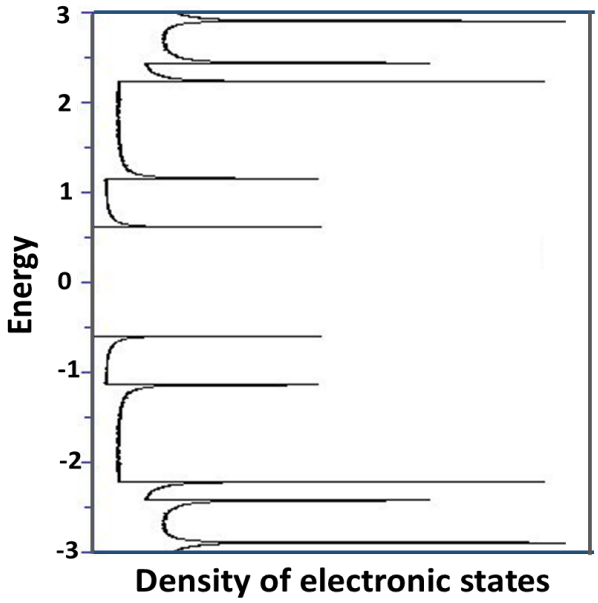

Figure 1-4 van Hove singularity in DOC of a (6, 4) SWNTs. Data is from

http://www.photon.t.u-tokyo.ac.jp/~maruyama/kataura/discussions.html

1.3 Characterizations of SWNTs

Characterization methods for SWNTs used in this work are described here. They are optical spectroscopies including: Raman spectroscopy, absorption spectroscopy, and photoluminescence excitation spectroscopy and microscopies including: scanning electron microscope (SEM) and transmission electron microscope (TEM). Properties and chirality of SWNTs were analyzed by Raman spectroscopy with 5 lasers, photoluminescence and absorption spectroscopies. Morphology was occasionally confirmed by SEM or TEM.

1.3.1 Raman spectroscopy

As a sensitive and powerful method, Raman spectroscopy is wildly used for the characterizing SWNTs bundles. General principle will be described as following.

Scattering can be divided into elastic scattering and inelastic scattering. In the case of Rayleigh scattering, there is no energy losing or obtaining for a photon (an elementary particle that descries quantum of light and terms of electromagnetic radiation) collision with a molecular, this is elastic scattering. Contrast with elastic scattering, Raman spectroscopy observes the inelastic scattering along the lattice to obtain the structure information of the matter. In inelastic scattering, molecular can get a quantum transition to an higher energy level or a lower energy level, which depends on its initial energy level and process of emitting or absorbing energy. When a excited electron absorbed energy from ground states then emitted photon energy to excited state, energy loses happened ($-h(V_0-V_v)$) in this scattering called stokes process; on the other hand, when a excited electron absorbed energy from excited states then emitted emit photon energy to ground state, energy obtaining happened ($-h(V_0+V_v)$) in this scattering called anti-stokes process. Scatting schematic is shown in the figure 1-5. The Raman shift is basically rising due to the energy difference between the incident and released photon. Due to 1D confinement of electronic and phonon states in SWNTs, when the energy gap of valence and conduct is matched with the energy of incident photon energy, resonant enhancement which is observed by Raman can obtain the vibrational properties of SWNTs will be occurred correspondingly.

Abundant information about structure, properties and purity of SWNTs can be obtained from Resonance Raman spectroscopy [12-16]. Main features of the Raman spectra from SWNTs bundles were shown in figure 1-5. Generally, Here introduces the dominant features of SWNTs from first-order Raman features Radial breath mode (RBM) and G band , and double resonance D band mainly analyst in this work.

RBM mode is one of the first-order Raman mode coming from coherent atomic vibration of the carbon atoms in radial direction of a nanotube, when the energy of the incident laser matches with the energy gap E_{ii} in DOS of an SWNT, RBM peaks obviously enhanced in the frequency of 100–500 cm^{-1}, Usually Raman shift in the RBM region can distinguish the diameter (d_t) of a SWNT and used to perform an assignment for a SWNT. Relationship of Raman shift and diameter considered as $\omega_{RBM} = \frac{A}{dt} + B$,

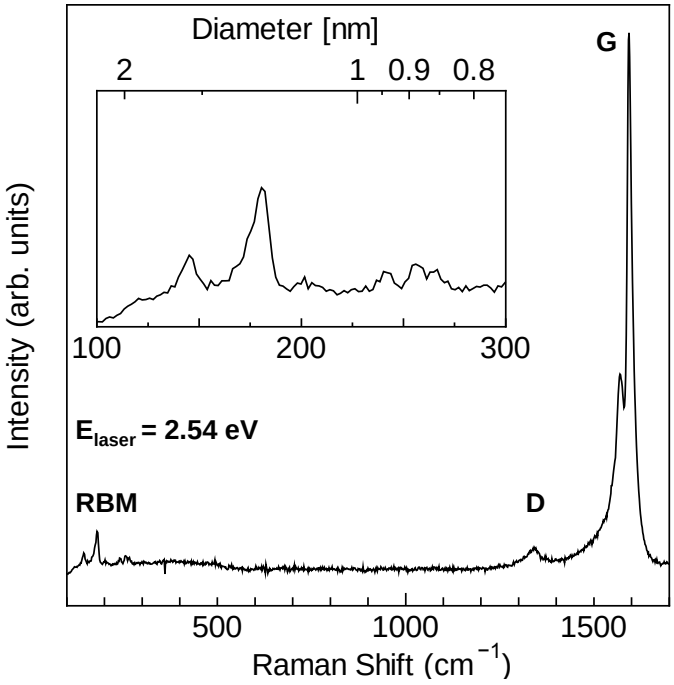

Figure 1-5 Typical Raman spectra of SWNTs

where A and B can be experimentally determined [17]. And with Kataura plot, almost fully assignment (*n*,*m*) of SWNTs bundles containing different SWNTs in resonance with the lasers of different excitation energies can be took in RBM spectra [18]. When using many laser lines, a diameter distribution of samples can be well obtained [19], the more accuracy the more laser lines used. And the ratio of semiconducting tubes to metallic tubes also can be determined when using many laser lines [20].

Another first-order Raman mode is G-band, which presents the nature of a SWNT for the in-plane atomic vibrational mode. The separation of G^+ (high frequency) related to axial atomic vibration (LO) and G^- modes (lower frequency) circumferential atomic vibration (TO) from G-band slipping can be used to characterize the diameter of SWNTs [18, 21] and identify semiconducting (lorentzian lineshape) and metallic (Breit-Wingner-Fano lineshape) in G mode SWNTs [22, 23], and the position of G-band also can be used to investigate the charge transfer of SWNTs [24].

A broaden and weak feature appears around 1350 cm^{-1} is disorder-band (D-band)

clarify the information of defects of atom structure or impurities in SWNTs. It is a common peak of a second-order feature in Raman of SWNTs, and the frequency of D-band exhibits a strong dependence on the excitation laser energy [25].

1.3.2 Optical absorption spectroscopy

To characterize the optical properties of SWNTs, absorption band observed from infrared to visible region were also checked by using UV-vis-NIR absorption spectroscopy. Usually, when light pass a medium, it may collide with medium, the matched energy result in the wavelength of absorbance, and the intensity of absorbance can show the concentration of detected species in the sample according to Beer's law. So UV-vis-NIR absorption spectroscopy also can identify samples quantity.

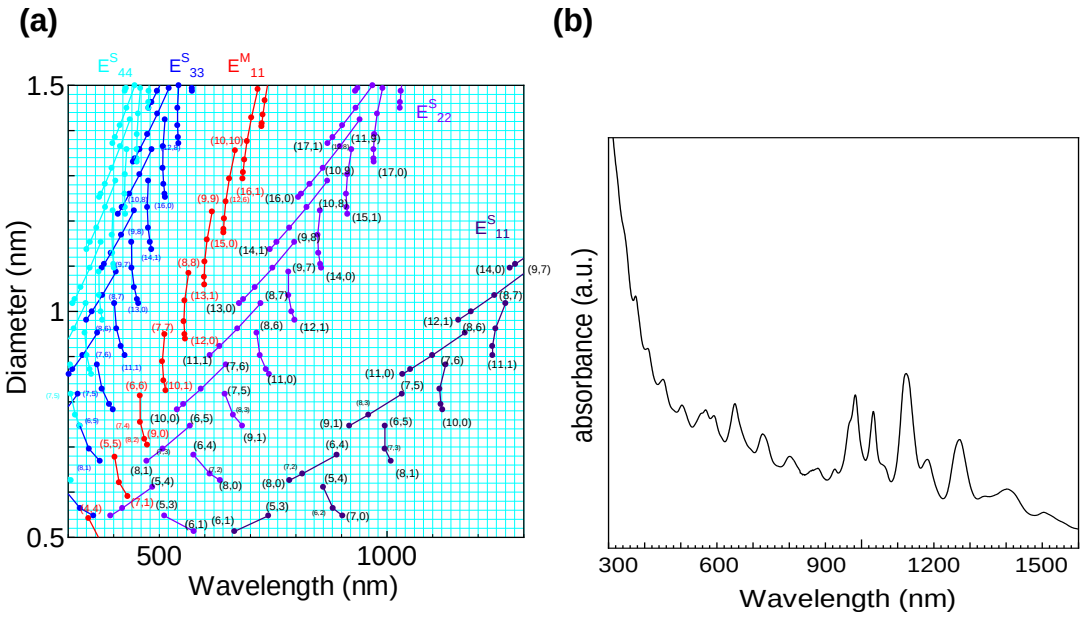

Figure 1-6 (a) Kataura plot and (b) absorption spectrum of dispersed SWNTs sample.

In case of SWNTs, when photon energy matches the vHS in DOC that is different with different chirality of SWNTs, absorbed photon will be increased significantly, which result in the rising peaks in the absorption spectrum. The electronic energy separation of the first vHS is called E_{11}, when the photon energy match it, absorbance can happen involving into peaks, which provide the chirality information of observed SWNTs sample.

Metallic SWNTs also have very weak absorbance called E_{11}^{M} even with a continuous band structure. By analogy the electronic energy separation of the second, third,… vHS is called E_{22}, E_{33}…. Combining the peaks of E_{11} and E_{22} obtained from the absorption spectra would provide enough information to recognize and assign an SWNT. Figure 1-6, (b) shows the absorption spectrum of one dispersed SWNTs sample and corresponding Kataura plot in (a). From the absorption peak shift of a dispersed SWNTs sample, we can clearly identify the exact diameter of one peak, diameter shift and diameter distribution. And ratio of metallic and semiconductor SWNTs can be estimated from the intensity of absorption features [10, 26]. The information obtained from absorption spectra comparing to Raman measurements observation further confirms the assignment of charities of SWNTs.

1.3.3 Photoluminescence excitation spectroscopy

Photoluminescence can be described as one electron excited into high energy level with absorbing energy, then return to low energy level with emitting a photon energy. It can check many properties of semiconductor SWNTs only [27], because this process cannot be produced in metallic materials where electron is excited by optical absorption, but hole is occupied by another electron immediately. The other limitation is that bundled SWNTs do not luminesce [28], it is necessary to isolate SWNTs bundles in surfactant wrapped solution by sonication for detecting.

Photoluminescence excitation (PLE) spectroscopy provides useful information about optical properties, chirality and chirality distribution of semiconducting SWNTs on the bases of vHSs. Once the electron of SWNTs is excited by absorbing an excited energy equal to energy separation E_{22}, the PLE spectra can be obtained by energy separation

E_{11} corresponds to the returned electron to the first transition energy through emitting. Figure 1-7 presents the PLE spectra of one dispersed SWNTs sample, chirality were assigned by the obtained pairs information of E_{11} and E_{22} corresponding to specific SWNTs. PLE can provide powerful information for identify and assignment of dispersed SWNTs sample by accompanies with absorption spectroscopy that observe optical properties in the same way [29].

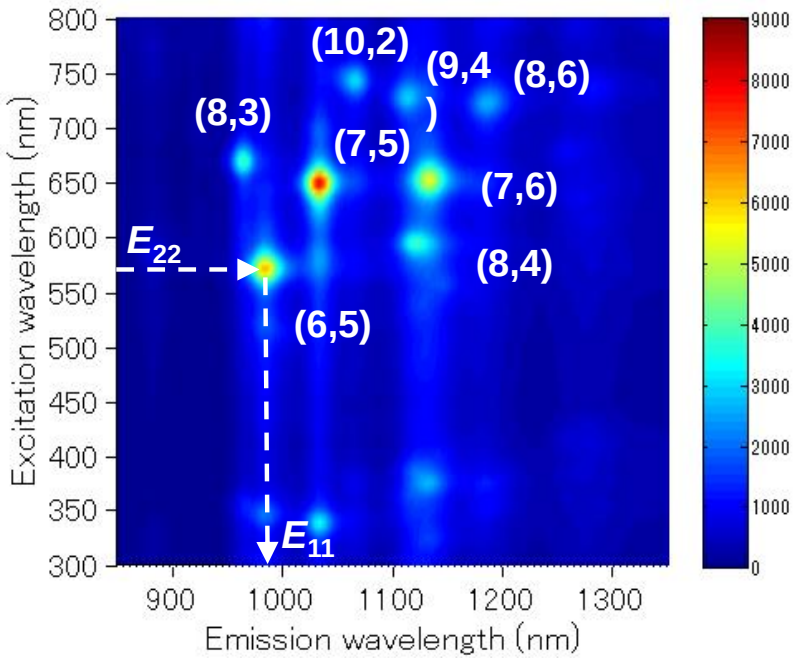

Figure 1-7 PL map of one dispersed SWNTs sample, chirality were assigned by the obtained information of E_{11} and E_{22} corresponding to specific chirality of SWNTs.

1.3.4 Electron microscope

Morphology of as-grown SWNTs were observed by scanning electron microscope (SEM) and transmission electron microscope (TEM) in this work. In SEM, electron beam with several acceleration voltage scan the surface of sample, an image is obtained by detecting the secondary electron. From the SEM image of SWNTs sample, general morphology such as networking, vertical align or horizontally align of SWNTs can be

identified. Yield of SWNTs can be roughly determined by SEM. However, clear diameter, layer and purity cannot detected by it.

TEM with acceleration voltage (60-200 keV) improve the observation of SWNTs [2], electron beam with high acceleration voltage transmit the sample then reach CCD camera under sample with very high magnification. Quality of SWNTs, such as information diameter and purity were observed by TEM in this work.

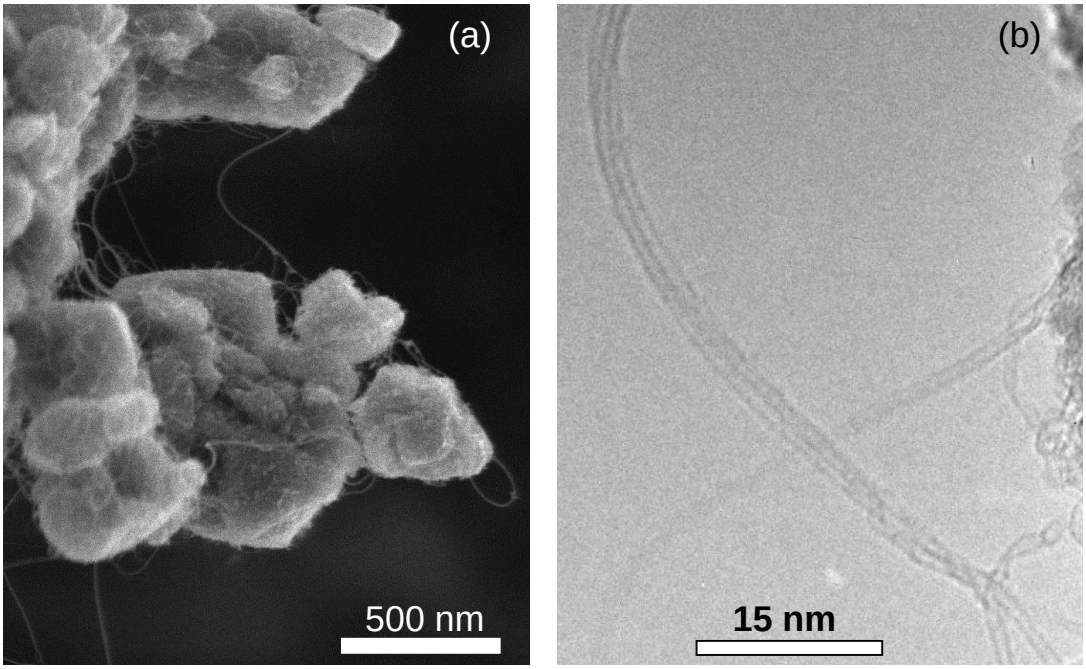

Figure 1-8 (a) SEM and (b) TEM images of SWNTs obtained in this work.

1.4 Application of SWNTs

Due to the one dimensional structure of CNTs, when think about the cross-section of wall of SWNTs, SWNTs has very high mechanical strength compare to other industrial fibers [30]. Meanwhile, thermal conductivity of SWNTs is also superior compare to diamond [31]. These attract a lot of interests from industry, as a basic application with

SWNTs [32]. The intellectual properties of application using SWNTs are continually growing.

As the SWNTs shows either metallic or semiconducting properties depends on the orientation of graphene lattice with respect to chirality, more and more applications of microelectronics have been investigated. The chirality decided property, where SWNTs with relative larger diameter shows metallic conductivity which is expect to apply as interconnection to substitute Cu wire according to Moore's law. SWNTs has purported ballistic transport and ability to carry large current densities in the absence of electro migration [33, 34]. As for semiconducting property, one dimensional structure shows quantum confinement effect rather than bulk material. With decreasing the diameter, as mentioned above, band gap of SWNT increased from 0.5 eV to 2 eV. Chiral (4,2) SWNTs is the smallest nanotube has been synthesized so far which has theoretical band gap of 2 eV. Furthermore, SWNT is compatible with field effect transistor and high-k architectures [35]. The first transistor has been studied more than 15 years ago [36]. Thin film transistor (TFT) is another example of SWNTs. Small diameter and crossed alignment can make transparent SWNTs network and shows higher mobility than conventional amorphous silicon [37]. This will helpful for a low-temperature process to organic light-emitting diode (OLED). Sufficient current can pass through RGB lighting from CNT network at a lower voltage [38].

Very recently, due to potential controllable of SWNTs diameter, controllable band gap of semiconducting SWNTs is expect to widen application of solar cells which improve the light absorbing from different band gap energy [39, 40]. And because of the quantum confinement of SWNTs and experimental and numerical observation of their multi excitation phenomenon, it was assuming single p-n junction that maximum solar conversion efficiency was placed with band gap around 1.34 eV from Shockley–Queisser limit, which is close to that of the small diameter SWNTs about 0.6 nm. It is promising for SWNTs-based solar cell (especially small diameter SWNTs) by breakdown the Shockley–Queisser limit.

As the large scale synthesis of SWNTs becomes popular, more and more low-end and high-end applications are already transferred to production. For instance, multi walled CNT has capability to reduce biofouling which can be act as anti-fouling coating to ships, automotives [41]. SWNTs-based transparent conducting films is applied to touch panel and other displays which are promising to replace indium-based compound [42]. SWNTs-based composition can also improve the electrical connectivity and mechanical integrity where adding to ion batteries [43]. Fiber-like structure can also apply to environmental application such as water purification [44].

Furthermore, SWNTs' optical properties enable its application in biotechnology, such as bio-maping [45] and near-infrared localized heating [46]. SWNTs is also found to be internalized by cells with binding tips to receptor of cell membrane. Drug delivery system (DDS) as an example with using SWNTs to load anti-cancer drug [47].

1.5 Chemical vapor deposition (CVD) synthesis of SWNTs

Due to their nanoscale structure and outstanding mechanical, thermal, optical and electronic properties, SWNTs have been one of the central topics in nanotechnology research. The preparation of high-quality SWNTs has been the goal of many research endeavors, and great efforts have been made to optimize the production of SWNTs. Up to date, Arc discharge, laser oven and chemical vapor deposition (CVD) are the main methods to obtain SWNTs. CVD as a powerful method forward to scale-up production, widely used for growth of SWNTs. In this work, experiments were implement in catalyst CVD (CCVD), CCVD synthesis of SWNTs is mainly introduced here.

Furthermore, Depends on geometry of catalysts, CCVD also can be generally divided into three strategies as shown in table 1-1: supported catalysts on porous substrates, supported catalysts on flat substrate and unsupported metal catalyst. As shown in table, the features of these strategies present clear different direction for different study purpose. CVD synthesis of SWNTs by nanoparticles will be demonstrated here, which has great assistant for observation of SWNTs, commercializes, chirality control of as-grown SWNTs [48-55]. SWNTs can be obtained from many kinds of carbon contained chemicals such as Methane, ethylene, acetylene, ethane, carbon monoxide.

Ethanol is one of the most widely used carbon sources for the synthesis of SWNTs. various morphologies of SWNTs, including random networks, vertically aligned arrays, horizontally aligned arrays, etc. have been successfully obtained using ethanol [52, 56-60].

Even now, we still face the questions about controlling and freely tuning the diameter during SWNTs growth process, though lots works have achievements on separating SWNTs to dispersion target diameter, or controllable growth directly [50, 51, 54, 61-65], more learning of direct realizing controllable growth in produce process is still needed for the aspect of fundamental knowledge and application.

Strategy	Geometry of catalyst support	Diameter of SWNTs	Morphology of SWNTs	Feature
Growth on plane substrate※	2-D structure	Relative large	Vertically aligned spaghetti	Good for mechanism
	2-D structure	Relative large	Horizontally aligned	Good for application
Floating catalyst	No confin-ement	Broaden distribution	Random oriented	HiPCo: bulk growth for PL
Growth on particle*	**3-D structure**	**Small Narrow distribution**	**Random**	**Quantity scale up Spectroscopy observation Good for mechanism**

Metallic catalyst (high carbon solubility)	Metallic catalyst (low carbon solubility)
Fe, Co, Ni	Pt, Au, **W**, Pd, **Cu**, Ag, Mo

Carbon feedstock
Methane, acetylene, carbon oxide, ethylene, **ethanol, dimethyl ether, acetonitrile**

Table 1-1 Strategies of SWNTs growth by CVD; catalysts and carbon feedstock used in CVD. ※ is using quartz, silicon and * is using Zeolite, MgO and microporous silica.

1.6 Motivation and overview of this thesis

The elementary process of CVD growth of SWNTs on catalyst are [66]: thermal decomposition of feedstock compound, surface dissociation on the catalyst, carbon diffusion through the catalyst bulk or over the catalyst surface, and nucleation, which are schematically shown in the figure 1-9. In these steps toward the formation of SWNTs, many effective points can be studied to understand the whole process. And in this work, experiment condition were mostly low temperature condition, where it was believed that carbon diffusion step is only surface diffusion as shown in figure 1-9 (a).

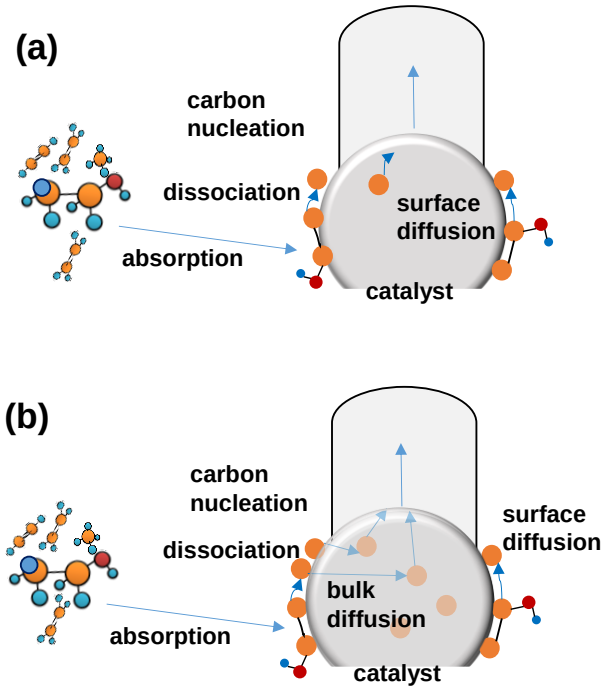

Figure 1-9 Schematic of SWNTs growth process

In the gas phase of CVD, carbon sources are decomposed at proper temperature and pressure before reaching the surface of catalyst, decomposition degree decides whether the final arrived carbon components were original carbon source or decomposed byproducts. Strong influence of carbon decomposition degree on the thickness of

SWNTs and SWNTs quality were observed [67-69].

Besides thermal phase decomposition, carbon absorb and dissociate on catalyst also strongly affect as-grown SWNTs, which is the reason carbon components reached on different catalysts result in different SWNTs. Of course, catalyst also affect the surface dissociation. Therefor carbon feedstock and sorts of catalyst are necessary parameters when we discussed the effect of surface dissociation. In the solid phase, carbon will be through diffusion in bulk or over surface and nucleation for growth of SWNTs, carbon solubility which verified by catalysts and formation of SWNTs controlled by crystalline or morphology of catalysts determined during this process. This process directly go forward to the cap based lift-up growth of SWNTs, therefor the effect from catalyst sorts are the key points to chirality/diameter controlled growth of SWNTs.

On the basis of understanding the effect from thermal decomposition, carbon sorts of feedstock and catalyst in CVD synthesis of SWNTs, simulation and experimental of thermal decomposition of carbon feedstock ethanol and dimethyl ether (DME) will be studied in the chapter 2, effect from different carbon components dissociated on surface and different catalysts will be discussed in chapter 4.

On the other hand, as we known, properties of SWNTs depend on its chirality, a varying types of properties are distinguished even only by small diameter differences or chirality. Unique chirality structures of SWNTs arouse researchers challenge and chance. Under low temperature, aggregation and/or Ostwald ripening lead to a decrease of the metal nanoparticle diameter [48-51, 53, 54, 59]. Generally, performance of catalysts has strong dependence on CVD conditions, exploration for SWNTs growth in expanding CVD condition were studied in chapter 3, and effect of catalysts on the selective growth will also be presented in chapter 4.

Significant breakthroughs were archived that synthesis small diameter SWNTs at low temperature while reducing defect in this work. Unignited problem on defects in SWNTs during extreme synthesis process is the bottle neck which need to be break through first, because defects in SWNTs not only affects their mechanical, thermal and optical properties, but also limit their application in SWNTs-based devices. Usually we

meet the big defect in SWNTs problem when the growth temperature is too low or the pressure is too high, because low active growth environment in low temperature usually arouse slow growth of SWNTs and over loading of carbon in high pressure bring too much carbon garbage, so it become a challenge that how to low down the defect in SWNTs in relative low temperature growth condition. All studies of this work were taken by temperature and pressure dependence strategy, from the exploration of temperature and pressure dependence in CVD, new CVD work window for good quality and broaden diameter distribution of SWNTs was extended, furthermore, super small diameter SWNTs rarely observed before were obtained, this core studies will present in chapter 3.

In this thesis, the study of decomposition of ethanol in SWNTs growth gives us the hint that can control the formation of SWNTs in gas phase. The work of expanding the CVD condition from high temperature and pressure to low temperature and pressure, bring us the systematic understanding on the key process that determine the efficiency growth of both the super-small diameter SWNTs and broaden diameter distribution SWNTs. And also we can get the important information from the quality modulating of SWNTs by changing the feedstock and catalysts, which is promising for controllable growth of SWNTs.

Reference:

[1] H. W. Kroto, J.R. Heath, S.C. O'Brien, R.F. Curl and R.E. Smalley, "C_{60}: Buckminsterfullerene," *Nature* 318, 162 **(1985)**

[2] S. Iijima, "Helical microtubules of graphitic carbon," *Nature* 354, 56 **(1991)**

[3] S. Iijima and T. Ichihashi, "Single-shell carbon nanotubes of 1-nm diameter," *Nature*, 363, 603 **(1993)**.

[4] K. S. Novoselov, A. K. Geim, S. V. Morozov, D. Jiang, Y. Zhang, S. V. Dubonos, I. V. Grigorieva, and A. A. Firsov, "Electric Field Effect in Atomically Thin Carbon Films," *Science*, 306, 666 **(2004)**

[5] R. Yuge, J. Miyawaki, T. Ichihashi, S. Kuroshima, T. Yoshitake, T. Ohkawa, Y. Aoki, S. Iijima, and M. Yudasaka, "Highly efficient field emission from carbon

nanotube− nanohorn hybrids prepared by chemical vapor deposition," *ACS nano*, 4, 7337 **(2010)**

[6] H. Li, X. He, Z. Kang, H. Huang, Y. Liu, J. Liu, S. Lian, C. H. A. Tsang, X. Yang and S.-T. Lee, "Water-soluble fluorescent carbon quantum dots and photocatalyst design," *Angew. Chem. Int. Ed.* 49, 4430 **(2010)**

[7] V. A. Krivchenko, S. A. Evlashin, K. V. Mironovich, N. I. Verbitskiy, A. Nefedov, C. Wöll, A. Ya. Kozmenkova, N. V. Suetin, S. E. Svyakhovskiy, D. V. Vyalikh, A. T. Rakhimov, A. V. Egorov, and L. V. Yashina, "Carbon nanowalls: the next step for physical manifestation of the black body coating," *Sci. Rep.* 3, 3328 **(2013)**

[8] A. G. Nasibulin, P. V. Pikhitsa, H. Jiang, D. P. Brown, A. V. Krasheninnikov, A. S. Anisimov, P. Queipo, A. Moisala, D. Gonzalez, G. Lientschnig, A. Hassanien, S. D. Shandakov, G. Lolli, D. E. Resasco, M. Choi, D. Tománek, and E. I. Kauppinen, "A novel hybrid carbon material," *Nat. Nanotechnol.* 2, 156 **(2007)**

[9] R. Saito, M. Fujita, G. Dresselhaus, and M. S. Dressejkljlhaus, "Electronic Structure of Chiral Graphene Tubules," *Appl. Phys. Lett.* 60 (18), **(1992)**

[10] H. Kataura, Y. Kumazawa, Y. Maniwa, I. Umezu, S. Suzuki, Y. Ohtsuka and Y. Achiba, "Optical properties of single-wall carbon nanotubes," *Synthesis Metals* 103, 2555 **(1999)**

[11] R. Saito, G. Dresselhaus, and M. S. Dresselhaus, "Trigonal warping effect of carbon nanotubes," *Physical Review B*, 61, 2981 **(2000)**

[12] M. S. Dressejkljlhaus, G. Dresselhaus, and R. Saito, "Raman spectroscopy of carbon nanotubes," *Physics Reports* 409, 47 **(2005)**

[13] C. Fantini, A. Jorio, M. Souza, M. S. Strano, M. S. Dresselhaus, and M. A. Pimenta, "Optical transition energies for carbon nanotubes from resonant Raman spectroscopy: environment and temperature effects," *Phys. Rev. Lett.* 93, 147406 **(2004)**

[14] H. Telg, J. Maultzsch, S. Reich, F. Hennrich, and C. Thomsen, "Chirality distribution and transition energies of carbon nanotubes," *Phys. Rev. Lett.* 93, 177401 **(2004)**

[15] S. K. Doorn, D. A. Heller, P. W. Barone, M. L. Usrey, and M. S. Strano, "Resonant Raman excitation profiles of individually dispersed single walled carbon nanotubes in solution," *Appl. Phys. A* 78, 1147 **(2004)**

[16] V. N. Popov and L. Henrard, "Comparative study of the optical properties of single-walled carbon nanotubes within orthogonal and nonorthogonal tight-binding models," *Phys. Rev. B* 70, 115407 **(2004)**

[17] A. Joria, R. Saito, J.H. Hafner, C.M. Lieber, M. Hunter, T. McClure, G. Dresselhaus, and M. S. Dressejkljlhaus, "structure (*n*,*m*) determination of isolated single-wall carbon nanotubes by resonant Raman scattering," Phys. Rev. Lett. 86, 1118 **(2001)**

[18] A. Jorio, M. A. pimento, A. G. Souza Filho, R. Saito, G. Dresselhaus, and M. S. Dresselhaus, "Characterizating carbon nanotube samples with resonance Raman scattering," New J. *Phys. 5*, 1.1 **(2003)**

[19] M. Milnera, J. Kurti, M. Hulman, H. Kuzmany, "Periodic resonance excitation and intertube interaction from quasi-continuous distributed helicities in single-wall carbon nanotubes," *Phys. Rev. Lett*. 84, 1324 **(2000)**

[20] Ge. G. Samsonidze, S. G. Chou, A. P. Santos, A. Selbst, M. S. Dresselhaus, A. K. Swan, M. S. Unlu, B. B. Goldberg, D. Chattopadhyay, S. N. Kim, F. Papadimitrakopoulos, "Quantitative evaluation of the octadecylamine-assisted bulk separation of semiconducting and metallic single wall carbon nanotubes by resonance Raman spectroscopy," *Appl. Phys. Lett.* 85, 1006 **(2004)**

[21] A. Jorio, A.G. Souza Filho, G. Dresselhaus, M.S. Dresselhaus, A.K. Swan, M.S. Unlu, B. Goldberg, M. A. Pimenta, J. H. Hafner, C. M. Lieber, and R. Saito, "G-band resonant Raman study of 62 isolated single wall carbon nanotubes," *Phys. Rev. B* 65, 155412 **(2002)**

[22] M. A. Pimenta, A. Marucci, S. A. Empedocles, M. G. Bawendi, E.B. Hanlon, A.M. Rao, P. C. Eklund, R.E. Smalley, G. Dresselhaus, M.S. Dresselhaus, "Raman modes of metallic carbon nanotubes," *Phys. Rev. B Rapid* 58, R16016 **(1998)**

[23] S. D. M. Brown, A. Jorio, P. Corio, M.S. Dresselhaus, G. Dresselhaus, R. Saito, K. Kneipp, "Origin of the Breit–Wigner–Fano lineshape of the tangential G-band feature of metallic carbon nanotubes," *Phys. Rev. B* 63, 155414 **(2001)**

[24] M. S. Dresselhaus, G. Dresselhaus, "Intercalation compounds of graphite," *Adv. Phys.* 30, 139 **(1981)**

[25] M. A. Pimenta, E. B. Hanlon, A. Marucci, P. Corio, S. D. M. Brown, S. A.

Empedocles, M. G. Bawendi, G. Dresselhaus, and M. S. Dresselhaus, “The anomalous dispersion of the disorder-induced and the second-order Raman bands,” *Brazil. J. Phys.* 30, 423 **(2000)**

[26] A. Hagen and T. Hertel, "Quantitative Analysis of Optical Spectra from Individual Single-Wall Carbon Nanotubes," *Nano Lett.* 3, 383 **(2003)**

[27] M. J. O’Connell, S. M. Bachilo, C. B. Huffman, V. C. Moore, M. S. Strano, E. H. Haroz, K. L. Rialon, P. J. Boul, W. H. Noon, C. Kittrell, J. Ma, R. H. Hauge, R. B. Weisman, and R. E. Smalley, "Band gap fluorescence from individual single-walled carbon nanotubes," *Science* 297, 593 **(2002)**

[28] J. Lefebvre, J. M. Fraser, P. Finnie, Y. Homma, “Photoluminescence from an individual single-walled carbon nanotube,” Phys Rev. B 69, 075403 **(2004)**

[29] S. M. Bachilo, M. S. Strano, C. Kittrell, R. H. Hauge, R. E. Smalley, and R. B. Weisman, "Structure-assigned optical spectra of single-walled carbon nanotubes," *Science* 298, 2361 **(2002)**

[30] B. Peng, M. Locascio, P. Zapol, S. Li, S. L. Mielke, G. C. Schatz, and H. D. Espinosa, "Measurements of near-ultimate strength for multiwalled carbon nanotubes and irradiation-induced crosslinking improvements," *Nat. Nanotechnol.* 3, 626 **(2008)**

[31] E. Pop, D. Mann, Q. Wang, K. Goodson, H. Dai, "Thermal conductance of an individual single-wall carbon nanotube above room temperature," *Nano Lett.* 6, 96 **(2006)**

[32] M. F. L. De Volder, S. H. Tawfick, R. H. Baughman, and A. J. Hart, "Carbon nanotubes: present and future commercial applications," *Science* 339, 535 **(2013)**

[33] B. Q. Wei, R. Vajtai and P. M. Ajayan, "Reliability and current carrying capacity of carbon nanotubes," *Appl. Phys. Lett.* 79, 1172, **(2001)**

[34] F. Kreupl, A. P Graham, G. S Duesberg, W. Steinhögl, M. Liebau, E. Unger, and W. Hönlein, "Carbon nanotubes in interconnect applications," *Microelectronic Engineering* 64, 399 **(2002)**

[35] A. M. Ionescu and H. Riel, "Tunnel field-effect transistors as energy-efficient electronic switches," *Nature* 479, 329 **(2011)**

[36] S. J. Tans, A. R. M. Verschueren, and C. Dekker, "Room-temperature transistor based on a single carbon nanotube," *Nature* 393, 49 **(1998)**

[37] D. M. Sun, M. Y. Timmermans, Y. Tian, A. G. Nasibulin, E. I. Kauppinen, S. Kishimoto, T. Mizutani, and Y. Ohno, "Flexible high-performance carbon nanotube integrated circuits," *Nat. Nanotechnol.* 6, 156 **(2011)**

[38] M. A. McCarthy, B. Liu, E. P. Donoghue, I. Kravchenko, D. Y. Kim, F. So, and A. G. Rinzler, "Low-voltage, low-power, organic light-emitting transistors for active matrix displays," *Science* 332, 570 **(2011)**

[39] K. Cui, T. Chiba, S. Omiya, T. Thurakitseree, P. Zhao, S. Fujii, H. Kataura, E. Einarsson, S. Chiashi, and Shigeo Maruyama, "Self-assembled microhoneycomb network of single-walled carbon nanotubes for solar cells," *J. Phys. Chem. Lett.* 4, 2571 **(2013)**

[40] K. Cui, A. S. Anisimov, T. Chiba, S. Fujii, H. Kataura, A. G. Nasibulin, S. Chiashi, E. I. Kauppinend and S. Maruyama, "Air-stable high-efficiency solar cells with dry-transferred single-walled carbon nanotube films," *J. Mater. Chem. A* 2, 11311 **(2014)**

[41] A. Beigbedera, P. Degeea, S. L. Conlanb, R. J. Muttonb, A. S. Clareb, M. E. Pettittc, M. E. Callowc, J. A. Callowc and P. Dubois, "Preparation and characterisation of silicone-based coatings filled with carbon nanotubes and natural sepiolite and their application as marine fouling-release coatings," *Biofouling* 24, 291 **(2008)**

[42] Z. Wu, Z. Chen, X. Du, J. M. Logan, J. Sippel, M. Nikolou, K. Kamaras, J. R. Reynolds, D. B. Tanner, A. F. Hebard., and A. G. Rinzler, "Transparent, conductive carbon nanotube films," *Science* 305, 1273 **(2004)**

[43] L. Dai, D. W. Chang, J.-B. Baek, and W. Lu, "Carbon nanomaterials for advanced energy conversion and storage," *Small* 8, 1130 **(2012)**

[44] M. S. Rahaman, C. D. Vecitis, and M. Elimelech, "Electrochemical carbon-nanotube filter performance toward virus removal and inactivation in the presence of natural organic matter," *Environ. Sci. Technol.* 46, 1556 **(2012)**

[45] A. De La Zerda, C. Zavaleta, S. Keren, S. Vaithilingam, S. Bodapati, Z. Liu, J. Levi, B. R. Smith, T.-J. Ma, O. Oralkan, Z. Cheng, X. Chen, H. Dai, B. T. Khuri-Yakub and S. S. Gambhiret, "Carbon nanotubes as photoacoustic molecular imaging agents in living mice," *Nat. Nanotechnol.* 3, 557 **(2008)**

[46] N. W. S. Kam, M. O'Connell, J. A. Wisdom, and H. J. Dai, "Carbon nanotubes as multifunctional biological transporters and near-infrared agents for selective cancer cell destruction," *Proc. Natl. Acad. Sci. U.S.A.* 102, 11600 **(2005)**

[47] Z. Liu, X. Sun, N. Nakayama-Ratchford, and H. Dai, "Supramolecular chemistry on water-soluble carbon nanotubes for drug loading and delivery," *ACS nano* 1, 50 **(2007)**

[48] Y. Miyauchi, S. Chiashi, Y. Murakami, Y. Hayashida, S. Maruyama, "Fluorscence spectroscopy of single-walled carbon nanotubes synthesized from alcohol," *Chem. Phys. Lett.*, 387, 198 **(2004)**

[49] S. M. Bachilo, L. Balzano, J. E. Herrera, F. Pompeo, D. E. Resasco, and R. B. Weisman, "Narrow (n,m)-distribution of single-walled carbon nanotubes grown using a solid supported catalyst," *J. Am. Chem. Soc.* 125, 11186 (**2003**)

[50] M. He, A. I. Chernov, E. D. Obraztsova, H. Jiang, E. I. Kauppinen, and J. Lehtonen, "Synergistic effects in FeCu bimetallic catalyst for low temperature growth of single-walled carbon nanotubes," *Carbon* 52, 590 **(2013)**

[51] M. He, H. Jiang, B. Liu, P. V. Fedotov, A. I. Chernov, E. D. Obraztsova, F.Cavalca, J. B. Wagner, T. W. Hansen, I. V. Anoshkin, E. A. Obraztsova, A. V. Belkin, E. Sairanen, A. G. Nasibulin, J. Lehtonen and E. I. Kauppinen, "Chiral-selective growth of single-walled carbon nanotubes on lattice-mismatched epitaxial cobalt nanoparticles," *Scientific Reports* 3, 1460 **(2013)**

[52] Y. Murakami, S. Chiashi, Y. Miyauchi, M. H. Hu, M. Ogura, T. Okubo, S. Maruyama, "Growth of vertically aligned single-walled carbon nanotube films on quartz substrates and their optical anisotropy," *Chem. Phys. Lett*. 385, 298 **(2004)**

[53] C.Z.Loebick, D. Abanulo, M. Majewska, G. L. Haller, L. D. Pfefferle, "Effect of reaction temperature in the selective synthesis of single wall carbon nanotubes (SWNT) on a bimetallic CoCr-MCM-41 catalyst," *Applied catalysis A.* 374 213(**2010**)

[54] M. He, C. Alexander I, P. V. Fedotoy, E. D. Obraztsova, J. Sainio, E. Rikkinen, H. Jiang, Z. Zhu, Y. Tian,E.I. kauppinen, M. Niemela, A. Q. I. Krause, "Predominant (6,5) single-walled carbon nanotube growth on a copper-promoted catalyst," *J. Am. Chem. Soc.* 132, 13994 **(2010)**

[55] T. Fujimori, S. Tsuruoka,B. Fugetsu, S. Maruyama, A. Tanioka, M. Terrones, M. Dresselhaus, M. Endo, K.Kaneko, "Enhanced X-ray shielding effects of carbon nanotubes," *Materials Express* 1, 273 (**2011**)

[56] S. Noda, H. Sugime, T. Osawa, Y. Tsuji, S. Chiashi, Y. Murakami, S. Maruyama, "A Simple Combinatorial Method to Discover Co-Mo Binary Catalysts That Grow Vertically Aligned Single Walled Carbon Nanotubes," *Carbon* 44, 1414 **(2006)**

[57] K. Hasegawa and S. Noda, "Diameter increase in millimeter-tall vertically aligned single walled carbon nanotubes during growth," *Appl. Phys. Express* 3, 045103 **(2010)**

[58] K. Hasegawa and S. Noda, "Millimeter-tall single-walled carbon nanotubes rapidly grown with and without water," *ACS nano* 5, 975 **(2011)**

[59] S. Maruyama, R. Kojima, Y. Miyauchi, S. Chiashi, M. Kohno, "Low-temperature synthesis of high-purity single-walled carbon nanotubes from alcohol," *Chem Phys Lett* 360, 229 **(2002)**

[60] Y. Murakami, Y .Miyauchi, S. Chiashi, S. Maruyama, "Direct synthesis of high-quality single-walled carbon nanotubes on silicon and quartz substrates," *Chem Phys Lett*, 377, 49 **(2003)**

[61] P. Zhao, E. Einarsso, G. Lagoudas, J. Shiomi, S. Chiashi, S. Maruyama, "Tunable Separation of Single-Walled Carbon Nanotubes by Dual-Surfactant Density Gradient Ultracentrifugation," *Nano Res.*, 623, 4 **(2011)**

[62] F. Yang, X. Wang, D. Zhang, J. Yang, D. Luo, Z. Xu, J. Wei, J.Wang, Zhi Xu, F. Peng, X. Li, R. Li, Y. Li, M. Li, X. Bai, F. Ding and Y. Li., "Chirality-specific growth of single-walled carbon nanotubes on solid alloy catalysts," Nature 510, 522 **(2014)**

[63] B. Wang, C. H. Patrick Poa, L. Wei, L. J. Li, Y. Yang, and Y. Chen, "(*n*,*m*) Selectivity of Single-Walled Carbon Nanotubes by Different Carbon Precursors on Co−Mo Catalysts," *J. Am. Chem. Soc.*, *129* (29), 9014 **(2007)**

[64] Y. Yuan, L. Wei, W. Jiang, K. Goh, R. Lau, and Y. Chen, "Sulfur induced chirality changes in single-walled carbon nanotube synthesis by ethanol chemical vapor deposition on Co/SiO_2 catalyst," *Journal of Materials Chemistry A*, 3, 3310 **(2015)**

[65] H. Wang, Y. Yuan, L. Wei, K. Goh, DS Yu, Y. Chen, "Catalysts for chirality selective synthesis of single-walled carbon nanotubes," *Carbon*, 81, 1 *(***2015)**

[66] C. T. Wirth, C. Zhang, G. Zhong, S. Hofmann, and J. Robertson, "Diffusion and reaction limited growth of carbon nanotube forests," *ACS nano*, 3, 3560 **(2009)**

[67] B. Hou, R. Xiang,T. Inoue, E. Einarsson, S. Chiashi, J. Shiomi, A. Miyoshi and S. Maruyama, "Decomposition of ethanol and dimethyl ether during chemical vapor deposition synthesis of single-walled carbon nanotubes," *Jpn. J. Appl. Phys*. 50, 065101-1 **(2011)**

[68] R. Xiang, E. Einarsson, J. Okawa, T. Thurakitseree, Y. Murakami, J. Shiomi, Y. Ohno, S. Maruyama, "Chemical vapor deposition for controlled synthesis of vertically aligned single-walled carbon nanotubes," *J. Nanosci. Nanotech*. 10, 3901 **(2010)**

[69] R. Xiang, E. Einarsson, Y. Murakami, J. Shiomi, S. Chiashi, Z. Tang, and S. Maruyama, "Diameter modulation of vertically aligned single-walled carbon nanotubes," *ACS nano* 6, 7472 **(2012)**

Chapter 2

Thermal decomposition of feedstock compounds (Ethanol and Dimethyl Ether) for SWNTs

2.1 Background and objective

During the CVD synthesis of SWNTs, carbon-containing compound is decomposed in gas phase and/or on the surface of catalyst nanoparticles. The carbon precipitates from the surface or bulk of the catalyst particle to form a tubular structure. There have been extensive explorations on the influence of the carbon feedstock, catalyst, and operating parameters such as temperature and pressure [1-4]. In the case of ACCVD, alcohol can undergo significant thermal decomposition before reaching the catalyst [5]. Different from other carbon sources like methane, ethylene, and acetylene, one unique feature of ethanol is that the molecule contains two inequivalent carbon atoms. An interesting proposition that arises from this asymmetric structure is whether or not both carbon atoms are incorporated into the final SWNTs. It is particularly important for ethanol to study its thermal decomposition processes before the carbon precursor arrives at the catalyst. So the extent of thermal decomposition, which strongly influences the gas composition around the catalyst, will undoubtedly affect the growth of SWNTs.

This chapter describes the systematic studies on the thermal decomposition of ethanol under typical CVD conditions by using both numerical simulation and experimental investigations. Understanding the possible reactions before the formation of SWNTs, and the analysis of the gas-phase composition and its influence on SWNT quality is the study described in this chapter.

This study also includes the dimethyl ether (DME) --- an isomer of ethanol --- as a potential candidate for the feedstock for SWNTs synthesis. This is based on the similar decomposition rates and some common products between DME and ethanol. Moreover, DME offers two potential advantages over ethanol. Different from ethanol, DME is a gaseous compound at room temperature, which allows easier handling, particularly in large-scale systems. Secondly, since its combustion produces very little soot [6], DME may produce cleaner SWNTs than those from alcohol. This part shows the work on the synthesis of SWNTs from DME, as well as the influence of temperature and pressure on the thermal decomposition of DME. These findings will be useful for understanding the complicated reaction pathways leading to the formation of SWNTs.

2.2 Simulation and experimental methods

2.2.1 Gas-phase kinetic simulation

Gas-phase decomposition of carbon-source materials was simulated by using SENKIN [7], a computer program that predicts the time-dependent chemical-kinetic behaviour of a homogeneous gas-mixture in a closed system. It is a part of CHEMKIN-II [8], which is a package of computer codes for the analysis of gas-phase chemical kinetics. Constant-temperature and constant-pressure conditions were chosen for the calculations using temperatures and pressures that had been experimentally found to be optimum for SWNT growth. Ethanol and DME oxidation kinetic model [9, 10] was used without modification.

2.2.2 Experimental

Concentrations of gaseous species were estimated from peak intensities of Fourier transform infra-red (FT-IR) spectra. It should be noted that these measurements were made for the gas sampled downstream of the CVD apparatus, rather than *in situ*. As shown in figure 2-1, DME or ethanol was fed into a quartz tubular reactor, which was maintained at constant temperature and pressure. The temperature profile in the quartz tube during typical CVD at 800 ºC has been studied previously [5], and the transient preheating length before the temperature-regulated region is known to be very short,

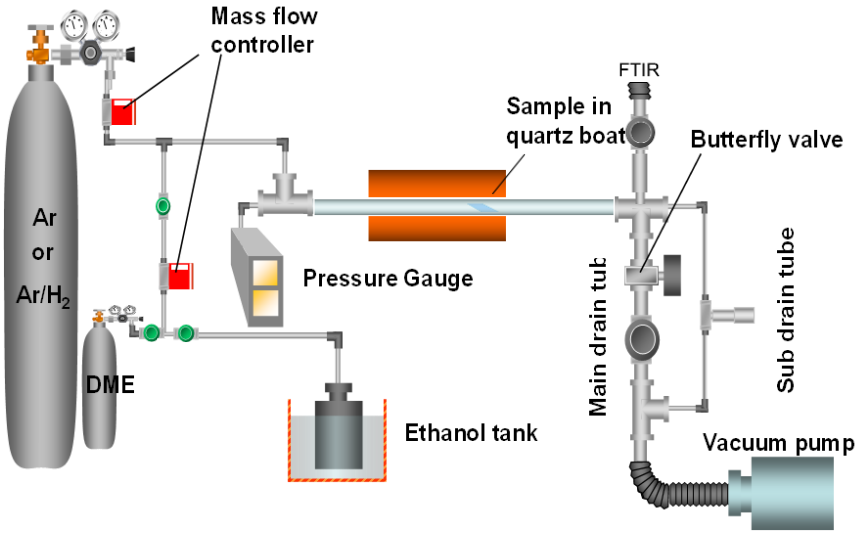

Figure 2-1 CVD apparatus, modified from ref [11].

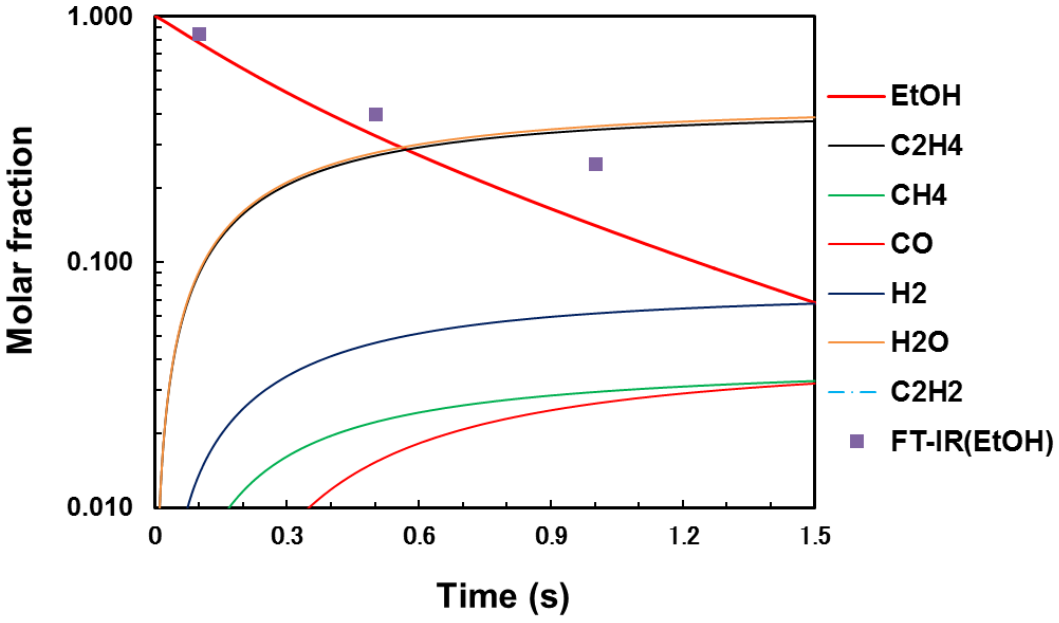

Figure 2-2 Mole fraction profile of the major species during the thermal decomposition of ethanol at 800 °C and 1.3 kPa calculated at constant temperature and pressure.

even at high flow rates exceeding those used in this study. This means that the feedstock is heated up to 800 °C promptly after entering the CVD reactor. The residence time in the heated region was fixed by adjusting the gas flow rate, and the time-history of the concentrations of carbon feedstock was measured by FT-IR.

The residence time (decomposition time) can be calculated from the ideal gas equation, $PV = nRT$. The volume V can be calculated from the dimensions of our equipment, where the inner diameter of the quartz tube is 2.54 cm and the length from entering the furnace until reaching the substrate position is 30 cm. The pressure and temperature were fixed at 1.3 kPa and 1073 K, respectively, so the remaining parameter to be found is *n*, where

$$n = \frac{V_{gas}}{k}. \tag{1}$$

k is a proportionality constant, and

$$V_{gas} = Qt, \tag{2}$$

Where Q is the volumetric flow rate and t is residence time. For a known flow rate, the residence time can be calculated from the following equation

$$t = \frac{PVk}{QRT}. \tag{3}$$

SWNTs were synthesized on a quartz or silicon substrate by ACCVD using ethanol or DME as carbon source. Cobalt and molybdenum catalyst nanoparticles were loaded onto the substrate by a dip-coating method. The details and procedures have been described in previous reports [12, 13]. The as-grown SWNTs were characterized by resonance Raman spectroscopy and SEM observation. *In situ* measurement of the transmitted intensity of a 488 nm laser was used to record the array thickness during growth [12].

2.3 Thermal decomposition of ethanol in CVD conditions

2.3.1 Effect of ethanol decomposition on the growth of SWNTs

Figure 2-2 indicates the mole fraction profile of major species during the thermal decomposition of ethanol at 800 °C and 1.3 kPa calculated at constant temperature and pressure, showing that approximate 90% of ethanol decomposes within 1.5 s. The typical flow rate of ethanol was 450 sccm, which corresponds to a residence time of approximately 0.1 s. Time profile of ethanol measured by FT-IR (symbols) is in good agreement with the simulation (line). Trace amounts of CO, methanol, and acetylene are also found by calculation. Though the experimentally measured decomposition is slightly slower than the simulation, the predicted concentration of ethanol agrees quite well.

Figure 2-3 (a) shows the calculated concentration profiles in expanded logarithmic scales, the decomposition times at which SWNTs growth were measured were marked by dashed lines in the figure.

Interestingly, by the change of the residence time (achieved by changing the flow rate), SWNTs growth curves changed significantly, as shown in figure 2-3 (b). Decrease of the flow rate, which increases the residence time of ethanol in the heated region, enhanced both the catalyst lifetime and the final film thickness. Since all the other conditions were the same, the difference can only be ascribed to the difference of gas composition. That is, for longer resident times, a larger fraction of ethanol decomposes before reaching the catalyst. The enhanced growth is thus attributed to the increased concentration of active species resulting from the decomposition of ethanol.

This study confirmed the importance of gas phase reaction of ethanol before reaching catalyst, which is the important growth rate-limiting step and cannot be ignored the kinetic and mechanistic studies of SWNTs formation [14,15].

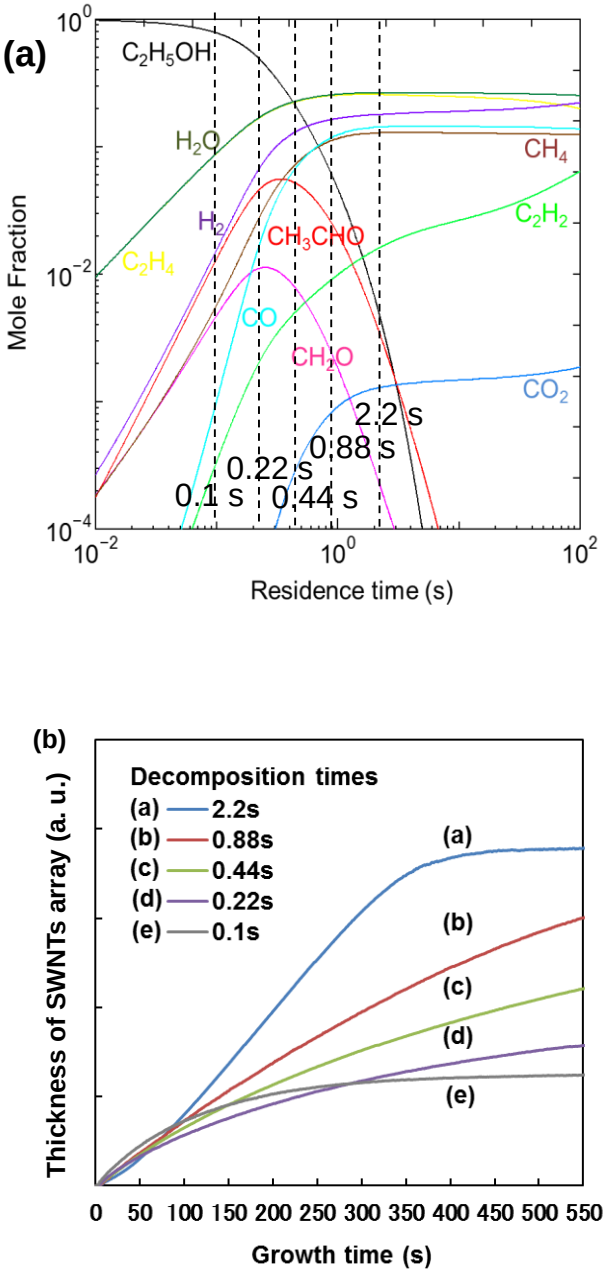

Figure 2-3 (a) Concentration-time profile of relevant species in the thermal decomposition of ethanol at 800 °C and 1.3 kPa. The decomposition times used in (b) were marked by dashed lines. (b) Obtained growth curves at 800 °C at different gas-phase decomposition times.

2.3.2 Temperature and pressure dependence of the thermal decomposition

Thermal decomposition of ethanol at 500 and 600 ^{o}C was simulated in this part. As shown in figure 2-4 (a), ethanol very slowly decomposes below 500 ^{o}C. The calculations shown in figure 2-4 (b) suggests that, at 600 ^{o}C for 100 s, the gas composition would be approximately 95% ethanol with trace of C_2H_4, CO, C_2H_2, etc. On the other hand, figure 2-4 (c) confirmed that ethanol quickly and thoroughly decomposes above around 850 ^{o}C. Figure 2-4 (c) and (d) show time evolution of ethanol concentration at different temperatures and pressures.

Concentration of ethanol changes more than 20 times depending on the residence time and temperature. This implies that in the conventional ACCVD condition, the gaseous precursor species for SWNTs should be a competition between the original ethanol and decomposition products. Considering the much smaller concentration and relatively lower reactivity of CH_4, CH_2O and CO [16, 17], the predominant contributors for the growth will be ethanol, C_2H_4 or C_2H_2. On the other hand, in the low-temperature or low-pressure ACCVD condition where ethanol decomposes only slightly, the precursor species for SWNTs maybe ethanol itself.

These simulations allow us to visualize how ethanol going through to the catalyst surface to the final formation of SWNT. During this gas-phase decomposition stage, ethanol maybe partially or totally decomposed into ethylene and water mainly, decomposition degree can be differential into lightly decomposition and thoroughly decomposition depending on the temperature, pressure and residence time. After reaching the surface of catalyst, the surface dissociation causes ethanol further decomposed on surface, and then carbon-contained molecules diffuse through the catalyst support and/or diffuse over the surface of catalyst in order to participate the growth of SWNTs. One phenomenon generally observed by TEM in CVD process is that at high reaction temperature [18], the outer walls of produced SWNTs are often covered with a significant amount of amorphous carbon soot when ethanol is thoroughly decomposed in the gas phase; but when gas-phase thermal decomposition of ethanol is reduced, the SWNT walls are much cleaner.

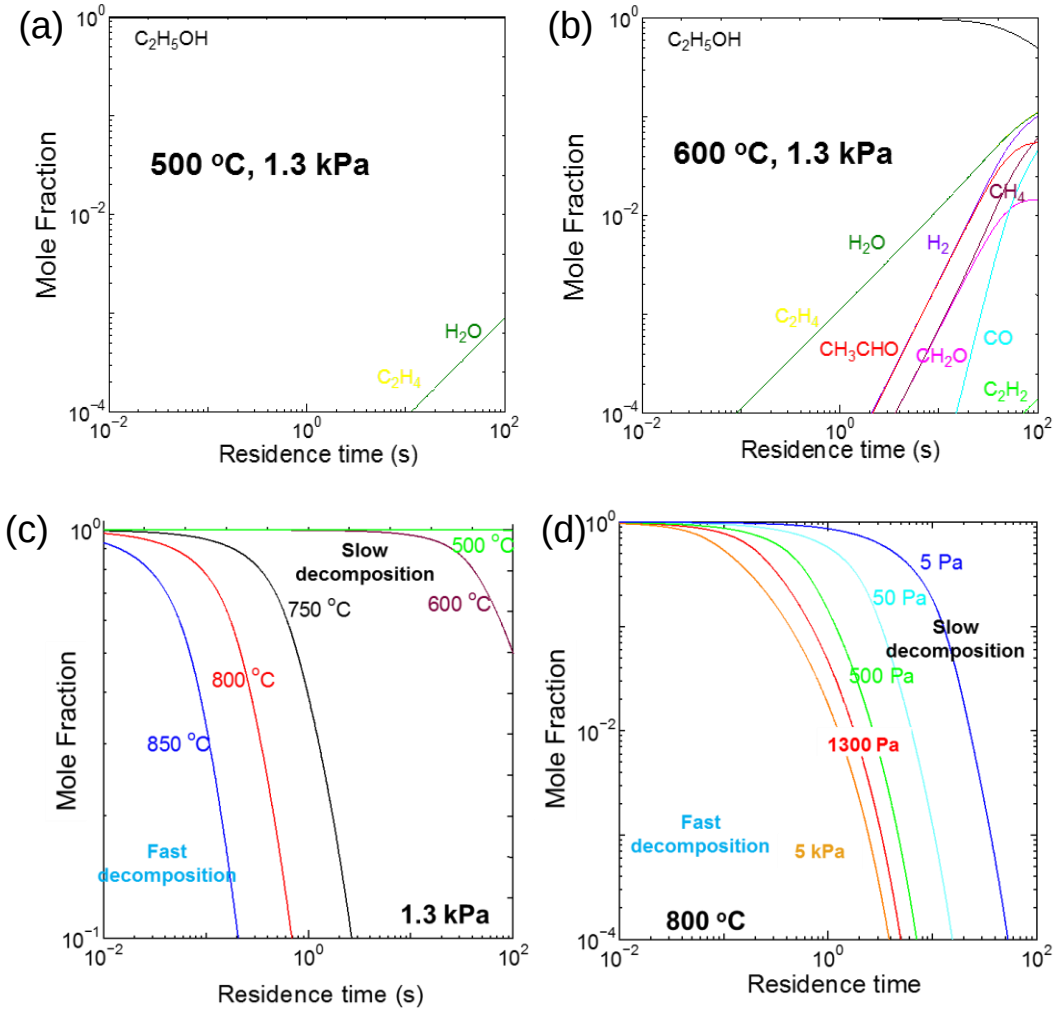

Figure 2-4 Simulation of the thermal decomposition of 1.3 kPa ethanol at (a) 500 °C and (b) 600 °C, (c) at 1.3 kPa and at five different temperature and (d) at 800 °C and at five different pressures.

This is likely due to the relative over-loading reactive carbon products from thoroughly thermal decomposition colliding into the formation of amorphous carbon. However, the decomposed product (such as C_2H_2 and even some radicals) could be possibly more efficient for the growth [19-21], also as shown in figure 2-3 (b), growth rate of SWNTs enhance while thoroughly decomposition increasing. Therefor decreasing gas-phase decomposition while increasing decomposition on catalyst surface through proper CVD condition is a possible way to enhance the abundance of clean and high-quality SWNTs.

These preliminary results may motivate further discussion on the details of the SWNT growth mechanism, and assist to improve controlling over the quality and purity of SWNTs. Also, disassociation or reaction on catalyst is the strong influence on the final formation of SWNTs besides decomposition of ethanol in gas-phase. It is important to choose a proper catalyst for specific purpose of SWNTs, which will be further discussed in chapter 4.

In this part, the direct relationship between the condition of carbon feedstock and the final quality of SWNTs is clearly implied. Through these understanding, when the other carbon source was chosen to be the feedstock in CVD synthesis of SWNTs, it is helpful to modify the optimal CVD condition during the preliminary experimental design. Therefore, on the basis understanding of ethanol CVD for SWNTs growth, DME used CVD for SWNTs were studied in the next section.

2.4 Thermal decomposition of DME in CVD conditions

4.1 Thermal decomposition of DME in comparison with ethanol

Thermal decomposition of ethanol was calculated using the CHEMKIN-II software package, as described in Section 2. The time-dependent gas composition of ethanol (at 1.3 kPa and 800°C) is shown in figure 2-2. Approximately 90% of ethanol decomposes in 1.5 s, and the major products of decomposition are C_2H_4, H_2O, C_2H_2, CH_4, CO, and H_2.

In contrast, as shown in figure 2-5, 90% of DME decomposes within 1 second, which is faster than the ethanol under the same conditions. The major decomposition products of DME are CH_4, CO, and H_2, as well as trace amounts of other species including CH_3OH and CH_2O. By comparing the breaking positions *a*, *a′*, and *b* of ethanol and DME, the dominant decomposition channels of ethanol are well known to be the molecular elimination channel to $H_2O + C_2H_4$ and the C-C bond fission channel to $CH_3 + CH_2OH$. The C–O fission channel (to $C_2H_5 + OH$) is known to be minor. It can determine that ethanol is more likely to form C_2 or CH_3OH, the latter of which can be further decomposed into CH_4, CO, and H_2. For DME, however, there is only one breaking position *b*, the dominant decomposition channel of DME is the C–O bond fission, thus should produce CH_4, CO, and H_2, as predicted by simulation.

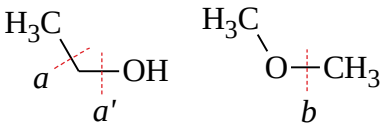

(4)

An FT-IR spectrum of the decomposed gas is shown in figure 2-6. The concentration of the feedstock gas was determined from the relative intensity of the characteristic peak in the spectra. For example, the C-O stretching mode at 1200 cm^{-1} was considered to be the characteristic peak for DME, this peak is very strong and is not interfered by any of

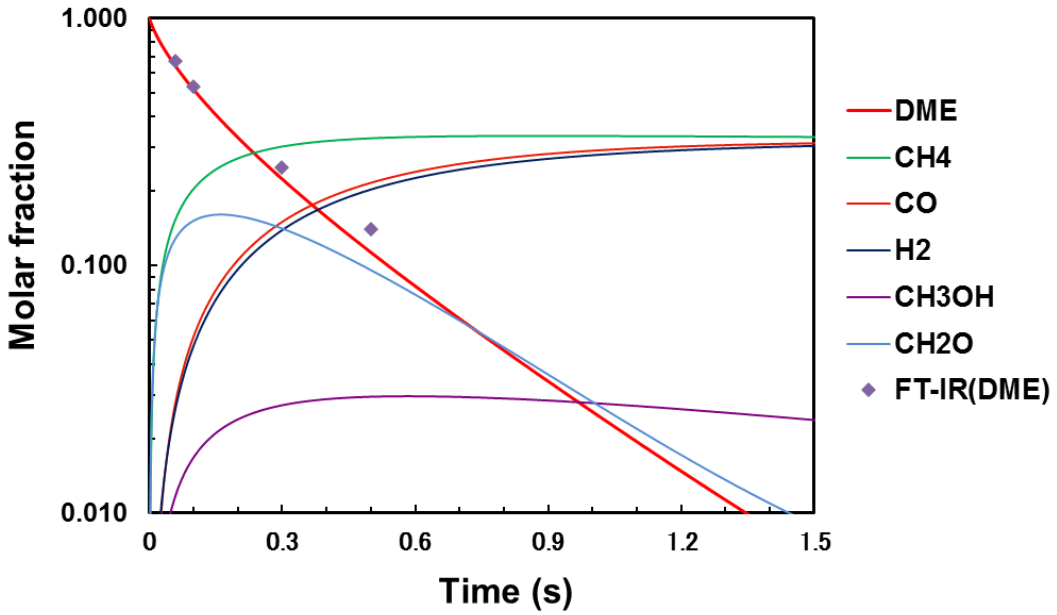

Figure 2-5 Numerical simulation of the thermal decomposition of DME at 800 °C and 1.3 kPa. More than 90% of DME decomposes within approximately 1 s. Experimental results by FT-IR (symbols) are in good agreement with the simulation (lines).

the decomposition products. The DME decomposition in figure 2-5 can be compared with that of ethanol in figure 2-2. Both of these results are for a furnace temperature of 800 °C and a feedstock pressure of 1.3 kPa. The relative concentrations of DME measured by FT-IR are in good agreement with the simulation.

At the high temperature condition of our experimental measurement, the decomposition of DME can be approximated as

$$CH_3OCH_3 \rightarrow CH_4 + CO + H_2 \quad (5)$$

This means that for cases in which DME decomposition is ~90% or more (and for no pressure gradient), the outgoing volumetric flow rate becomes three times larger than at the inlet, where only DME existed. The real residence time thus becomes 1/3 of that calculated from the volumetric flow rate at the inlet. This decreasing residence time was considered when calculating the relative concentration of DME based on the FT-IR spectra. The similar estimation for ethanol was also considered [5].

In addition to the decreasing residence time, we also considered potential overlap of FT-IR spectral features of DME with those from decomposition products. This could result in the overestimation of the DME concentration, especially at low DME concentrations and high product concentrations. The C-O band, which exists only for DME, avoids this interference. The flow in the reactor, however, is not a fully formed plug flow, especially at low pressures where the diffusion of gas becomes significant, thus some of the DME may escape to the exit faster than the calculated residence time. However, this effect is insignificant due to the small inner diameter of the CVD quartz tube, thus possible diffusion of DME was not considered.

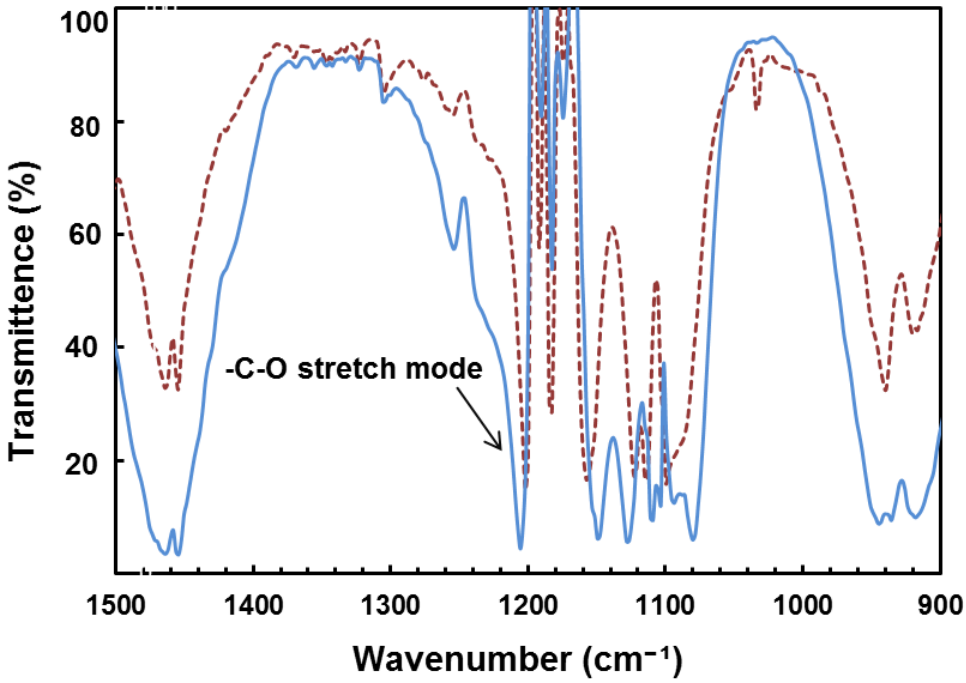

Figure 2-6 FT-IR spectra of DME at different degrees of decomposition. The dashed line indicates thorough decomposition and the solid line indicates light decomposition.

Based on the results of DME decomposition, some of the products are similar to those produced from ethanol decomposition, indicating that DME is a potential carbon source for the growth of SWNTs. More importantly, however, is that although ethanol yields SWNTs with little amorphous carbon, DME is known to produce even less soot during combustion than ethanol [6]. Therefore, the product grown from DME could be an even cleaner carbon source if the process and synthesis conditions were well optimized. And also from the study of effect of decomposition of ethanol on the quality of as-grown SWNTs, lightly decomposition of ethanol can result in cleaner and better quality SWNTs, therefor DME, which has the similar decomposition rate and decomposed species with ethanol, can grow high-quality SWNTs at optimized condition with lightly gas-phase decomposition. To understand the effect of CVD condition on the decomposition degree of DME, the influence of temperature and pressure on the thermal decomposition of DME is implied in the next section.

2.4.2 Influence of temperature and pressure on the thermal decomposition of DME

Some prediction of temperature and pressure influence on the thermal decomposition will be helpful for experimental optimization, so to investigate the temperature dependence we fixed the pressure at 1.3 kPa and performed various time-integrations of DME decomposition. The pressure dependence was similarly investigated by fixing the temperature at 800 °C. Temperature and pressure dependences of DME decomposition are shown in Figure 2-7. When the temperature increases to 950 ºC, DME is more than 90% decomposed within 0.1 second, which means CH_4 and CO become the major precursors for SWNT growth. At 800 ºC, the DME concentration decreased very quickly for pressures near 0.5 kPa, whereas less than 15% of DME was decomposed when the pressure was increased from 1 kPa up to 7 kPa. After adjusting integration time and experimental conditions (primarily by adjusting the flow rate), results of DME decomposition within 0.1 s at various temperatures and pressures are found to be in good agreement with the simulation results (Fig. 2-5).

From the temperature dependence of DME, the thermal decomposition of DME at 700 ºC, 1.3 kPa when the residence time is 0.1 s, is similar to the decomposition of

ethanol at 800 ºC. It can be assumed that high-quality SWNTs can be synthesized at lower temperature than ethanol by using DME.

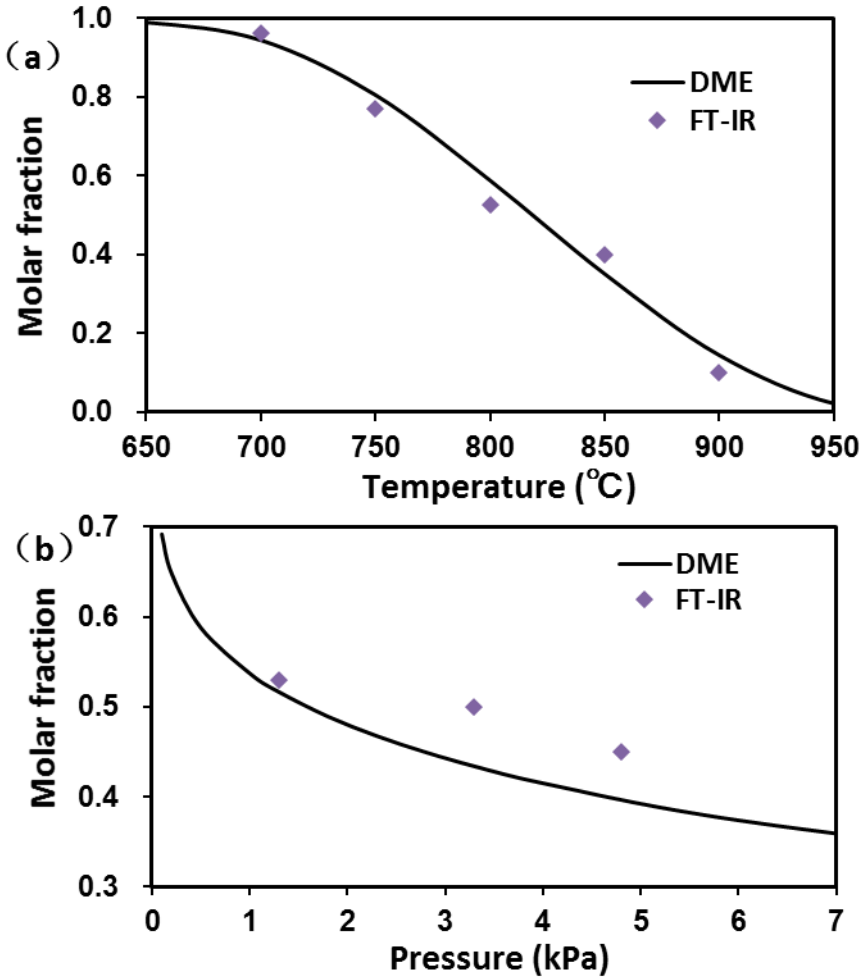

Figure 2-7 (a) Temperature dependence and (b) pressure dependence of thermal decomposition of DME (time-integration) in conventional CVD conditions.

2.4.3 SWNTs growth using DME as a carbon source

To investigate the potential of DME as a novel carbon source for SWNT synthesis, ethanol was replaced in conventional ACCVD process with DME. Preliminary results clearly confirm that SWNTs can be synthesized from this new precursor at lower temperature 700 ºC. A resonance Raman spectrum from the DME-synthesized SWNTs is shown in figure 2-8, and no clear difference from ethanol was found. DME will also be used in low temperature and low pressure CVD, results will be shown and discussed in detail in the chapter 4.

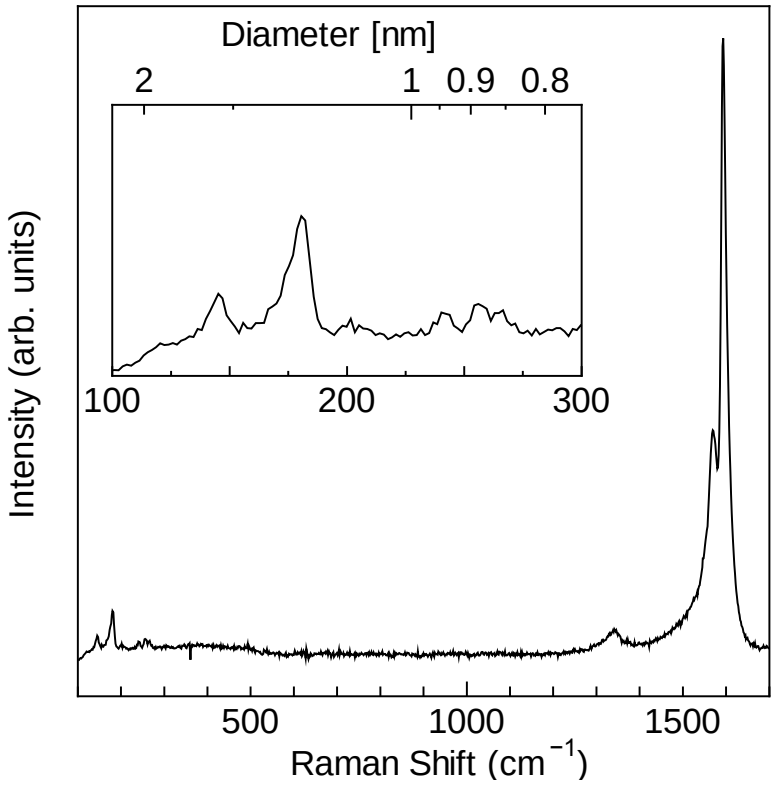

Figure 2-8 Raman spectra of SWNTs synthesized from DME at 700 ºC, 5 kPa. Inset shows enlarged RBM region.

2.5 Conclusion

Gas-phase thermal decomposition of ethanol and DME was simulated using the chemical kinetic model under typical SWNT growth conditions. Profiles of reaction species concentrations were plotted as predicted as thermal decomposition mechanism, which confirmed the simulation reaction trends and products. FT-IR spectroscopy was used to measure the concentrations of reactant (ethanol and DME) resulting from decomposition, and the molar fractions were correlated against residence time in the reactor by adjusting the flow rate of the feedstock gas. FT-IR experimental results at various temperatures and pressures were found to be in agreement with corresponding simulations.

Effect of thermal decomposition of ethanol on the quality was discussed, generally light gas-phase decomposition of ethanol can result in high quality SWNTs comparing to heavy decomposition of ethanol. In this chapter it was also shown that SWNTs could be synthesized by replacing ethanol with DME. The relatively lower optimal CVD temperature of SWNTs growth by DME also confirmed the assumption on the effect of decomposition of carbon feedstock on the final SWNTs formation and its dependence on CVD conditions.

References

[1]S. Maruyama, R. Kojima, Y. Miyauchi, S. Chiashi and M. Kohno, "Low-temperature synthesis of high-purity single-walled carbon nanotubes from alcohol," *Chem. Phys. Lett.* 360, 229 **(2002)**

[2] Y. Murakami, S. Chiashi, Y. Miyauchi, M. H. Hu, M. Ogura, T. Okubo and S. Maruyama "Growth of vertically aligned single-walled carbon nanotube films on quartz substrates and their optical anisotropy," *Chem. Phys. Lett.* 385, 298 **(2004)**

[3] S. Noda, K. Hasegawa, H. Sugime, K. Kakehi, Z. Zhang, S. Maruyama and Y. Yamaguchi, "Millimeter-thick single-walled carbon nanotube forests: hidden role of catalyst support," *Jpn. J. Appl. Phys.* 46, 808 **(2007)**

[4] S. Noda, H. Sugime, K. Hasegawa, K. Kakehi and Y. Shiratori, "A simple combinatorial method aiding research on single-walled carbon nanotube growth on substrates," *Jpn. J. Appl. Phys.* 49, 02BA02-1 **(2010)**

[5] R. Xiang, E. Einarsson, J. Okawa, T. Thurakitseree, Y. Murakami, J. Shiomi, Y. Ohno and S. Maruyama "Parametric study of alcohol catalytic chemical vapor deposition for controlled synthesis of vertically aligned single-walled carbon nanotubes," *J. Nanosci. Nanotechnol.* 10, 3901 **(2010)**

[6] Z. W. Zhao, M. Chaos, A. Kazakov, and P. L. Dryer, "Thermal decomposition reaction and a comprehensive kinetic model of dimethyl ether,", *Int. J. Chem. Kinet.* 40, 1 **(2008)**

[7] A. E. Lutz, R. J. Kee and J. A. Miller: Sandia Report SAND87-8248 (1995)

[8] R. J. Kee, F. M. Rupley and J. A. Miller: Sandia Report SAND89-8009B (1995)

[9] N. M. Marinov, "A detailed chemical kinetic model for high temperature ethanol oxidation," *Int. J. Chem. Kinet.* 31, 183 **(1999)**

[10] E. W. Kaiser, T. J. Wal/lington, M.D. Hurley, J. Platz, H. J. Curran, W. J. Pitz and C. K. Westbrook "Experimental and modeling study of premixed atmospheric-pressure dimethyl ether−air flames," *J. Phys. Chem. A* 104, 8194 **(2000)**

[11] K. Ogura, M. Kadowaki, J. Okawa, E. Einarsson, and S. Maruyama, "Growth mechanism of vertically aligned SWNTs by in-situ absorption measurements," 33rd Fullerene Nanotube General Symposium **(2007)**

[12] S. Maruyama, E. Einarsson, Y. Murakami and T. Edamura "Growth process of vertically aligned single-walled carbon nanotubes," *Chem. Phys. Lett.* 403, 320 **(2005)**

[13] E. Einarsson, M. Kadowaki, K. Ogura, J. Okawa, R. Xiang, Z. Zhang, Y. Yamamoto, Y. Ikuhara and S. Maruyama, "Growth mechanism and internal structure of vertically aligned single-walled carbon nanotubes," *J. Nanosci. Nanotechnol.* 8, 6093 **(2008)**

[14] G. F Zhong, T. Iwasaki, J. Robertson, H. Kawarada, "Growth Kinetics of 0.5 cm Vertically Aligned Single-Walled Carbon Nanotubes,". *J. Phys. Chem. B* 111, 1907. **(2007)**

[15] R. Xiang, Z. Yang, Q. Zhang, G. Luo, W. Qian, F. Wei, M. Kadowaki, E. Einarsson, and S. Maruyama, "Growth Deceleration of Vertically Aligned Carbon Nanotube Arrays: Catalyst Deactivation or Feedstock Diffusion Controlled," J. Phys. Chem. C 112, 4892 **(2008)**

[16] H. Dai, A. G. Rinzler, P. Nikolaev, A. Thess, D. T. Colbert, and R. E. Smalley, "Single-wall nanotubes produced by metal-catalyzed disproportionation of carbon monoxide," *Chem. Phys. Lett.* 260, 471 **(1996)**

[17] J. Kong, A. M. Cassell, and H. Dai, "Chemical vapor deposition of methane for single-walled carbon nanotubes," *Chem. Phys. Lett.* 292, 567 **(1998)**

[18] R. Xiang, B. Hou, E. Einarsson, P. Zhao, S. Harish, K. Morimoto, Y. Miyauchi, S Chiashi, Z. Tang, and S. Maruyama, "Carbon Atoms in Ethanol Do Not Contribute Equally to Formation of Single-Walled Carbon Nanotubes," *ACS nano*, 7, 95 **(2013)**

[19] J. H. Hafner, M. J. Bronikowski, B. Azamian, P. Nikolaev, A. G. Rinzler, D. T. Colbert, K. A. Smith, and R. E. Smalley, "Catalytic growth of single-wall carbon nanotubes from metal particles," *Chem. Phys. Lett.* 296, 195 **(1998)**

[20] R. T. K. Baker, P. S. Harris, R. B. Thomas, R. J. Waite, "Formation of Filamentous Carbon from Iron, Cobalt and Chromium Catalyzed Decomposition of Acetylene," *J. Catal.* 30, 86 **(1973)**

[21]R. Xiang, E. Einarsson, J. Okawa, Y. Miyauchi, S. Maruyama, "Acetylene-Accelerated Alcohol Catalytic Chemical Vapor Deposition Growth of Vertically Aligned SingleWalled Carbon Nanotubes," *J. Phys. Chem. C* 113, 7511 **(2009)**

Chapter 3

Expansion of CVD conditions: growth of super-small diameter SWNTs

3.1 Background and motivation

Until now, we still face the questions about controlling growth and freely tuning the diameter of SWNTs, though lots works had achievements on separating SWNTs to dispersion target diameter [1,2], to realize directly growth of specific SWNTs is still a challenge, especially for the growth of small diameter SWNTs with relative higher band gap which is useful towards application, rarely reports demonstrated the direct growth of small diameter SWNTs and sufficient spectroscopy observation on the as-grown small diameter SWNTs.

Owing to relative high catalytic activity and carbon solubility, Fe and Co are usually considered as the main catalysts widely used for SWNTs growth, just because their high ability for growth of SWNTs by this binary catalyst, usually a relative broad diameter distribution SWNTs can be obtained using Fe-Co catalyst. In the contrary, the catalyst Cu, which recently used cooperate with Co to grow narrow diameter distribution SWNTs aroused interests to grow specific SWNTs such as (6,5) and (7,5) [3,4]. Choosing these two kinds catalysts in the extending CVD system, the modulating of diameter control can be comprehensively reviewed from broad distributed samples to narrow ones.

Usually, to achieve the small diameter SWNTs, two strategies are used: lowering the

growth temperature and confine the catalysts from Oswald ripening [5] and aggregation, small diameter SWNTs were promised for growing on relative small catalysts. Or controlling the morphology of catalyst to fix the initial cap of SWNTs growth. Generally, growth of small diameter SWNTs were realized by the former methodology which is using lower temperature. On the other hand, particle morphology of zeolite enhanced yield and widen CVD work window of temperature and pressure for SWNTs growth, there are a lot of reports for that small diameter SWNTs can be obtained at relative low temperature on particle support catalysts [6-11]. In this work, zeolite was used as particle morphology catalyst support.

Previous conventional CVD temperature for SWNTs growth using ethanol was considered only in a narrow range, from 600 °C to 800 °C at stable pressure [8, 9], controllable growth of SWNTs is very limited only through moderating CVD condition. In this chapter, low temperature, which is low down to 430 °C, coupled with low pressure were tried in CVD by zeolite support Fe-Co catalyst. Expanded CVD work window implied a chance to produce new chirality of SWNTs with super-small diameter which cannot be obviously obtained in conventional CVD, and revealed new understanding of growth mechanism in CVD system.

3.2 Experiments and characterization

3.2.1 Catalysts preparation and CVD procedure

Metal catalyst Fe and Co used in this work for CVD condition exploration were supported by USY-zeolite powder [HSZ-390HUA from Tosoh], which support widen temperature growth in previous reported works [8-11], preparation process of miscible iron acetate [$(CH_3CO_2)_2Fe$] and cobalt acetate [$(CH_3CO_2)_2Co\text{-}4H_2O$] into USY-zeolite powder was similar to reported methods [8, 9]. 2.5 wt % weight concentrations of both Fe and Co of iron acetate and cobalt acetate dissolved in 30ml ethanol were mixed into the zeolite powder. Then the solution was sonicated in 10 mines and dried for 1 hour at 80 ^{o}C. After repeat this sonication and drying steps twice, solution was dried 24 hours at 80 ^{o}C. Absolutely dried powder with light brown color was grinded carefully, since

more molar powder is better for the touch between carbon source and catalyst. Prepared powder can be kept in small bottle for the usage each time.

For the usage in CVD, the zeolite support catalyst carried by a quartz boat was set in a quartz tube (i.d. 27 mm) inside an electric furnace as shown in figure 3-1. During heating to target temperature by the electric furnace, 300 sccm (standard cc/min) of Ar/H_2 (3 % H_2) was employed so as to maintain the pressure inside the quartz tube at 40 ± 1 kPa. The quartz tube was evacuated by a rotary pump after the electric furnace reached the growth temperature, and at the same time with Ar/H_2 was stopped. Ethanol vapor or the other kinds of carbon source (such as DME) from a reservoir with carrier gas Ar (500 sccm) were then introduced at a constant pressure. After completion of the CVD reaction, carbon source were stopped, 500 sccm Ar was closed when temperature cooled down below 600 ºC (only for the case that growth temperature was higher than 600 ºC) then 300 sccm of Ar/H_2 was flowed through the tube while it cooled to room temperature. Growth temperature was varied between 350 ºC and 900 ºC, and growth

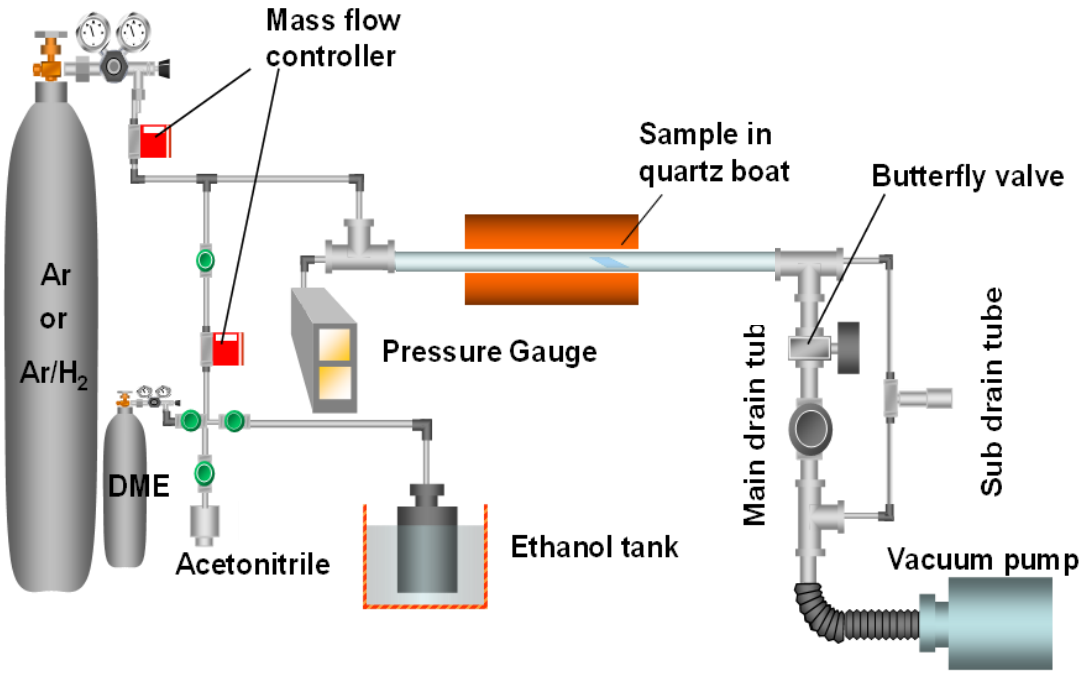

Figure 3-1 CVD apparatus, modified from ref [12]

partial pressure was between 0.02 Pa and 1300 Pa. After cooling down, as-grown SWNTs sample in the quartz boat was took out for characterizations originally or further treatment.

3.2.2 Characterization: Raman, PL, absorption, SEM and TEM

As-grown SWNTs were characterized by resonant Raman scattering and optical absorption. The Raman spectra were measured by Renishaw inVia Raman Microscope using 5 lasers of 488 nm, 532 nm, 633 nm, 785 nm and l064 nm. As shown in figure 3-2 (a), 4 excitation energies laser used in this work were marked in Kataura plot combining with Raman spectra in the RBM region, and G-band shown in (b). Raman results shown in this work for assignment will be presented as this format to identify chirality assignment by Raman [13,14]. SEM (SEM, 1 kV acceleration voltage, S-4800, Hitachi Co.,Ltd.) and TEM (TEM, JEOL 2000EX operating at 120 kV) were also used to observe the morphology of as-grown SWNTs directly.

In order to perform an optical measurement, as-grown sample sometimes need to get treatment for obtaining suspended SWNTs or smaller bundles, [15] The as-grown sample was dispersed in 6 ml D_2O with 4 wt % surfactant sodium deoxycholate (DOC) by heavy sonication with an ultrasonic processor (UP-400s with S3/Micro Tip 3, Hielscher Ultrasonics) for 1 h at a power flux level of 400 W/cm^2. Then dispersion was centrifuged (Micro ultracentrifuges CS150GXL/CS120GXL, Hitachi Koki) at 40000 rpm (163,000 g) for 20 min (keep in 22 °C). The 80% upper supernatant, rich in isolated SWNTs, was decanted and used in measurement of absorption and photoluminescence excitation spectroscopy.

In addition to optical measurements, The UV-vis-NIR absorption spectra arranged the wavelength from 300 cm^{-1} to 1600 cm^{-1} for dispersed SWNTs liquid were measured with UV-3150, (Shimadzu Co., Ltd.). The photoluminescence excitation spectroscopy arranged the emission wavelength from 850 nm to 1350 nm and excitation wavelength from 300 nm to 850 nm were measured through a PLE, HORIBA Jobin Yvon Fluorolog *i*HR320, equipped with a liquid-nitrogen-cooled GaAs detector. PLE map is also shown

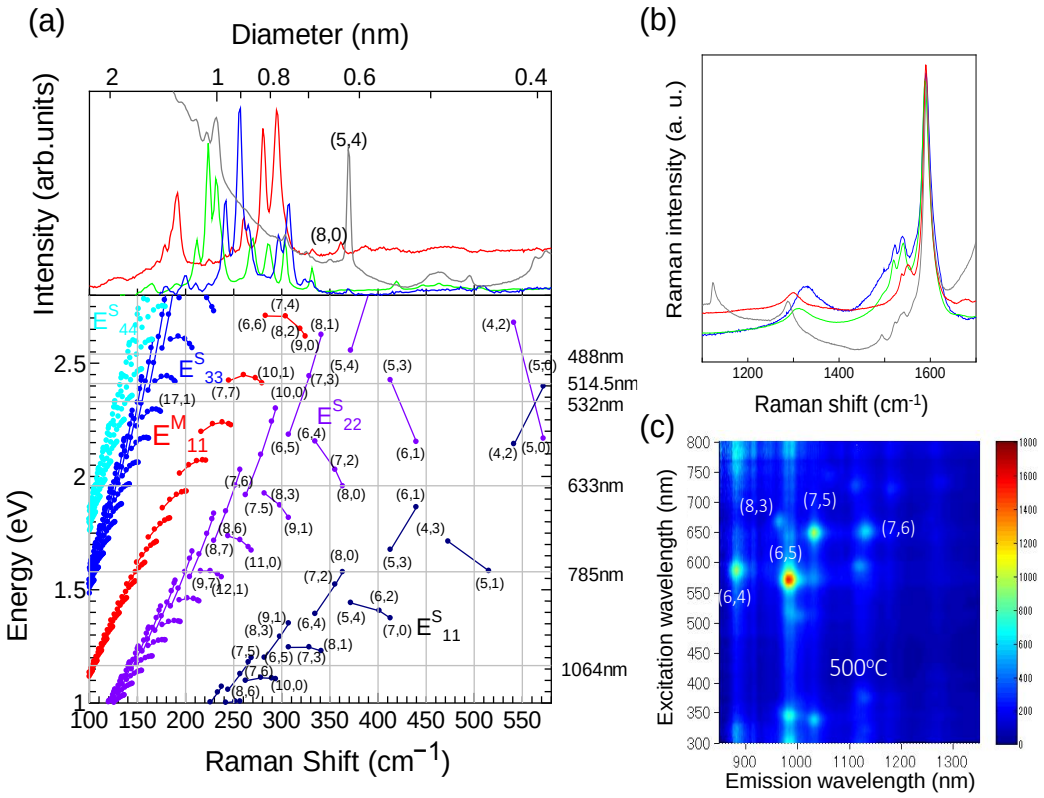

Figure 3-2 (a) and (b) spectra of Raman, and (c) PLE map of the sample obtained at 500°C, 5 Pa in CVD using Fe-Co. Kataura plot in bottom of (a) was used for assigning the observed SWNTs in Raman and absorption [13, 14].

in the figure 3-2 (c).

In addition, during the observation of small diameter SWNTs by Raman spectroscopy, usually resonance peaks raised in RBM region were in higher frequency of Raman shift, where noise maybe interrupt the accuracy of identifying each peak corresponded to specific chirality. In order to eliminate the interruption of noise in RBM region of Raman spectra, as-grown SWNTs sample was annealed in the air from 420 °C to 600 °C. Raman spectra were shown in figure 3-3.

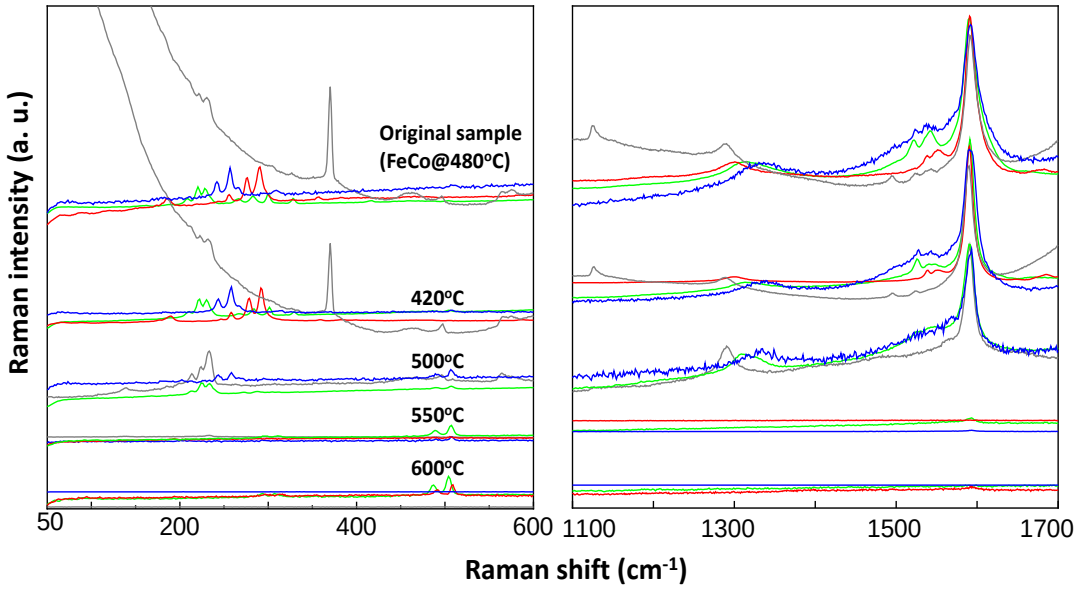

Figure 3-3 As-grown sample was annealed in the air, the signals obtained when all SWNTs burned out reveal the noise signals in RBM region (left one) of Raman spectra.

By comparing the original sample, a procedure of SWNTs burned out gradually was observed by Raman spectra especially in the RBM region. From figure 3-3, when the annealing temperature reached 500 ^{o}C, it seems that SWNTs with small diameter were disappeared. All SWNTs were gone until 550 ^{o}C from the totally disappeared peaks in RBM and G-band, while there were peaks left around Raman shift 500 cm^{-1}, these are the noises that probably from effect of zeolite and should be pay attention that they cannot be considered in the assignment for the small diameter SWNTs.

3.3 Expansion of CVD condition for high quality SWNTs

3.3.1 CVD experimental map

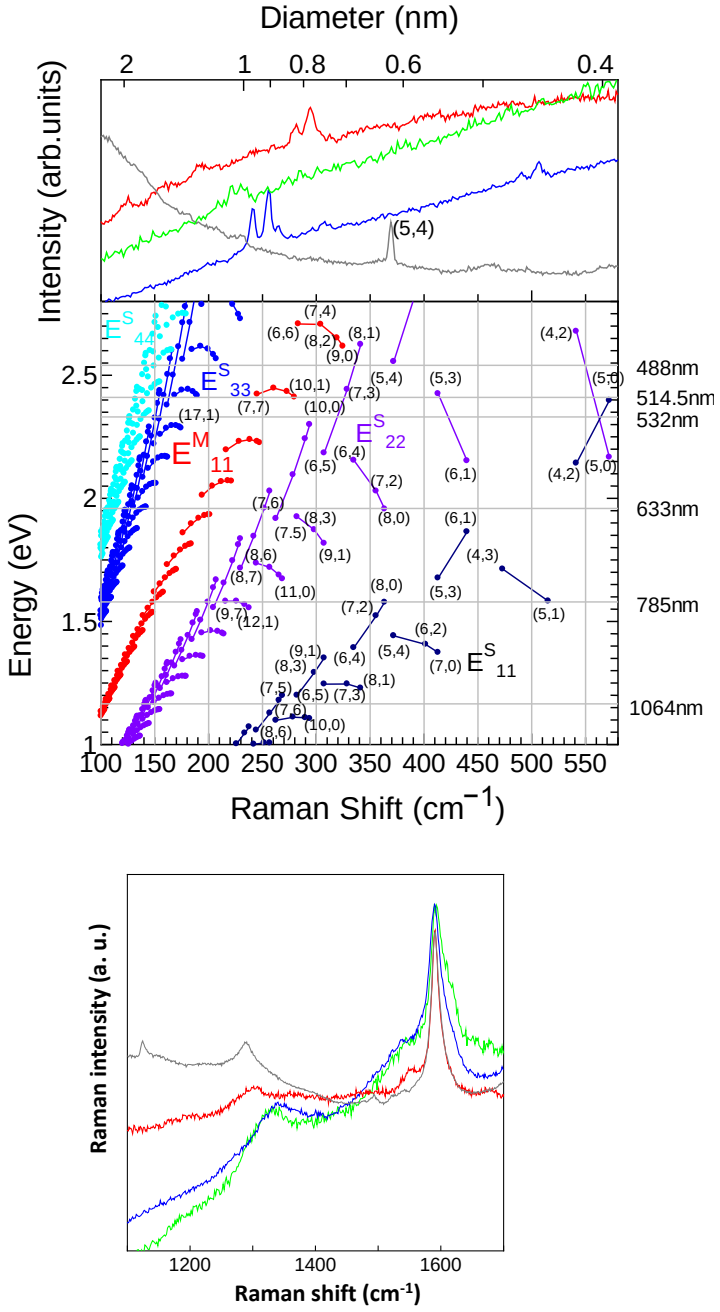

Figure 3-4 Raman spectra of good quality SWNTs synthesized in low temperature and pressure CVD.

As introduced in section 3.1, previously conventional CVD temperature using ethanol for SWNTs growth was considered only in a narrow range, from 600 °C to 800 °C [8, 9], controllable growth of SWNTs is very limited only through moderating CVD condition. Low temperature, which is low down to 430 °C, coupled with low pressure 0.02 Pa were used in CVD by zeolite support Fe-Co catalyst. Figure 3-4 presents that the good-quality and small diameter SWNTs with less chirality were obtained at 430 °C and 0.02 Pa.

As shown in figure 3-4, only several chirality of SWNTs observed by Raman spectra, they can be assigned by Kataura plot, and a relative good G/D ratio reveal the good quality of synthesized SWNTs at low temperature and pressure. From comparing with Kataura plot, the features resonance to 488 nm laser and 532 nm laser in RBM region, reveal metallic SWNTs were observed by these two laser lines, broad G^- peak in BWF line shape also confirms the observation for metallic SWNTs. In the contrary, mainly semiconductor SWNTs were observed by 633 nm and 785 nm lasers from peaks resonance in RBM region. Compare to the sample obtained at conventional CVD condition, most SWNTs disappeared at this extreme condition, but small diameter ones such as (5,4) survived, which also demonstrated that the strategy of obtaining small diameter SWNTs by low down growth temperature. New operation window implies a chance to produce new chirality of SWNTs which cannot be obviously obtained in conventional CVD, and provides new understanding of growth mechanism in CVD system.

Figure 3-5 presents all experimental CVD condition done in this work, one spot is corresponding to one pair of temperature and pressure, green ones mean SWNTs can be synthesized which was determined by Raman observation for the G-band. In the contrast, red ones mean there was no SWNTs growth at this temperature and pressure condition. Temperature range was fixed from 350 ^oC to 900 ^oC while pressure range was from 0.02 Pa to 1300 Pa.

Through analyzing the experimental conditions in this map, the trend of quality of as-grown SWNTs, temperature and pressure dependence on the formation of SWNTs,

and limitation for SWNTs growth with a specific catalyst were systematically and clearly demonstrated. Many information for controllable growth of SWNTs can be considered as refer for the future modification and application, theoretical discussion also can be revealed by the trend shown in this map for understanding the growth mechanism of SWNTs.

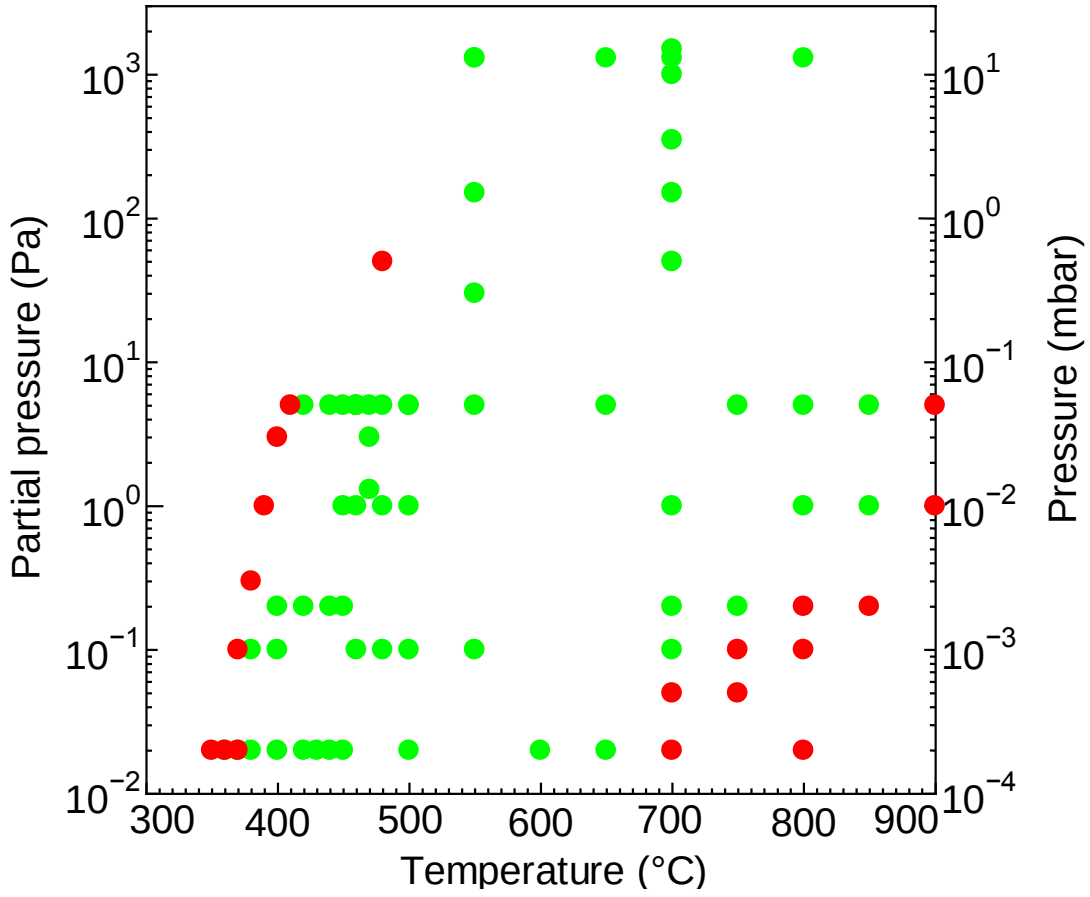

Figure 3-5 Experimental map which include all temperature and pressure information of experiments done in CVD of this work. Green dots mean SWNTs can be obtained, Red dots mean G-band of SWNTs cannot be observed by Raman.

3.3.2 Effect of temperature and pressure on synthesis of super-small diameter SWNTs

As demonstrated in the experimental map, temperature and pressure dependence of synthesis of SWNTs were checked in this work, through this exploration step by step, conventional CVD condition was successfully shift from high temperature and pressure condition to low temperature and pressure condition. Most importantly, small diameter even super-small diameter SWNTs which were rarely obtained in conventional synthesis process and catalyst were obtained through expanding CVD condition. Here,

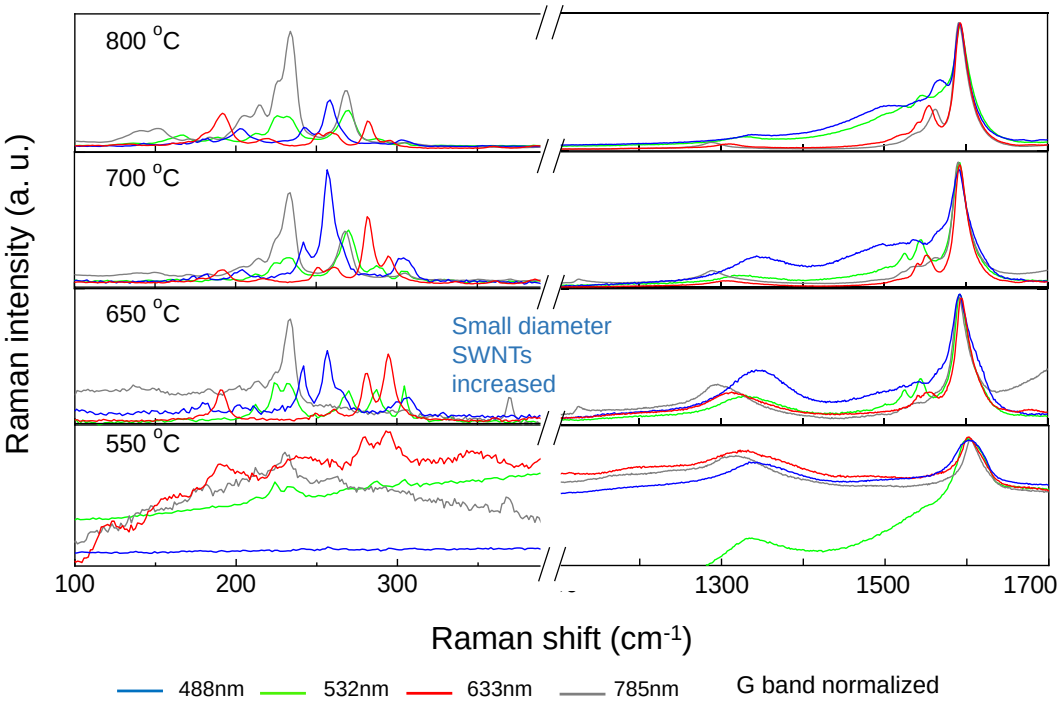

Figure 3-6 Raman spectra of SWNTs growth at different temperature and at 1300 Pa, 4 excitation energies lasers were used in Raman spectroscopy, where shows differences in the RBM region and increased D-band of SWNTs synthesized in different temperature.

effect of temperature and pressure on synthesis of SWNTs are discussed on the observation by Raman spectroscopy, PLE map and absorption.

Figure 3-6 shows Raman spectra in the temperature range from 550 ºC to 800 ºC at 1300 Pa, 4 excitation energies lasers were used, where shown different RBM region. When all G-band are normalized, a clear Raman up-shift can be observed from the peaks in RBM region, such as the peak appeared around 300 cm^{-1} observed by 633 nm laser, it is quite enhanced with temperature decreasing while peaks around 200 cm^{-1} reduced a lot. A very small peak around 370 cm^{-1} observed by 785 nm laser also confirms the appearance of small diameter SWNTs with decreasing temperature; however, at the same time, defects observed by D-band enhance a lot with the decreasing temperature, it is no doubt that the formation of SWNTs were getting worse or more amorphous carbon obtained when temperature decreasing. It can be seen the

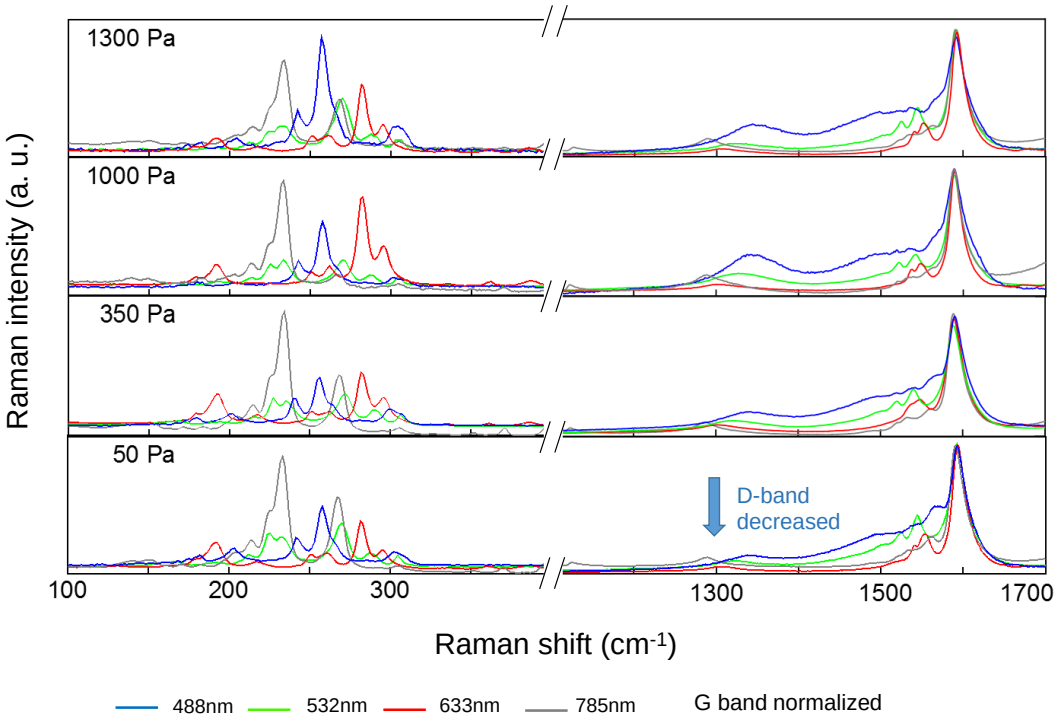

Figure 3-7 Raman spectra of SWNTs growth at different pressure and at 700 ºC, 4 lasers used in Raman scatterings, where shows differences in the RBM region and decreased D-band caused by different pressure.

small diameter SWNTs appears at low temperature but with fulfill defects formation of SWNTs or abundant amorphous carbon, how to overcome this problem became critical to realize small SWNTs growth.

On the other hand, pressure dependence were also checked as shown in figure 3-7, the SWNTs samples were synthesized in the pressure range from 50 Pa to 1300 Pa at 700 ^{o}C. It seems there is no effect from pressure on the diameter of SWNTs, but a clear trend on the D-band reducing is obtained. When pressure decreased, defects or of SWNTs and impurity correspondingly decreased obviously.

From the experiments of temperature and pressure dependence, hints for resolving the impossible growth of SWNTs at low temperature revealed through more exploration of CVD condition. Low pressure can assist with the decreasing of defects in SWNTs structure or decreasing the amorphous carbon. Coupling low pressure and low temperature become reasonable. In figure 3-8, low temperature experiments at 550 ^{o}C were employed with the decreasing pressure. From 1300 Pa to 30 Pa, with the pressure decreasing, a significant change not only in the RBM region but also in G-band and D-band are observed by Raman spectra. Super-small diameter (d_t < 0.8 nm) is observed and the quality of as- grown SWNTs is better and better with the decreasing pressure. The assumption of pair of low temperature and low pressure for high quality of SWNTs is confirmed by the good G/D ratio of Raman spectra.

On the basis of these temperature and pressure dependence results, finally, SWNTs were successfully synthesized at very low temperature 480 ^{o}C only coupling with low pressure, the pressure dependence at this low temperature are shown in figure 3-9. No doubt, D-band was still decreased with decreasing pressure. In the contrast, when pressure low down to 0.1 Pa, diameter distribution of SWNTs became more broad. This is probably because the pressure can be considered as the amount of carbon loading on the catalyst, at extreme low temperature, where both small size catalyst and big size catalyst existed. With proper carbon loading, broad diameter distribution of SWNTs can be obtained. However, when the carbon loading is over for the capacity of catalyst especially big size catalyst, over-loading carbon will collide to amorphous

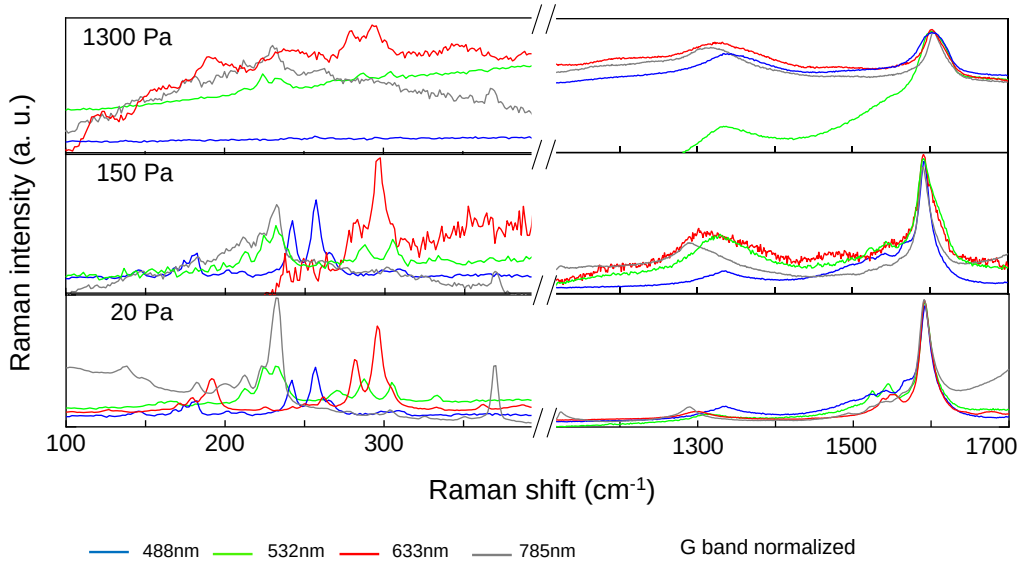

Figure 3-8 Raman spectra of SWNTs growth at different pressure and at 550 ºC, 4 lasers used in Raman scatterings, where shows differences in the RBM region and decreased D-band caused by different pressure.

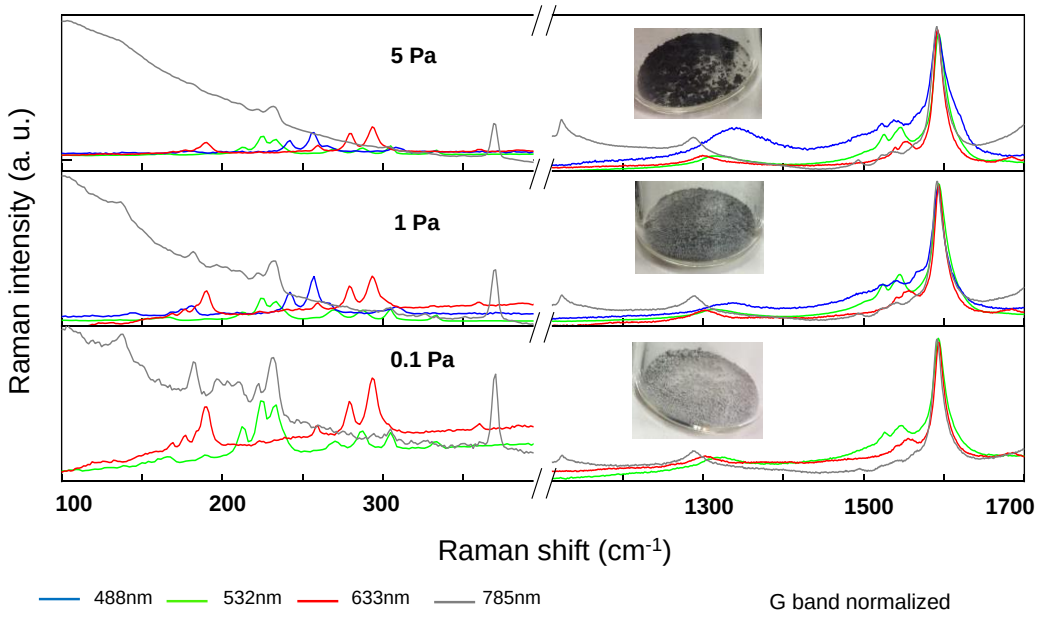

Figure 3-9 Raman spectra of SWNTs growth at different pressure and at 480 ºC, 4 lasers used in Raman scatterings, where shows differences in the RBM region and decreased D-band caused by different pressure. Inset pictures roughly show the appearance of samples.

carbon then encapsulate and poison the catalyst or SWNTs, therefor, diameter distribution of SWNTs become narrow and D-band is increased. The image inset Raman figures presents the exterior of as-gown SWNTs. The color of sample directly indicates the carbon loading of the formation of SWNTs or amorphous carbon.

Regardless how other factors affected on the formation of SWNTs, the most critical parameter for small diameter and diameter distribution is temperature, and proper pressure assists the quality and diameter distribution of SWNTs. Therefore, for the purpose of growth of small diameter SWNTs, temperature range from 500 ^{o}C to 850 ^{o}C at low pressure 5 Pa were checked. All samples obtained in this condition were observed by Raman, absorption and PL.

To confirm the growth of SWNTs, morphology of SWNTs were also observed by SEM and TEM. SEM images of SWNTs sample obtained are shown at figure 3-10 (a) 800 ^{o}C, 1300 Pa and (b) 800 ^{o}C, 5 Pa; TEM images are shown in figure 3-10 (c) and (d) for SWNTs obtained at 500 ^{o}C, 5 Pa.

In figure 3-11, PLE maps reveal the chirality of dispersed as-grown SWNTs. (6,5) became predominant when growth temperature was lower than 550 ^{o}C, where (7,5) was predominant with growth temperature 650 ^{o}C. (6,4) was efficiently enhance when temperature was lower than 550 ^{o}C, which is also observed by absorption results shown in figure 3-14. In the Raman spectra of figure 3-13, RBM region clear reveals that mainly super-small diameter SWNTs (d_t < 1 nm) obtained when temperature low down to 550 ^{o}C, quality of SWNTs are relative good according to the low pressure growth condition. And the signals in the high frequency of Raman shift raised efficiently, means the abundant appearance of super-small diameter SWNTs.

For the new appearance of super-small diameter SWNTs, observation for them were very rarely and it is very important to determine the assignment for these new SWNTs. Our understanding and knowledge expended to a new area with the expended CVD condition and first observed chirality of SWNTs in conventional catalyst ethanol CVD. The critical assignment of super-small diameter SWNTs by Raman, PLE map and absorption corresponding to Kataura plot will discussed and concluded in section 3.4.

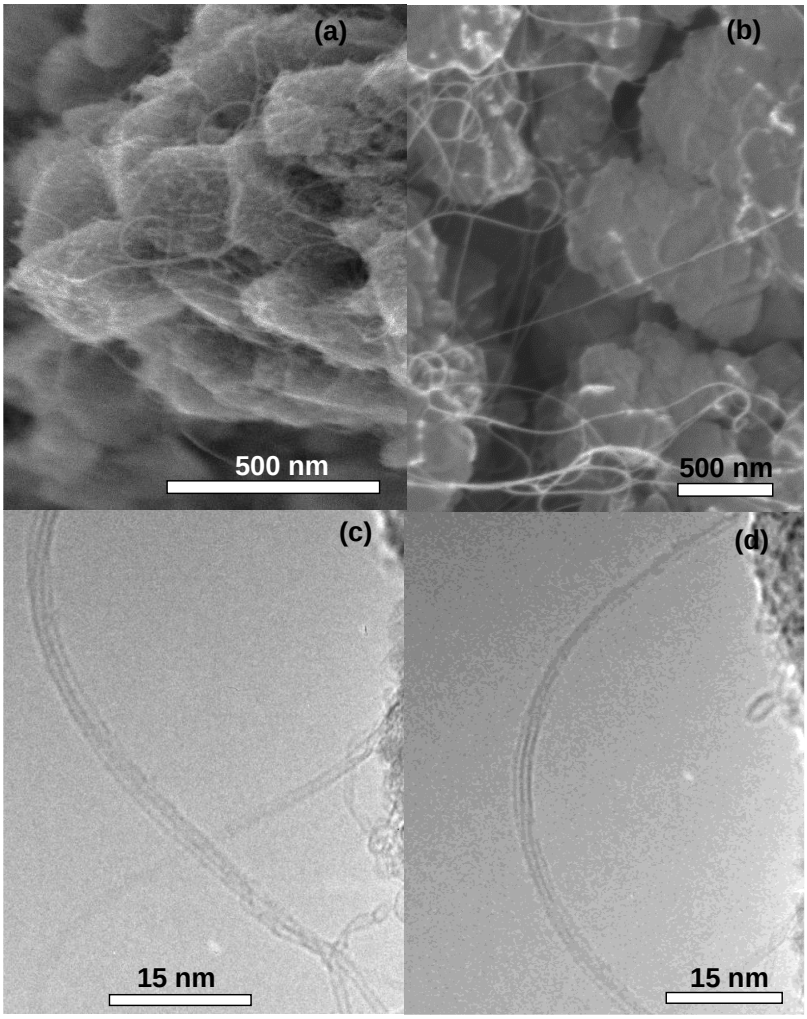

Figure 3-10 SEM images of SWNTs sample growth at (a) 800 ºC, 1300 Pa and (b) 800 ºC, 5 Pa; TEM images (c) and (d) for SWNTs obtained at 500 ºC, 5 Pa.

3.3.3 Broad diameter distribution of SWNTs in high temperature and low pressure CVD

A very interesting phenomenon was revealed from the observation on the SWNTs obtained in the range of temperature 500 ºC ~ 800 ºC at 5 pa by PLE map and Raman spectra. It is believed that small diameter SWNTs are hardly obtained at high

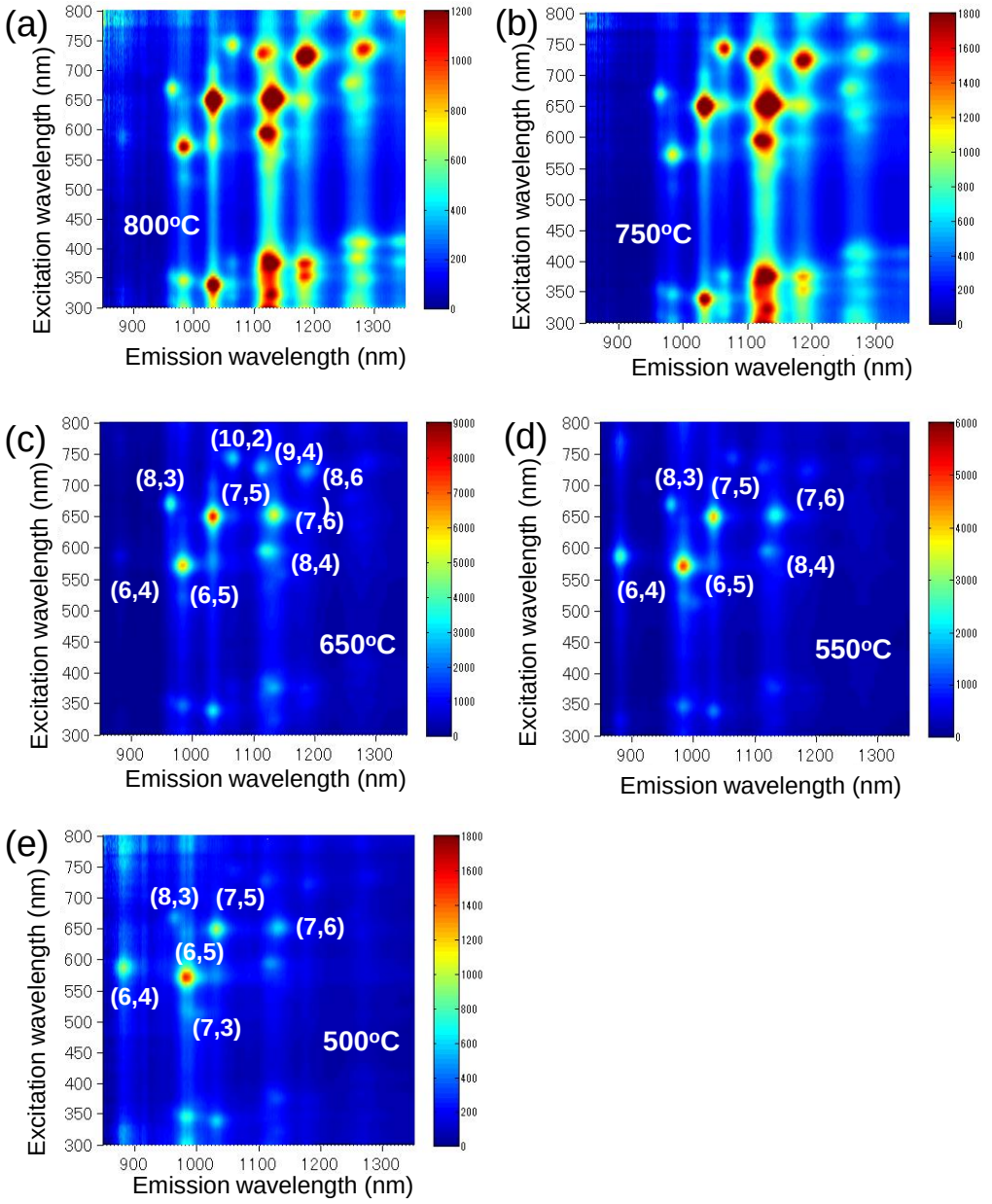

Figure 3-11 PLE maps of dispersed SWNTs growth from 800 ºC to 500 ºC at 5 Pa.

temperature, it indeed observed that small diameter SWNT reduced a lot from 500 ^{o}C to 750 ^{o}C, dominant chirality shift from small diameter SWNTs (6,5) to relative bigger diameter SWNTs (7,6), (8,6) and so on. But when temperature was increased to 800 ^{o}C, PL intensity of small diameter SWNTs (6,5), (6,4) and (8,3) became obviously enhanced again, and weak signals can be detected for even super-small diameter SWNTs such as (7,3). This trend also can be clearly observed in figure 3-12, which presents the normalized PL intensity of (7,5), (6,5), (6,4) and so on. Broad diameter distribution SWNTs similar to HiPCo sample [16] were obtained at this high temperature and low pressure condition.

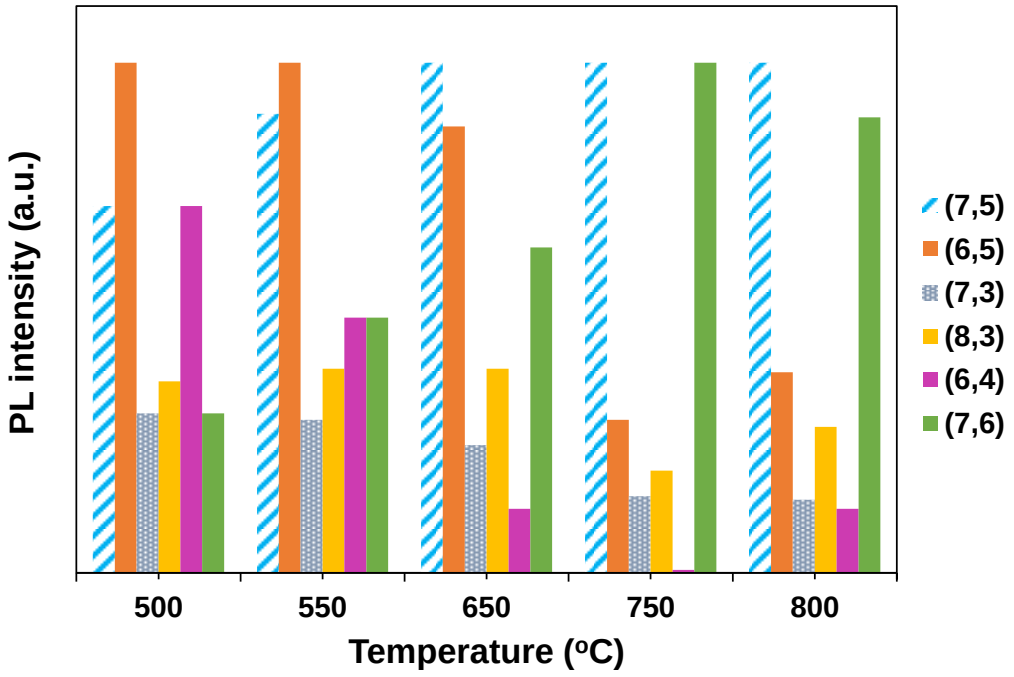

Figure 3-12 PL intensity for specific chirality of dispersed SWNTs growth from 800 ^{o}C to 500 ^{o}C at 5 Pa.

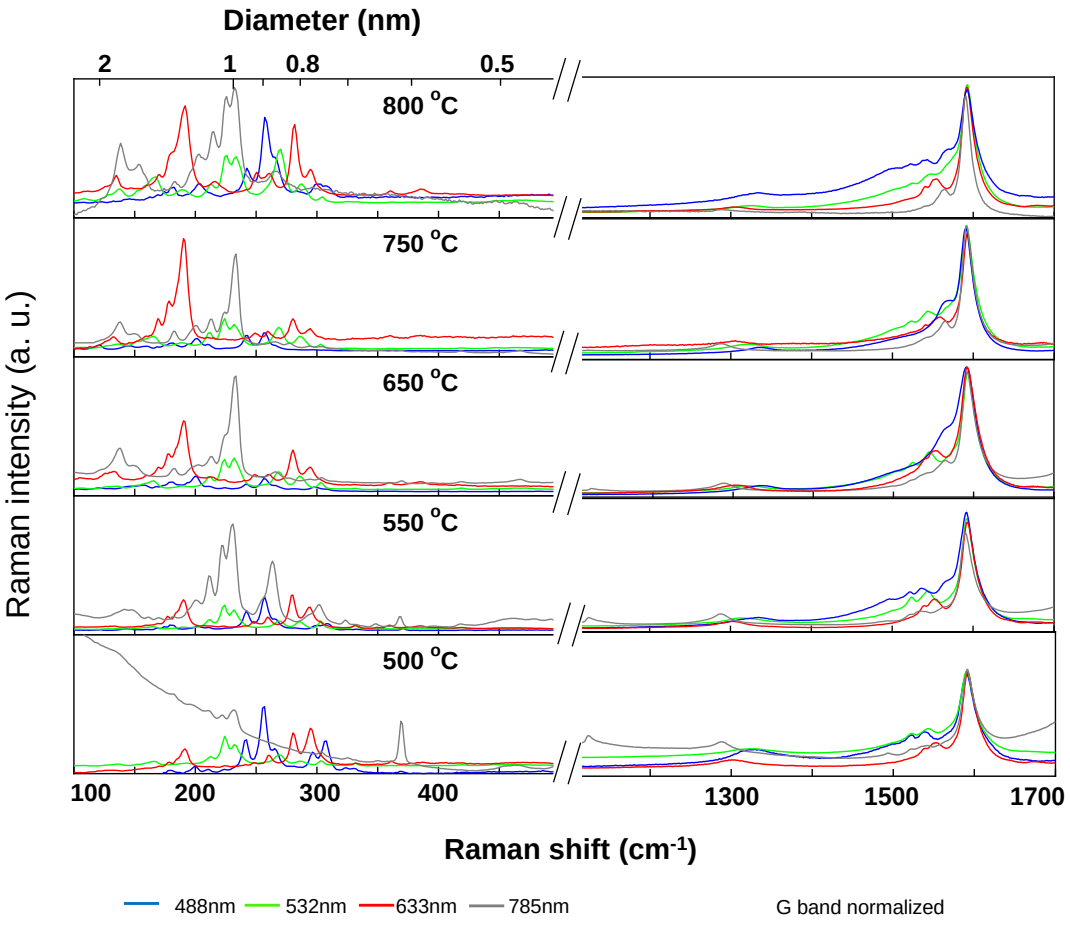

Figure 3-13 Raman spectra of SWNTs growth at different temperature and at 5 Pa, 4 excitation energies lasers used in Raman spectroscopy, which shown differences in the RBM region and D-band caused by different temperature and different chirality of SWNTs.

In addition, Raman spectra also confirmed this trend, abundant features raised in RBM region including both small diameter SWNTs and big diameter SWNTs. And besides semiconducting observed by PLE map of the SWNTs sample obtained at 800 ºC and 5 Pa, metallic SWNTs were also quite synthesized revealed by the broad G^- peak in BWF line shape of Raman spectra by 488 nm laser and 532 nm laser. Absorption

spectra shown in figure 3-14 further confirm the results of Raman and PLE map.

Compare with the SWNTs obtained at 800 ºC and 1300 Pa, more broad diameter distribution SWNTs sample can be obtained at 800 ºC and 5 Pa, this phenomenon indicates that proper carbon loading determined by pressure strongly affect the diameter distribution of SWNTs, over loading carbon maybe poison catalysts, which probably result in narrow diameter distribution.

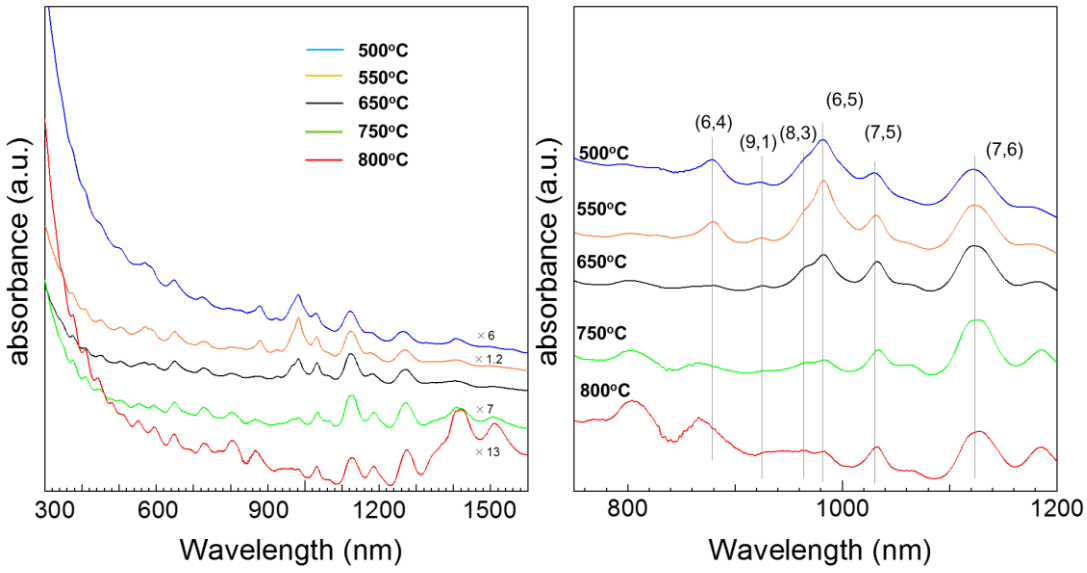

Figure 3-14 Absorption spectra of SWNTs in the range of temperature 500 ºC ~800 ºC at 5 Pa, chirality of SWNTs are shown in E_{11}^{S} region.

3.3.4 Growth boundary of SWNTs

According to figure 3-5, boundary of SWNTs growth can be roughly demonstrated by red dots. There are two boundary areas, one of them is around low temperature and

the other one is around high-temperature and low-pressure area. We believe SWNTs cannot be growth at low temperature because of insufficient activation energy for carbon towards the formation of SWNTs and the deactive catalyst. On the other hand, at high-temperature and low-pressure conditions, it is hypothesized that little amount of carbon is eaten by the catalyst and potential energy is not enough for nucleation of carbon.

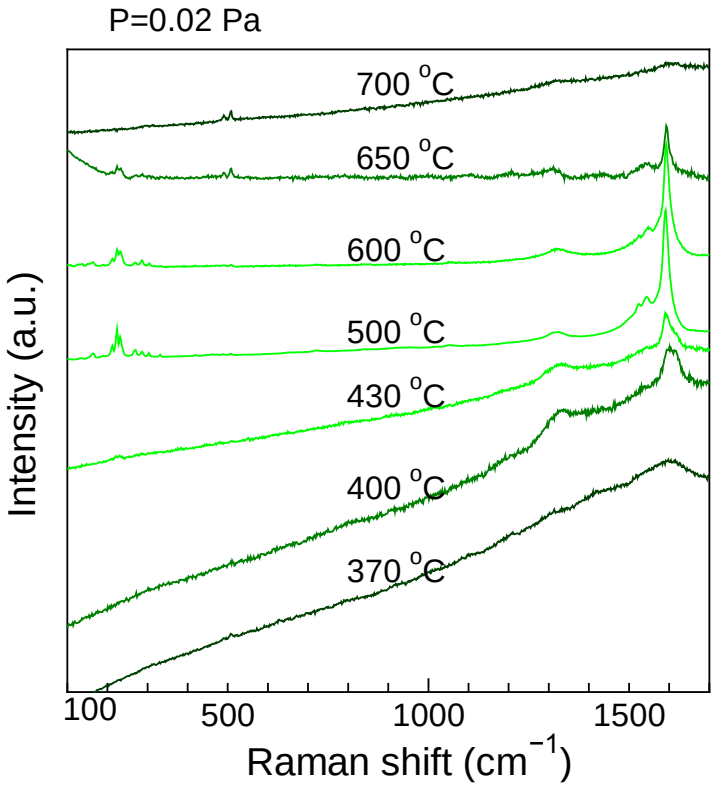

Figure 3-15 Observation of SWNTs by Raman (λ=532 nm) from 370 ºC to 700 ºC at 0.02 Pa.

To track the change of SWNTs growth along the boundary conditions, SWNTs obtained from 370 ºC to 700 ºC at 0.02 Pa were observed by Raman spectroscopy with excitation energy laser 532 nm. As shown in figure 3-15, SWNTs can be synthesized from 400 ºC to 650 ºC at 0.02 Pa, neither 370 ºC nor 700 ºC cannot grow SWNTs, which indicates two growth boundaries of SWNTs at 0.02 Pa.

3.3.5 Effect of carrier gas

Some other parameters also effect the growth of SWNTs in CVD, in this work, carrier gas employed were Ar and Ar/H_2, they usually act the roles of reduction gas in the annealing process or cooling gas taking away heat during cooling process, here discussion was focus on their influence on the usage of carrier gas for carbon feedstock at the low pressure system.

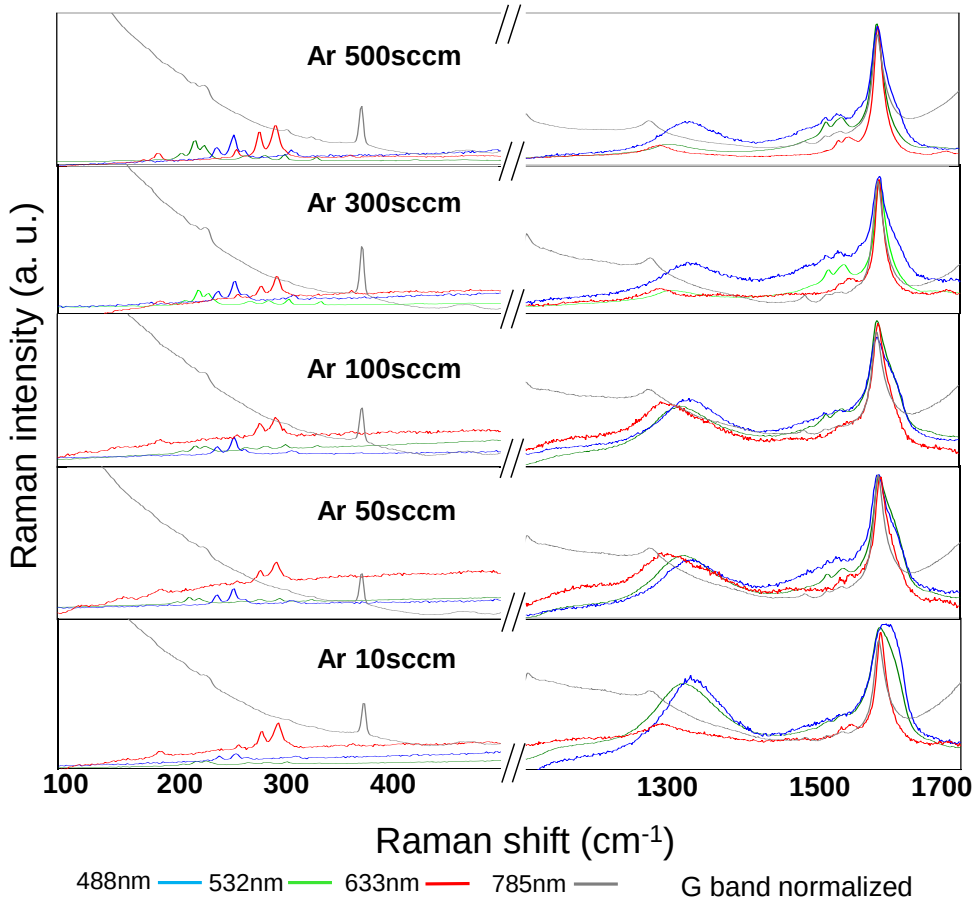

Figure 3-16 Raman spectra of SWNTs growth under different flow rate of Ar carrier gas, 4 excitation energies lasers used in Raman spectroscopy, where show enhanced D-band caused by decreased flow rate of Ar.

In figure 3-16, Raman spectra of sample growth at 480 ^{o}C 5 pa with different flow rate of carrier gas Ar were presented. A clear changing trend of D-band can be obtained by varying flow rate from 10 sccm to 500 sccm. D-band is reduced with the increasing flow rate of Ar, which can be explained as that, the partial pressure of carbon feedstock was decreasing, because the flow rate of carrier gas is increasing while flow rate of carbon feedstock fixed at constant pressure.

At low-temperature CVD condition, carbon loading over or not is critical as discussed in section 3.3.2, this is probably because the partial pressure of carbon feedstock can be considered as the amount of carbon loading on the catalyst, at extreme low temperature 480 ^{o}C, with proper carbon loading, broad diameter distribution of SWNTs can be obtained. However, when the carbon loading is over for the capacity of catalysts, over-load carbon will collide into amorphous carbon then encapsulate catalysts or SWNTs, therefor, diameter distribution of SWNTs becomes narrow and D-band increased. The results from carrier gas demonstrate a good agreement with the discussion of carbon loading discussion, which also confirmed the importance of carbon loading ability for catalyst or reaction active energy, which will be theoretical discussed in the next section.

The effect of Ar/H_2 was also studied by replacing Ar/H_2 with Ar in CVD experiment, results in figure 3-17 shown a significant difference between the condition using Ar and Ar/H_2. In the upper left of figure 3-17, small diameter SWNTs are disappeared obviously when using Ar/H_2 especially at temperature 500 ^{o}C, this is probably because of the etching effect from H_2 on the reaction especially small diameter SWNTs growth. In the bottom right of figure 3-17, Ar/H_2 also affect D-band of as-grown SWNTs, H_2 probably destroyed the carbon order in SWNTs. Ar/H_2 is not suitable as carrier gas for low temperature and pressure growth of small diameter SWNTs in this work.

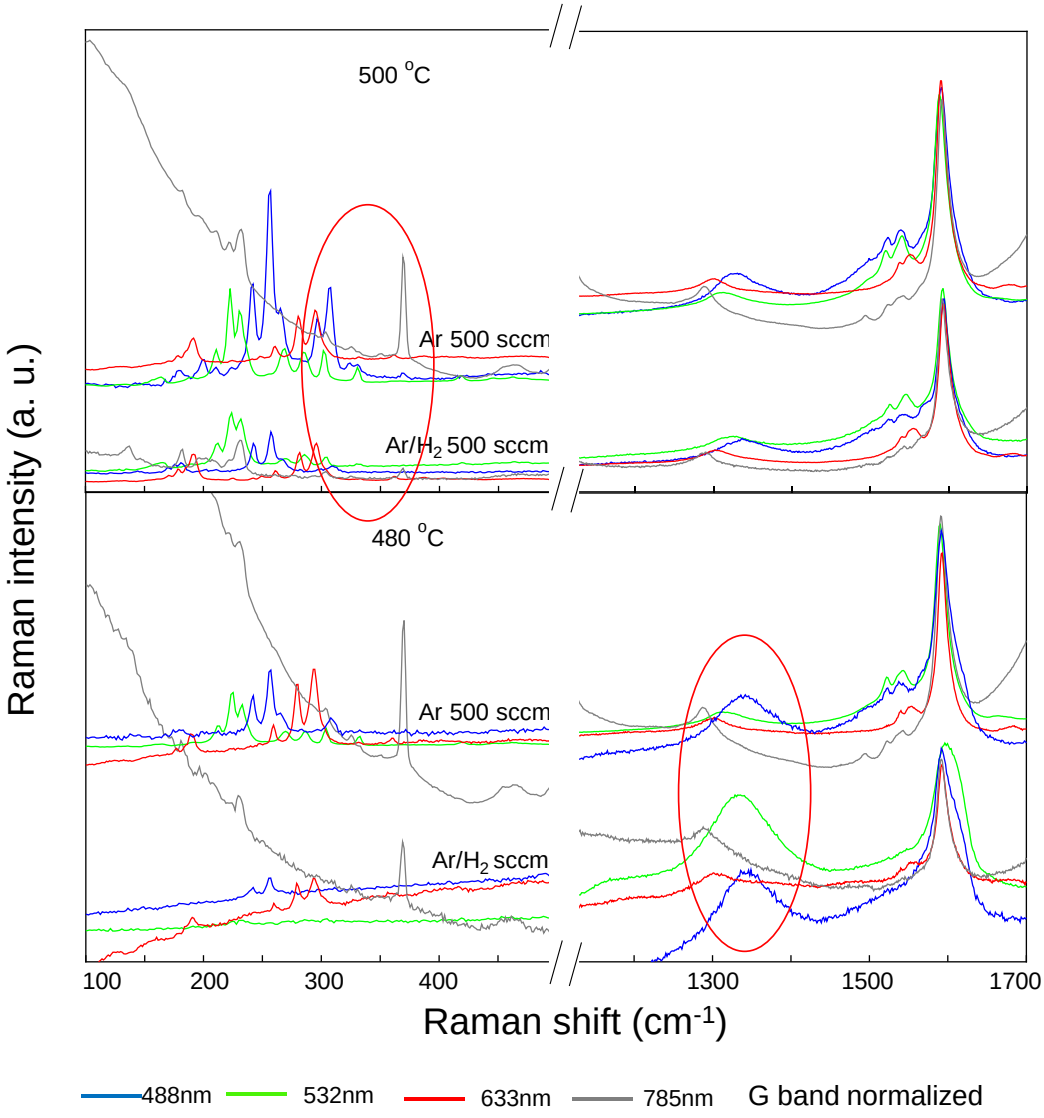

Figure 3-17 Raman spectra of SWNTs synthesized by using different carrier gas, 4 excitation energies lasers used in Raman spectroscopy.

3.4 Assignment of the super-small diameter SWNTs beyond (6,5)

SWNTs obtained in this work were characterized by Raman, absorption and PL spectroscopies. Assignment of the observed SWNTs especially the new ones grown in expansion catalyst ethanol CVD is very important. To realize assignment of a SWNT, the full spatial symmetry of a SWNT is expressed by Kataura plot, the index of its chirality and electron energy band were interpreted by absorption spectra, PLE mapping and Raman spectra.

In general, resonance Raman process shows a strong diameter-dependence when Raman measurement on the bundles or isolated SWNTs SWNTs with a typical diameter [17-20]. And Raman signal is significantly enhanced when energy of laser used in Raman machine matches an energy separation E_{ii} of vHS in the bands between valence and conducting. This behavior for the typical SWNTs with typical diameter (1 nm< d_t) can also be employed to assign the RBM and G-band modes qualitatively in the small diameter SWNTs ($d_t \approx 0.4$ nm) [21, 22], which is helpful to assign the SWNTs obtained in this work smaller than (6,5) (d_t < ~0.8 nm). 5 excitation energies lasers 488 nm, 532 nm, 633 nm, 785 nm and 1064 nm were used in Raman experiments, this wide E_{laser} lines can cover most resonant signals which are presented as spectral features from SWNTs with corresponding diameters.

Raman spectra peaks provide information for assignment of (n,m) of SWNTs, due to the features of observed SWNTs are invoked to identify the diameter. It is realized the (*n, m*) values of SWNTs for assignment. Equation of the diameters of as-grown SWNTs and Raman shift in RBM region was analyzed to set as:

$$\omega_{RBM} = \frac{A}{dt} + B \qquad (3\text{-}1)$$

A lot of reported works [22-27] confirmed *A* and *B* for assignment with good agreement. the parameters used in this work is reported in [14].

On the other hand, when photon energy matches the vHS in DOC that is different

with chirality of SWNTs, absorbed photon will be increased significantly, which result in the rising peaks in the absorption spectrum. The electronic energy separation of the first vHS is called E_{11}, when the photon energy match it, absorbance can happen involving into peaks, which provide the chirality information of observed SWNTs sample. Gap energies for all chiral index between mirror spikes can be indicated in Kataura work [13]. In the optical absorption spectra of SWNTs especially the small diameter SWNTs, three significant absorption features can be obtained, which have relationship to diameters like Raman spectroscopy. The peaks in the first and second lowest wavenumbers corresponding to E_{11} and E_{22} between spikes are from the semiconducting SWNTs with small diameter, and the third one is from the metallic tubes with the almost same diameter showing the overlap with E_{11} and E_{22} of semiconducting SWNTs, where we should pay more attention for accurate identification. Of course there are E_{33} and E_{44} in the observation of absorption, most obviously overlapping can confused the clear identifications, will not be included in this work for small diameter SWNTs observation.

From the diameter of SWNTs calculated by Raman, cooperating with the wavelength form optical absorption with corresponding original Kataura plot, particular assignment of SWNTs is classical presented in figure 3-18, 3-19, respectively.

In the figure 3-2, Raman spectra of SWNTs synthesized at 500 ^{o}C and 5 Pa condition were shown, Raman spectra by 4 lasers present an obvious up-shift compare to the SWNTs synthesized in conventional CVD condition using the catalyst, which means smaller diameter SWNTs can be obtained at low temperature and low pressure condition. G band and D band shows a good quality of SWNTs. So the assignment details for this sample were discussed here as an example.

In figure 3-18, Assignments of obtained SWNTs at low temperature and pressure by Raman spectra coupling with Kataura plot, 5 lasers were used. And Kataura plot was plotted to RBM region at the same time, laser lines were marked in it corresponding to the lasers used in this study. It can be clarified for the SWNTs beyond the (6,5) observed by 532 nm laser, several sharp Raman peaks assigned as (7,3),

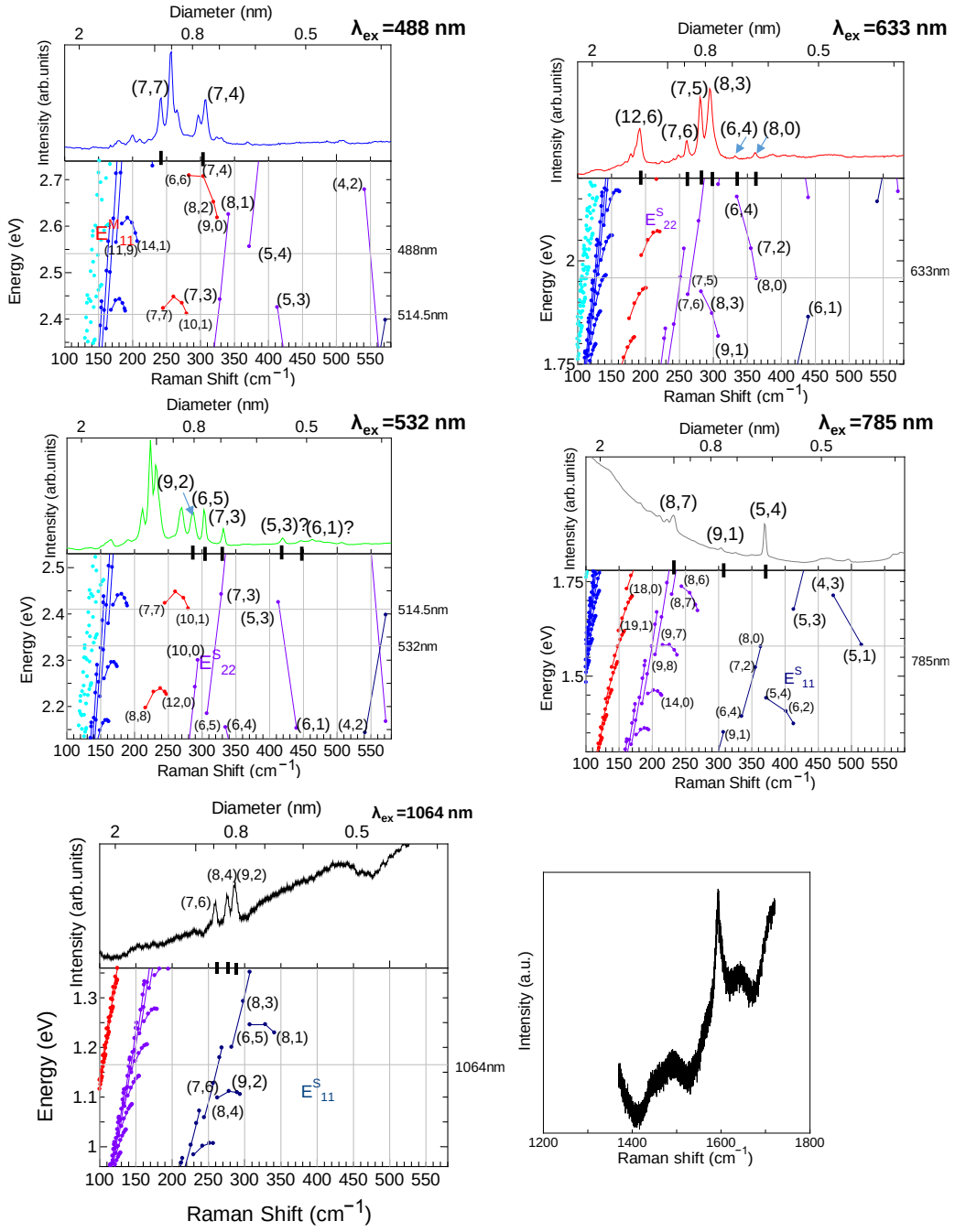

Figure 3-18 Assignments of SWNTs growth at low temperature and pressure by Raman spectra accompanied with Kataura plot, 5 excitation energies lasers were used by Raman.

(5,3) and (6,1) can be significantly observed by 532 nm; To confirm the assignment of super-small diameter SWNTs (5,3) and (6,1), observed frequencies in this work are compared to the reported DFT calculation and experiment observation results [28, 29]. And usually 10-30 cm^{-1} lower than calculated frequency in RBM peaks observation were acceptable, which is suggested by [22]. Based on these discussion, the peaks appeared at high frequency observed by 532 nm laser in this work are demonstrated as (5,3) and (6,1). (6,4) and (8,0) are determined by 633 nm; (9,1) and (5,4) were observed by 785 nm laser, and (7,4) was observed by 488 nm laser, respectively. Rarely used laser 1064 nm were also shown RBM of small diameter SWNTs (d_t < 1 nm) (7,6), (8,4) and (9,2) and clear G-band. Therefore Raman becomes a powerful method to observe the new existence SWNTs in this work.

Semiconducting SWNTs with transition energies E_{11} and E_{22} observed by PL, as shown in figure 3-19. (6,5) became the predominant one in as-grown sample, together with relative high concentration (6,4), (7,5) and so on. It has a good agreement with RBM of Raman to identify the chirality of SWNTs, for example, (7,5), (7,6), (6,4) and (8,3) observed by 633 nm laser and (6,5) (7,3) observed by 532 nm laser in Raman. However, comparing to the significant signals in Raman, which due to the strong resonance signal of (8,0) and (5,4) by 633 nm and 785 nm lasers, respectively, they cannot observed because of the limitation of emission range in PL apparatus, in the optical absorption spectroscopy, (5,4) can be observed.

The ratio of (6,4) to (6,5) can be roughly determined by the intensity of PL, almost 60% was achieved by this work. (6,4) SWNTs were rarely obtained in the past reported work. The ratio of (6,4) to (6,5) is smaller than 10% [28, 30, 31], even in some work that obtained small diameter ~0.6 nm, (6,4) cannot observed at all in the PL map. And in the recent report (6,5) predominant work, this ratio increased to ~20% estimate by PL intensity [32].

It can be seen that unignited signals appeared in the wave number bigger than 350 cm^{-1}, to clarify whether they are from the smaller SWNTs or noise, experiments of as-grown

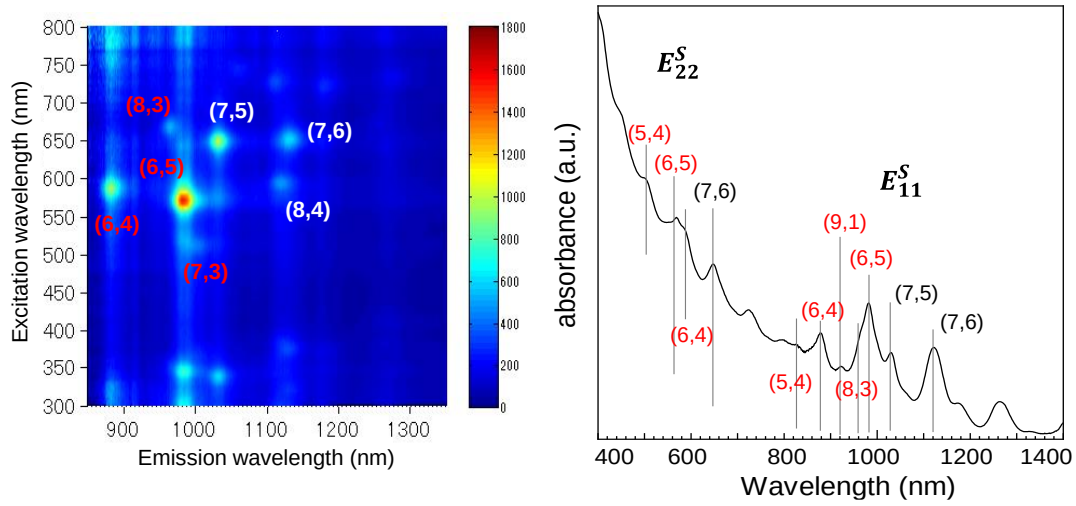

d_t of all marked charities < ~**1** nm

d_t of red marked charities < ~**0.8** nm

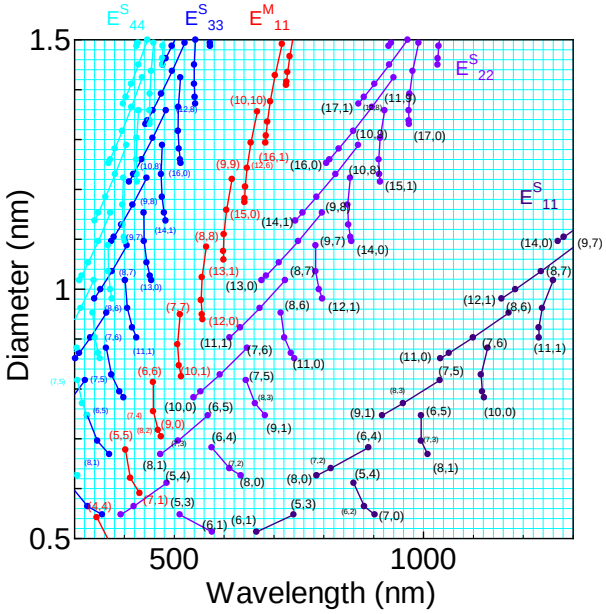

Figure 3-19 Assignments of SWNTs growth at low temperature and pressure by PL and absorption spectra.

SWNTs burned detected by Raman were implied in this chapter. SWNTs sample obtained at low temperature 480 ^{o}C and low pressure ~5 Pa were in situ annealed to atmosphere by opening CVD chamber to air in 10 mins. Figure 3-3 presents the Raman spectra in 4 lasers of as-grown sample after annealing in the air at various temperature. Raman spectra of SWNTs burned at 420 ^{o}C is similar to the original ones, however, big difference was occurred when annealing temperature increased to 500 ^{o}C where small diameter SWNTs < ~1 nm totally disappeared. In the Raman signals by 785 nm, the peaks around 500 cm^{-1} disappeared coupling with the signal (~370 cm^{-1}) of small diameter SWNTs, similar phenomenon obtained in the other works implied that the

	Raman shift (cm^{-1})					PL (nm)		Absorption (nm)		d_t (nm)
	λ_{ex}=1064nm	λ_{ex}=785nm	λ_{ex}=633nm	λ_{ex}=532nm	λ_{ex}=488nm	λ_{22}	λ_{11}	λ_{22}	λ_{11}	
(6,1)				445.47						0.521
(5,3)				419.98						0.556
(5,4)		370.35								0.620
(8,0)			361.85							0.635
(6,4)			331.88			578	878	578	878	0.692
(7,3)				331.40		505	985			0.706
(6,5)				303.69		565	981	565	981	0.757
(9,1)		303.62							920	0.757
(7,4)					304.85					0.765
(8,3)			294.54			660	960		960	0.782
(9,2)	286.76			286.31						0.806
(7,5)			280.31			650	1030		1030	0.829
(8,4)	277.21					592	1115			0.840
(7,6)	259.97		260.85			648	1123		1123	0.895
(7,7)					242.08					0.963
(8,7)		232.11								1.032

Table 3-1 Assignment for SWNTs (d_t < ~1 nm) observed by Raman, PL and absorption spectra.

peaks around 500 cm-1 to 1100 cm-1 are the IFM region which has a strong resonance with the signal (~370 cm^{-1}) of small diameter SWNTs (5,4). When the small diameter SWNTs burned out, the IFM region also will be eliminated correspondingly [33]. On the other hand, in the other 3 lasers, when all SWNTs removed in the air annealing, the peaks left can be clearly clarified they are not from the SWNTs, but probably from the zeolite or metal catalysts.

All assigned SWNTs with super-small diameter (optical band gap up to ~1.5 eV) are shown in Table 3-1. Each SWNT with corresponding Raman, PL or absorption data are shown in this table, for the smallest one observed in this work, which is only 0.52 nm, confirmed by Raman laser 532 nm. The similar observation for (6,1) by reported wok [28] and for (5,3) by one reported observation from separated SWNTs [29] confirm the

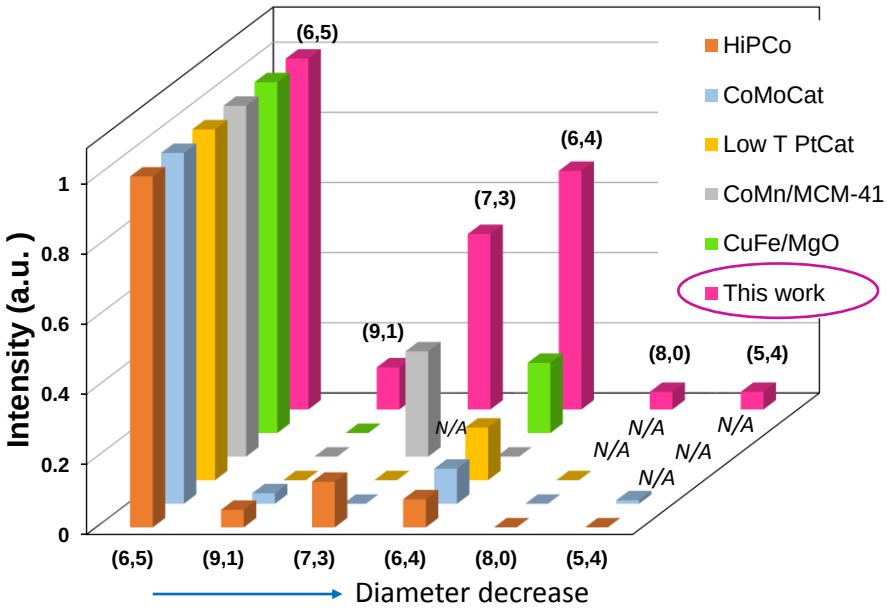

Figure 3-20 Comparison of small diameter SWNTs observed between previous works and this work [16, 30-32, 34].

accuracy of this work.

Efficient enhancement of super-small diameter SWNTs was achieved in this work, mostly, these super-small diameter SWNTs were rarely obtained in direct growth, for example, (6,4) was usually extracted from inner tube of a double-walled carbon nanotubes [35, 36]. Only a few works reported the observation of small diameter which breakthrough (6,5). And very few works can observe these small diameter SWNTs by PL or absorption besides Raman spectroscopy. In figure 3-20, previous reported works for observation smaller diameter SWNTs normalized to (6,5) were compared with this work. As one of the most efficient work to achieve the growth of super-small diameter SWNTs more than (6,5), this work showed excellent efficiency not only for the relative amount but also the chirality distribution of super-small diameter SWNTs.

3.5 Kinetic mode for SWNTs growth in low-temperature and low-pressure CVD: analysis of SWNTs growth map in ACCVD

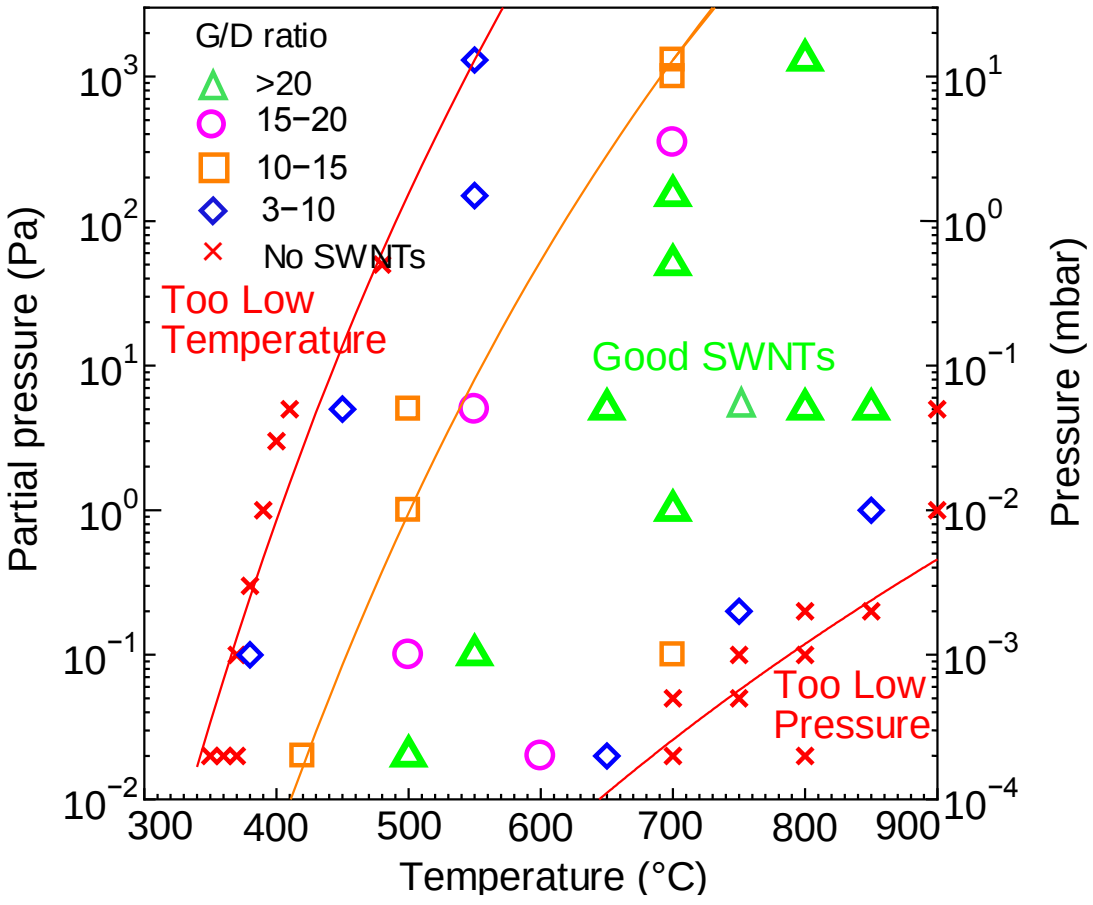

Figure 3-21 Experimental map which include all experimental information (temperature and pressure) done in expansion CVD. Different G/D ratio measured by Raman are marked by different color; orange line was fit by ideal gas equation through estimating activation energy as 2.3 eV.
Please refer details of G/D ratio in appendix I.

3.4.1 Growth mechanism

As the explanation for figure 3-5, more information are concluded in figure 3-21 after finishing parameter studies by experiments. All experimental CVD condition done in this work, one spot is corresponding to one pair of temperature and pressure, green ones mean SWNTs can be synthesized which is determined by Raman observation for the G-band. In the contrast, red ones mean there is no SWNTs growth at this temperature and pressure condition. Temperature range is fixed to 350 ^{o}C to 900 ^{o}C while pressure range is 0.02 Pa to 1300 Pa.

G to D ratio was added this map, different color and shape were added on corresponding experimental condition, and where orange squares mean G to D ratio of SWNTs is about 10-15 with high-quality as an example. Through comparing these value of G to D ratio, some particular discussion can present the influence of temperature and pressure on the quality of SWNTs obtained in the expansion CVD system from high temperature and pressure to low temperature and pressure.

From the temperature influence, G/D is gradually decreased with decreasing temperature, SWNTs were gradually terminate the growth with temperature decreasing, which confirm that the growth of SWNTs cannot be terminated suddenly, it should be gradually stopped with decreasing temperature. On the other hand, low temperature also limit both of the diameter of SWNTs and diameter distribution because of inducing the decreased size of catalyst, which can be described as small catalyst or aggregators formation due to the decreased mobility of catalyst migration at low temperature lead to small diameter SWNTs and diameter distribution [33].

In the case of influence from pressure, when pressure was increased, G/D is became decreasing and diameter distribution of SWNTs became narrow, which is constant with the explanation of carbon loading [5, 37]. With proper carbon loading, broad diameter distribution of SWNTs can be obtained. However, when the carbon loading is over for the capacity of catalyst, over-load carbon will collide into amorphous carbon then encapsulate or poison catalysts, therefor, diameter distribution of SWNTs become narrow and D-band increase.

One area should be paid attention is the part of high-temperature and low-pressure CVD, even high-quality SWNTs can be obtained at high temperature with proper low pressure, however, when the pressure was too low, which means the carbon loading was too low. Carbon will be easily participate into the formation of amorphous carbon quickly at high temperature and then covered the catalysts to stop the nucleation of SWNTs. Or low amount of carbon is just eaten by the catalyst without nucleation of SWNTs. Therefore, it can be observed that no SWNTs can be obtained at too high temperature with too low pressure. No SWNTs can be growth due to zeolite structure destroyed at 900 ^{o}C was also a probably reason.

3.4.2 Kinetic consideration on the growth map

In conclusion, whether carbon loading over or not is critical to judge the growth condition of SWNTs. In this temperature-pressure dependence map, relationship of temperature and pressure can be described as ideal gas equation as:

$$p / p^{*} = \sqrt{\frac{T}{T^{*}}} \exp\left(-\frac{E_a}{k_B}\left(\frac{1}{T} - \frac{1}{T^{*}} \right) \right) \tag{3-2}$$

In CVD condition, growth of SWNTs can be considered proportional to $\exp\left(-\frac{E_a}{k_B T} \right)$, while the growth of morphology of carbon can be considered as collision of carbon which is decided by number of density or velocity proportional to $\frac{p}{T}\sqrt{T} = \frac{p}{\sqrt{T}}$.

One stable growth of SWNTs, should have a constant value that ratio of reaction of SWNTs to collision of carbon for carbon, expressed as:

$$\frac{\text{Reaction Rate}}{\text{Collision Rate}} > C_{critical} \tag{3-3}$$

$$\frac{\sqrt{T}}{p} \exp\left(-\frac{E_a}{k_B T} \right) = const = \frac{\sqrt{T^{*}}}{p^{*}} \exp\left(-\frac{E_a}{k_B T^{*}} \right) \tag{3-4}$$

From this, the proportional relationship of temperature and pressure is clearly described here.

By the way, for the reaction active energy, E_a=2.3 eV was fitted by equation (3-2) covered five magnitude pressure range with orange line in figure 3-17, which was the value of growth active energy for SWNTs by ethanol have good agreement with previous reported calculation for ethanol [38], and this value of activation energy is a little higher than other works [39, 40] because of the reasonable influence from secondary reaction of ethanol during CVD synthesis of SWNTs.

3.6 Summary

Super-small diameter SWNTs are grown by alcohol catalyst chemical vapor deposition (ACCVD) method using USY-zeolite supported catalysts. In conventional ACCVD process, usually high-quality SWNTs were grown around 800 ^{o}C with 1.3 kPa, through studies of the influence of temperature and pressure on the formation of SWNTs in this work, the relationship of temperature and pressure was clarified: SWNTs can grow in lower CVD temperature accompanied with proper lower pressure, which was also confirmed by kinetic study on the formation of SWNTs. The temperature range of growing high-quality SWNTs was extended down to 430 ^{o}C combining with very low partial pressure of ethanol down to 0.02 Pa.

Extended temperature range of CVD open a new CVD work window for efficient growth of super-small diameter SWNTs. During the decreasing CVD temperature, super-small diameter SWNTs (0.8 nm < d_t < 0.52 nm) were obtained around 500 ^{o}C, 5 Pa. Previously, SWNTs with diameters smaller than (6,5) (~0.8 nm) are known to be very inefficient to grow unless inside of special zeolite pore or inside of an outer nanotube, super-small diameter SWNTs were rarely directly grown in reported works. By the low temperature growth with the conventional Fe-Co catalysts, we can extend the small diameter limit; ratio of smaller diameter tubes increased with lower temperature CVD with optimum low pressure. Resonant Raman with 5 excitation laser lines, absorption and Photoluminescence (PL) are used to characterize abundance of

small diameter nanotubes, and chirality of super-small diameter SWNTs were assigned as (6,4), (5,4), (5,3), (6,1) etc..

Reference

[1] P. Zhao, E. Einarsson, R. Xiang, Y. Murakami and S. Maruyama, "Controllable expansion of single-walled carbon nanotube dispersions using density gradient ultracentrifugation," *J. Phys. Chem. C*, 114, 48314834 **(2010)**

[2] P. Zhao, E. Einarsso, G. Lagoudas, J. Shiomi, S. Chiashi, S. Maruyama, "Tunable separation of single-walled carbon nanotubes by dual-surfactant density gradient ultracentrifugation," *Nano Res.*, 4, 623 **(2011)**

[3] M. He, A. I. Chernov, E. D. Obraztsova, H. Jiang, E. I. Kauppinen, and J. Lehtonen,"Synergistic effects in FeCu bimetallic catalyst for low temperature growth of single-walledcarbon nanotubes," *Carbon*, 52, 590 **(2013)**

[4] L. Ding, A. Tselev, J. Wang, D. Yuan, H. Chu, T. P. McNicholas, Y. Li, and J. Liu, "Selective Growth of Well-Aligned Semiconducting Single-Walled Carbon Nanotubes," *Nano Letters*, 9, 800 **(2009)**

[5]N. Fukuoka, Y. Mizutani, S. Naritsuka, T. Maruyama, and S. Iijima, "Low-temperature synthesis of single-walled carbon nanotubes in a high vacuum using Pt catalyst in alcohol gas source method," *Jpn. J. Appl. Phys.* 51, 06FD23 **(2012)**

[6] M. He, A. I. Chernov, E. D. Obraztsova, H. Jiang, E. I. Kauppinen, and J. Lehtonen, "Synergistic effects in FeCu bimetallic catalyst for low temperature growth of single-walled carbon nanotubes," *carbon* 52, 590 **(2013)**

[7] M. He, A. I. Chernov, E. D. Obraztsova, J. Sainio, E. Rikkinen, H. Jiang, Z. Zhu, A.Kaskela, A.G. Nasibulin, E. I. Kauppinen, M. Niemelä, and O. Krause, "Low Temperature Growth of SWNTs on a Nickel Catalyst by Thermal Chemical Vapor Deposition," Nano Res., 4, 334 **(2011)**

[8] S. Maruyama, R. Kojima, Y. Miyauchi, S. Chiashi, and M. Kohno, "Low-temperature synthesis of high-purity single-walled carbon nanotubes from alcohol," *Chem. Phys. Lett.* 360, 229 **(2002)**

[9] Y. Murakami, Y. Miyauchi, S. Chiashi, and S. Maruyama, "Characterization of single-walled carbon nanotubes catalytically synthesized from alcohol," *Chem. Phys. Lett.* 374, 53 **(2003)**

[10] K. Mukhopadhyay, A. Koshio, N. Tanaka, and H. Shinohara, "A simple and novel way to synthesize aligned nanotube bundles at low temperature," *Jpn. J. Appl. Phys.* 37, L1257 **(1998)**

[11] K. Mukhopadhyay, A. Koshio, T. Sugai, N. Tanaka, H. Shinohara, Z. Konya, and J. B. Nagy, "Bulk production of quasi-aligned carbon nanotube bundles by the catalytic chemical vapour deposition (CCVD) method," *Chem. Phys. Lett.* 303, 117 **(1999)**

[12] K. Ogura, M. Kadowaki, J. Okawa, E. Einarsson, and S. Maruyama, "Growth mechanism of vertically aligned SWNTs by in-situ absorption measurements," 33rd Fullerene Nanotube General Symposium **(2007)**

[13] H. Kataura, Y. Kumazawa, Y. Maniwa, I. Umezu, S. Suziki, Y. Ohtsuka and Y. Achiba, "Optical properties of single-wall carbon nanotubes," *Synthesis Metals* 103, 2555 **(1999)**

[14] P. T. Araujo, S. K. Doorn, S. Kilina, S. Tretiak, E. Einarsson, S. Maruyama, H. Chacham, M. A. Pimenta, and A. Jorio, "The third and fourth optical transitions in semiconducting carbon nanotubes," *Phys. Rev. Lett.* **9**8, 067401 **(2007)**

[15] M. J. O'Connell, S. M. Bachilo, C. B. Huffman, V. C. Moore, M. S. Strano, E. H. Haroz, K. L. Rialon, P. J. Boul,W. H. Noon, C. Kittrell, J. P. Ma, R. H. Hauge, R. B. Weisman, and R. E. Smalley, "Band gap fluorescence from individual single-walled carbon nanotubes," *Science* 297, 593 **(2002)**

[16] S. M. Bachilo, M. S. Strano, C. Kittrell, R. H. Hauge, R. E. Smalley, R. B.e Weisman,"Structure-assigned optical spectra of single-walled carbon nanotubes," *Science* 298, 2361(**2002**)

[17] M. S. Dresselhaus and P. C. Eklund, "Phonons in carbon nanotubes," *Adv. Phys.* 49, 705 **(2000)**

[18] A. Jorio, R. Saito, J. H. Hafner, C. M. Lieber, M. Hunter, T. McClure, G. Dresselhaus, and M. S. Dresselhaus, "Structural (n,m) determination of isolated Single-Wall Carbon Nanotubes by resonant raman scattering," *Phys. Rev. Lett.* 86, 1118 **(2011)**

[19] A. Jorio, A. G. Souza Filho, G. Dresselhaus, M. S. Dresselhaus, R. Saito, J. H. Hafner, C. M. Lieber, F. M. Matinaga, M. S. S. Dantas, and M. A. Pimenta, "Joint density of electronic states for one isolated single-wall carbon nanotube studied by resonant Raman scattering," *Phys. Rev. B* 63, 245416 **(2001)**

[20] A. G. Souza Filho, A. Jorio, J. H. Hafner, C. M. Lieber, R. Saito, M. A. Pimenta, G. Dresselhaus, and M. S. Dresselhaus, "Electronic transition energy Eii for an isolated (*n*,*m*) single-wall carbon nanotube obtained by anti-Stokes/Stokes resonant Raman intensity ratio," *Phys. Rev. B* 63, 241404R **(2001)**

[21] Z. M. Li, Z. K. Tang, G. G. Siu and I. Bozovic "Raman characterization of 0.4 nm single-wall carbon nanotubes using the full-symmetry line group," *Appl. Phys. Lett.* 84, 4101 **(2004)**

[22] A. Jorio, A.G. Souza Filho, G. Dresselhaus, M.S. Dresselhaus, A. Righi, F.M. Matinaga, M.S.S. Dantas, M.A. Pimenta, J. Mendes Filho, Z.M. Li, Z.K. Tang, and R. Saito, "Raman studies on 0.4 nm diameter single wall carbon nanotubes," *Chem. Phys. Lett.* 351, 27 **(2002)**

[23] J.-L. Sauvajol, E. Anglaret, S. Rols, and L. Alvarez, "Phonons in single wall carbon nanotube bundles," *Carbon* 40, 1697 **(2002)**

[24] G. Sauve, P. V. Kamat, and R. S. Ruoff, "Excited triplet and reduced forms of C84," *J. Phys. Chem.* 99, 2162 **(1995)**

[25] Z. Yu and L. Brus, "(n, m) Structural assignments and chirality dependence in single-wall carbon nanotube Raman scattering," *J. Phys. Chem. B* 105, 6831 **(2001)**

[26] U. D. Venkateswaran, A. M. Rao, E. Richter, M. Menon, A. Rinzler, R. E. Smalley, and P. C. Eklund, "Probing the single-wall carbon nanotube bundle: Raman scattering under high pressure," *Phys. Rev. B* 59, 10928 **(1999)**

[27] L. Alvarez, A. Righi, T. Guillard, S. Rols, E. Anglaret, D. Laplaze, and J.-L. Sauvajol, "Resonant Raman study of the structure and electronic properties of single-wall carbon nanotubes," *Chem. Phys. Lett.* 316, 186 **(2000)**

[28] L. Kavan, O. Frank, A. a Green, M. C. Hersam, J. Koltai, V. Zólyomi, J. Kürti, and L. Dunsch, "In situ raman spectroelectrochemistry of single-walled carbon nanotubes: Investigation of materials enriched with (6,5) tubes," *J. Phys. Chem. C* 112, 14179 **(2008)**

[29] S. Cambre, B. Schoeters, S. Luyckx, E. Goovaerts, and W. Wenseleers, "Experimental observation of single-file water filling of thin single-wall carbon nanotubes down to chiral index (5,3)," *Physical Review Letters*, 104, 207401 **(2010)**

[30] T. Maruyama, Y. Mizutani, S. Naritsuka and S. Iijima "Single-walled carbon nanotube growth in high vacuum using Pt catalyst in alcohol gas source method," *Materials Express* 1, 267 (**2011**)

[31] C. Z. Loebick, S. Derrouiche, N. Marinkovic, C. Wang, F. Hennrich, M. M. Kappes, G. L. Haller and L. D. Pfefferle, "Effect of Manganese Addition to the Co-MCM-41 Catalyst in the Selective Synthesis of Single Wall Carbon Nanotubes," *J. Phys. Chem. C* 113, 21611 (**2009**)

[32] He, M. A. I. Chernov, P. V. Fedotov, E. D. Obraztsova, J. Sainio, E. Rikkinen, H. Jiang, Z. Zhu, Y. Tian, E. I. Kauppinen, M. Niemela and A. O. I. Krause. "Predominant (6, 5) single-walled carbon nanotube growth on a copper-promoted iron catalyst," *J. Am. Chem. Soc.* 132, 13994 **(2010)**

[33] N. Li, X. Wang, F. Ren, G. L. Haller, and L. D. Pfefferle, "Diameter tuning of single-walled carbon nanotubes with reaction temperature using a Co monometallic catalyst," *J. Phys. Chem. C* 23, 113 **(2009)**

[34] S. M. Bachilo, L. Balzano, J. e E. Herrera, F. Pompeo, D. E. Resasco, and R. B. Weisman, "Narrow (*n*,*m*)-Distribution of single-walled carbon nanotubes grown using a solid supported catalyst," *J Am Chem Soc* 125,11186 (**2003**)

[35] Y. Miyata, M. Suzuki, M. Fujihara, Y. Asada, R. Kitaura, and H. Shinohara, "Solution-phase extraction of ultrathin inner shells from double-wall carbon nanotubes," *ACS Nano* 4, 5807 **(2010)**

[36] H. Shiozawa,C. Kramberger, R. Pfeiffer, H. Kuzmany, T. Pichler, Z. Liu, K. Suenaga, H. Kataura, and S.R.P. Silva, "Catalyst and chirality dependent growth of carbon nanotubes determined through nano-test tube chemistry," *Advanced Materials* 22,3685 (**2010**)

[37] B. Wang, C. H. P. Poa, L. Wei, L. J. Li, Y. Yang, and Y. Chen, "(*n*,*m*) Selectivity of single-walled carbon nanotubes by different carbon precursors on Co−Mo Catalysts," *J. Am. Chem. Soc.*, *129* (29), 9014 **(2007)**

[38] P. Vinten, J. Lefebvre, and P. Finni, "Kinetic critical temperature and optimized

chemical vapor deposition growth of carbon nanotubes," *Chem. Phys. Lett.* 469, 293 **(2009)**

[39] C.T. Wirth, C. Zhang, G. Zhong, S. Hofmann, and J. Robertson, "Diffusion and reaction limited growth of carbon nanotube forests", *ACS nano*, 3 3560 **(2009)**

[40] E. Einarsson, Y. Murakami, M. Kadowaki, and S. Maruyama, "Growth dynamics of vertically aligned single-walled carbon nanotubes from *in situ* measurements," *Carbon*, 46, 293 **(2008)**

Chapter 4

Influence of feedstock compounds (DME and acetonitrile) and zeolite support catalysts (Cu-Co and W-Co) on the CVD synthesis of SWNTs

4.1 Background and motivation

The influence of carbon source compounds and catalysts on the quantity and quality of SWNTs were studied and will be discussed in this chapter. During CVD synthesis of SWNTs, several processes limit growth rate and formation of SWNTs. In the gas phase, carbon feedstock go through thermal decomposition before reaching catalysts, decomposed carbon feedstock absorb and dissociate on the surface of catalyst, then carbon atoms diffuse bulk or surface, finally carbon atoms participate into the growth of SWNTs. Different carbon feedstock and catalysts present different performance during all these processes. Therefore, studies on the effect of carbon feedstock and catalysts are very important, especially for low temperature and pressure CVD synthesis of small diameter SWNTs.

DME was preferred not only because its potential for cleaner SWNTs [1] but also it is meaningful to compare its performance on the diameter of SWNTs in low temperature and pressure CVD to ethanol. Acetonitrile, [2-5] were also widely used in CVD to reduce diameter of SWNTs by nitrogen doping in SWNTs structure, rarely work report the low temperature CVD by using these carbon feedstock, therefore, CVD growth of small diameter SWNTs at 500 ^{o}C by acetonitrile was studied in this work.

On the other hand, some promising work published very recently present the advantage of Cu [6-8] and W [9] in the selective growth of SWNTs such as (6,5) and (12,6). Using these catalysts in the low temperature CVD system or zeolite support morphology is promising and meaningful trails toward better exploration not only for reducing diameter of SWNTs but also for controllable growth.

4.2 Catalysts preparation, CVD conditions and characterization

Metal catalysts W, Cu and Co used in this work for CVD growth of SWNTs were supported by USY-zeolite powder [HSZ-390HUA from Tosoh], which support low temperature growth in previous reported works [10-13].

Preparation process was the same as that described in section 3.2.1, the difference is only the original chemical. W and Cu are tungsten hexachroride (WCl_6) and copper acetate [$(CH_3CO_2)_2Co\text{-}6H_2O$] into USY-zeolite powder, respectively. 2.5 wt % weight concentrations of both Cu and Co of copper acetate and cobalt acetate were used in this work. But in the case of miscible of WCl_6 and cobalt acetate, weight concentration of W had a strong influence on the final formation of SWNT, therefore, many different concentration of W were employed from 0.5 wt% to 5 wt%, while Co is constant at 2.5 wt%.

CVD process is almost the same as section 3.2.1, the equipment can be checked in figure 3-1. DME from a reservoir with carrier gas Ar (500 sccm) were then introduced at a constant pressure. In the case of acetonitrile, vaporized acetonitrile from liquid acetonitrile carried by carrier gas Ar was introduced into CVD chamber by mass flow controller. The growth temperature was varied between 480 ºC and 800ºC, and the growth partial pressure was between 0.02 and 1300 Pa.

As-grown SWNTs were characterized by Raman spectroscopy and optical absorption. The results of Raman spectra were measured by Renishaw inVia Raman Microscope using 4 lasers of 488 nm, 532 nm, 633 nm, 785 nm. UV-vis-NIR absorption and PLE mapping were also used to character dispersed SWNTs sample, details stated in chapter 3 will not be described here.

4.3 Influence of feedstock compounds on the growth of SWNTs

Acetonitrile and DME were used as feedstock in the same low temperature and low pressure CVD condition using Fe-Co catalyst, even DME is the constitute isotope chemical of ethanol, they have the same atom substation, still induced different SWNTs, which is probably due to the different feedstock will absorb and dissociate differently on catalyst surface.

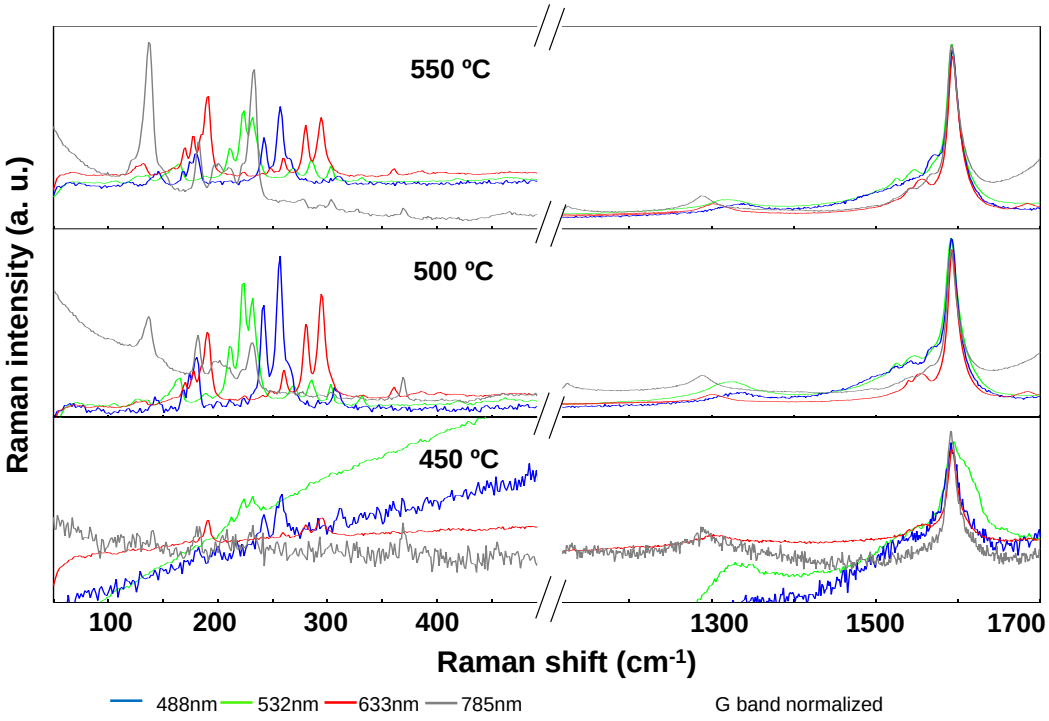

Figure 4-1 Raman spectra of SWNTs synthesized by DME at different temperature and at 5 Pa, 4 lasers used in Raman spectroscopy, where shows differences in the Raman spectra caused by different temperature.

4.3.1 Low-temperature low-pressure CVD using DME

DME replacing ethanol in low temperature and low pressure CVD growth of SWNTs was implement, as-grown SWNTs were observed by Raman spectroscopy. Temperature and pressure dependence on the formation of SWNTs were obtained by Raman spectra presented in figure 4-1 and 4-2.

In the low temperature range from 450 ^{o}C to 550 ^{o}C, reducing of diameter by decreased temperature was not obviously in the case of DME CVD, while there was significant diameter reducing in ethanol CVD. Raman spectra were obtained from SWNTs synthesized by DME in the range of temperature at 5 Pa, 4 lasers used in Raman spectroscopy, where shows differences in the RBM region and different G-band caused by different temperature. However, the differences did not obtained sufficient diameter tuning caused by temperature (450 ^{o}C to 550 ^{o}C) as shown in the case of ethanol. In RBM region, appearance of small diameter SWNTs raise the peaks at relative high Raman frequency, at the same time, existence of big diameter SWNTs still raise the peaks at low Raman frequency even temperature decreased. It seems that relative more broaden diameter distribution SWNTs were obtained by DME at low temperature (around 500 ^{o}C) condition.

From the decomposition studies in chapter 2, there is almost no gas phase decomposition in this low temperature experiment condition. Therefore, the difference of DME and ethanol on the formation of SWNTs in low temperature CVD is probably due to the different absorb on catalyst and catalyst surface dissociation, which is caused by different molecular structure of ethanol and DME themselves. On the other hand, when ethanol and DME undergo thoroughly gas-phase decomposition at high temperature, where mainly decomposition products participate SWNTs growth, SWNTs obtained at this condition seem very similar as shown in chapter 2. This is due to the common decomposition products between ethanol and DME.

In figure 4-2, Raman spectra of SWNTs synthesized by DME in the range of pressure at 450 ^{o}C, 4 lasers used in Raman scatterings, where shows diameter distribution of

sample at 0.2 Pa was increased compare to that at 1 Pa in the RBM region, but G-band became worse a lot when pressure is 0.02 Pa, almost no SWNTs can be obtained at 0.02 Pa. The changing in the RBM region is hard to identify the trend, it is probably 450 ^{o}C is an extreme low temperature for DME, only narrow work window of pressure can be fitted in this experimental condition. So only 0.2 Pa is relative best for SWNTs growth at 450 ^{o}C. And comparing to 0.2 Pa, carbon loading was over at 1 Pa, thus catalysts probably were poisoned by over carbon, which aroused the narrower diameter distribution.

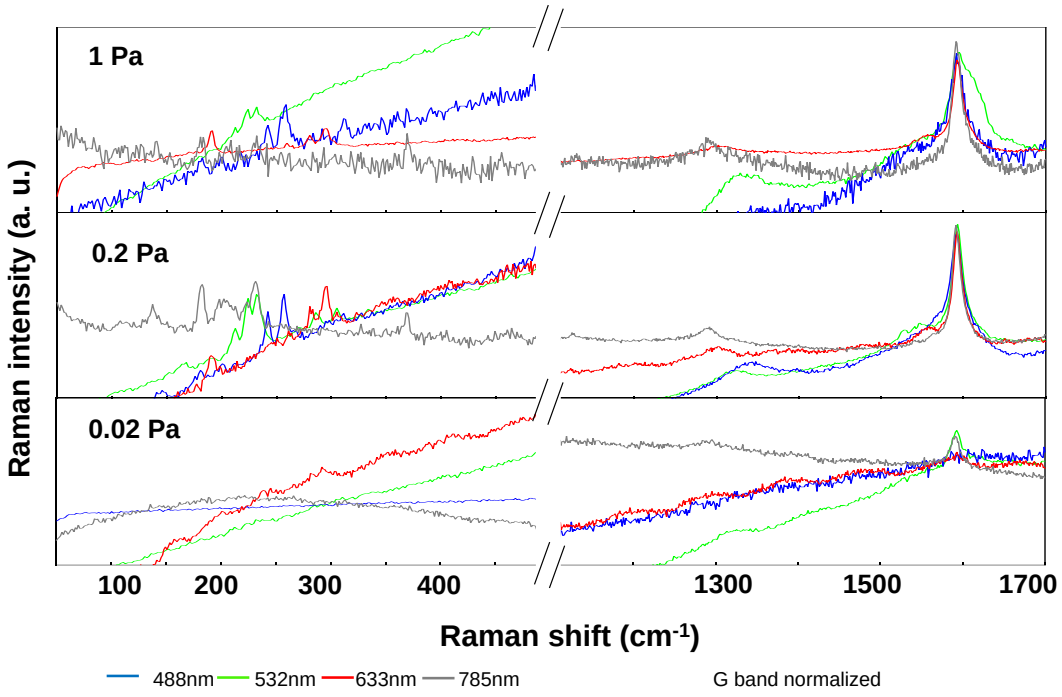

Figure 4-2 Raman spectra of SWNTs synthesized by DME from 0.02 Pa to 1 Pa at 450 ^{o}C, 4 lasers used in Raman spectroscopy, which reveals diameter distribution of sample at 0.2 Pa was increased compare to that at 1 pa, and SWNTs were hardly obtained when pressure is 0.02 Pa.

4.3.2 Low-temperature low-pressure CVD using acetonitrile

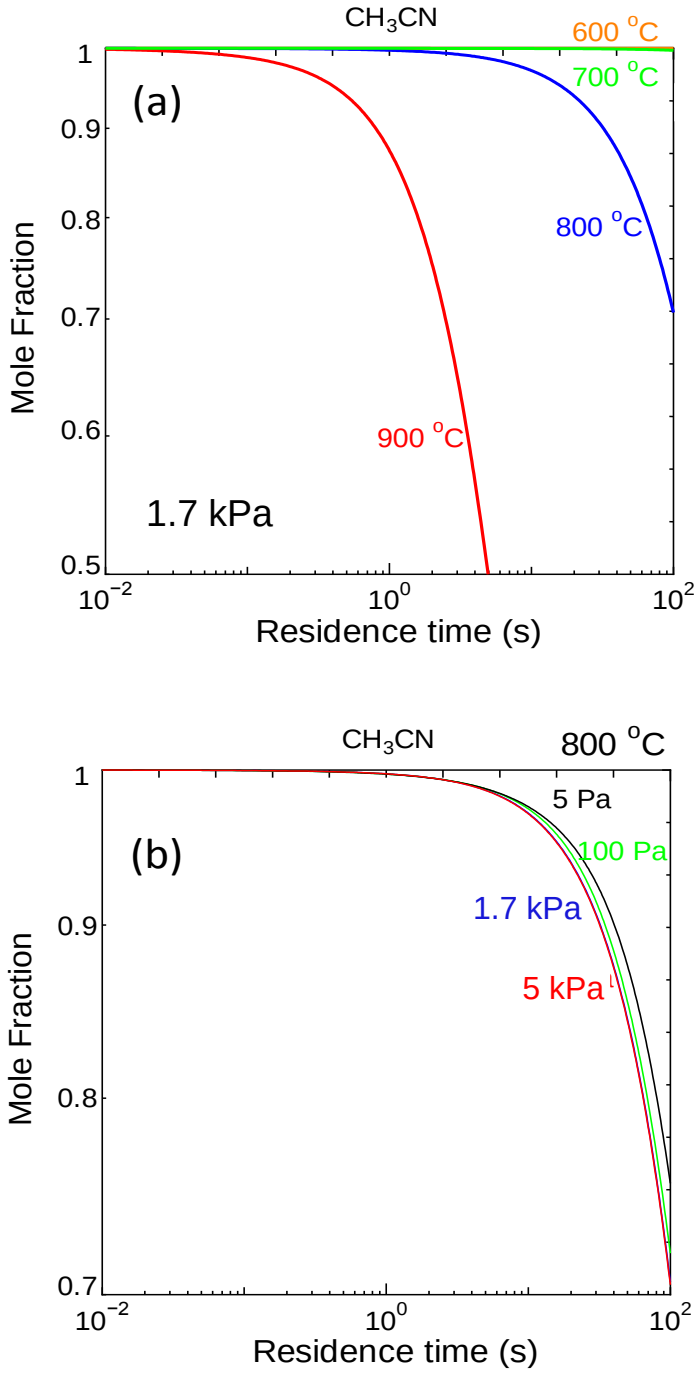

Figure 4-3 Temperature (a) and pressure (b) dependence of mole fraction of acetonitrile as the function of integration residence time.

Temperature and pressure dependence of acetonitrile decomposition were simulated by CHEMKIN, results are shown in figure 4-3. From the results, acetonitrile is hardly decomposed in gas phase even at high temperature and high pressure condition comparing to that of ethanol or DME. In most case, mainly acetonitrile contribute into the growth of SWNTs directly not decomposed products, but even there is no thermal decomposition, there may be difference on catalyst surface absorb and dissociation of acetonitrile, this can be clarified by the difference of formation of SWNTs at the same CVD condition with ethanol and DME. Of course, the effect from nitrogen doping also cannot be ignored at the same time.

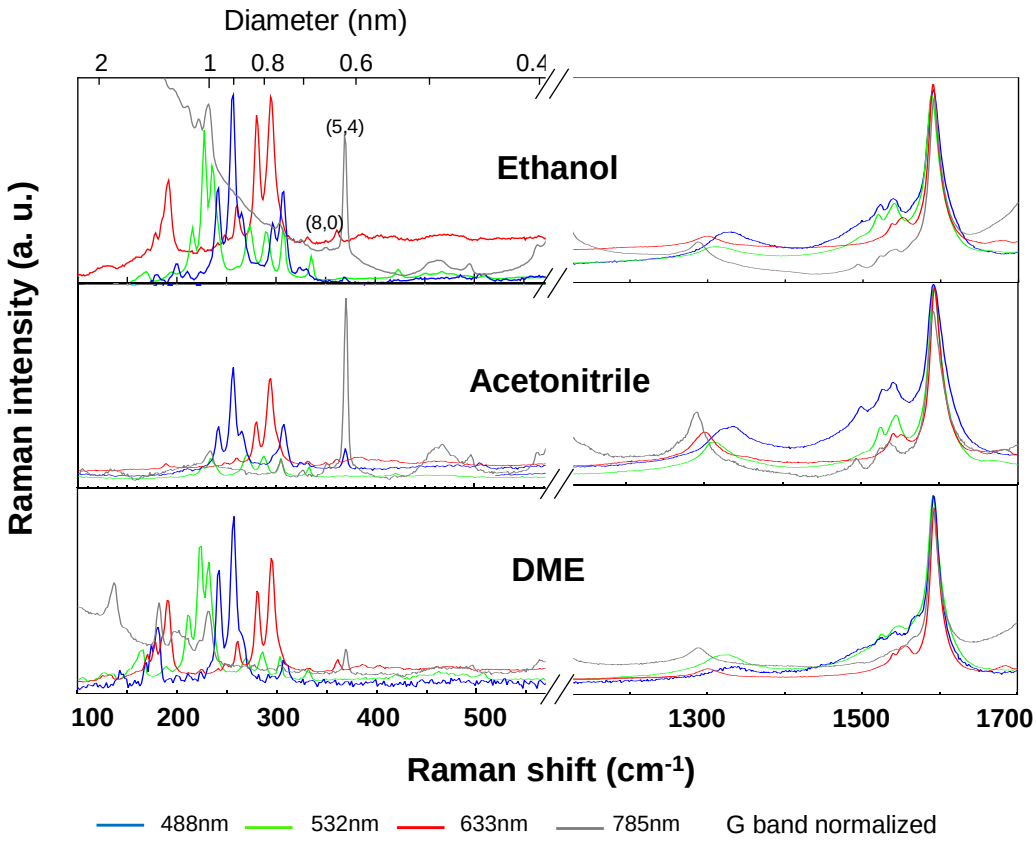

Figure 4-4 Raman spectra of SWNTs synthesized from ethanol, acetonitrile and DME at 500 ºC, 5 Pa.

4.3.3 Influence of feedstock compounds: comparison among ethanol, DME and acetonitrile

Raman spectra of SWNTs grown by using ethanol, acetonitrile and DME in 500 ^{o}C and 5 Pa CVD are shown in figure 4-4. In the RBM region, without doubt, acetonitrile significantly enhanced the growth of small diameter SWNTs, and diameter SWNTs (d_t > 1 nm) totally disappeared. Acetonitrile present an excellent ability to only grow small diameter SWNTs as expecting. However, compare to ethanol, its relative big defects cannot be ignored, in some case, these effect will limit its application.

In contrast, DME preferred growing bigger diameter SWNTs at the same time with small diameter SWNTs growth, broad diameter distribution of SWNTs can be observed in its sample by Raman even at low temperature, which is the condition ethanol and acetonitrile mainly grown super small diameter SWNTs without the existence of big diameter SWNTs. This can be identified as the feature of DME.

However, when we discuss the effect from different carbon feedstock, it should be noticed that the difference obtained in this section was from the same CVD condition (temperature and pressure) using ethanol, DME and acetonitrile. Especially at this CVD condition, these three carbon feedstock are all hardly decomposed in gas phase, details of thermal decomposition of ethanol, DME and acetonitrile at low temperature and low pressure can be found in appendix IV. Different molecular structure in carbon feeding components result in different efficiency reaction with catalyst, thus difference or very small difference on the growth of SWNTs can be obtained. But, when a proper CVD condition is implemented for these carbon feedstock individually, almost the similar SWNTs can be growth by different carbon feedstock, which was clarified that similar SWNTs can be obtained by both ethanol and DME at different CVD condition (resulted in similar decomposition products) in chapter 2 and reported work [14].

4.4 Comparison of various zeolite-supported catalysts

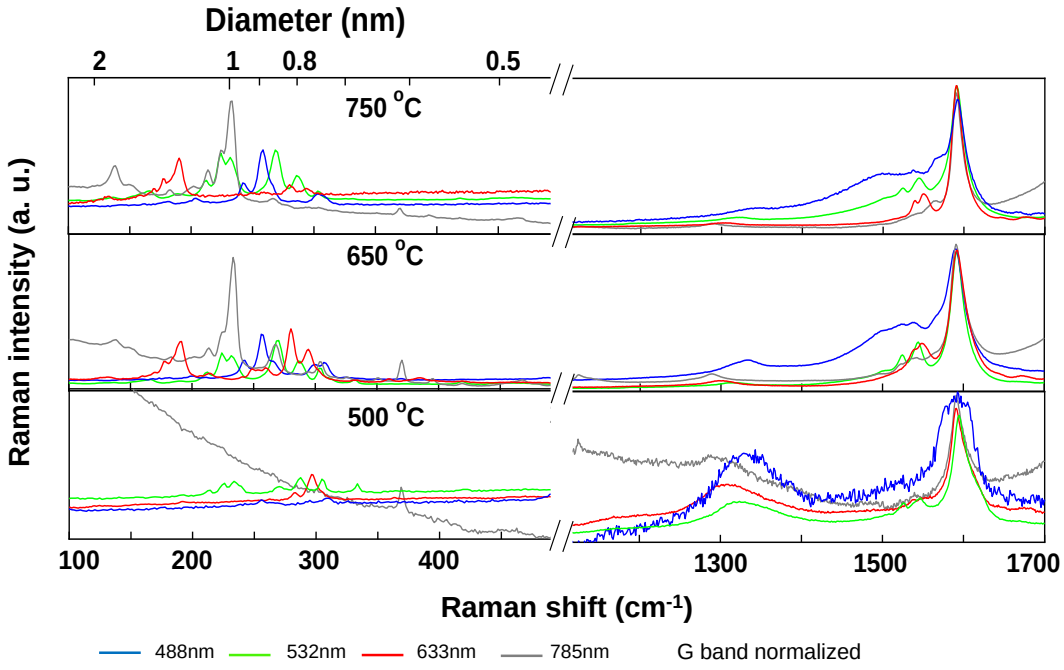

Figure 4-5 Raman spectra of SWNTs synthesized by Cu-Co zeolite at different temperature and at 5 Pa, 4 lasers used in Raman spectroscopy, where shows differences of the RBM region and different G-band in SWNTs obtained at different temperature.

4.4.1 Growth of super-small diameter SWNTs by Cu-Co

Catalyst Cu was widely used as introduced in section 4.1, many strategies for loading catalysts have been employed such as dip coating, spattering for ACCVD growth. Most reports of selective chiral growth were loading Cu into particle catalyst support, which is benefit for narrow down diameter distribution and applicable for optical observation. In this work, Cu and Co miscible into zeolite, this binary catalyst enhance both the selective

growth of small diameter SWNTs and growth efficiency.

Cu-Co zeolite was used in CVD at different temperature by ethanol, Raman spectra present the direct observation from as-grown SWNTs samples in figure 4-5. First of all, influence of temperature on the formation of SWNTs are identified by RBM region of Raman spectra, corresponding inverse diameter are also marked in figure 4-5, when temperature decreased from 750 ^{o}C to 650 ^{o}C, small diameter SWNTs only 0.6 nm is observed by 785 nm laser obviously, when temperature reached 500 ^{o}C most metallic SWNTs observed by 488 nm laser are disappeared, which is also confirmed by the soften and broaden G-band and increased G/D ratio, and at the same time the diameter distribution of SWNTs narrowed down.

Spectra of PLE mapping and absorption for the dispersed SWNTs sample are shown in figure 4-6. In PLE map, a clear decreasing of chirality of SWNTs is demonstrated. (7,5) is the dominant chirality and abundant small diameter SWNTs (8,3), (8,4), (7,6) and (6,5) show their existence at 750 ^{o}C. When temperature decreased to 650 ^{o}C, little bigger diameter SWNTs such as (10,2), (9,4) and (8,6) almost faded out, indicate small diameter SWNTs became the predominant when temperature decreasing. A promising achievement that only (6,5) as the absolutely dominant chirality was obtained when temperature decreased to 500 ^{o}C, which was also observed by absorption. Cu presented its ability for assistant of selective growth of (6,5) SWNTs, this became more efficiently when temperature was low down to 500 ^{o}C, where is the new explored expanding CVD condition. (6,5) SWNTs participated about 50% in the total population of SWNTs sample, which is roughly estimated by approximate peak intensities of both PLE map and absorption spectra.

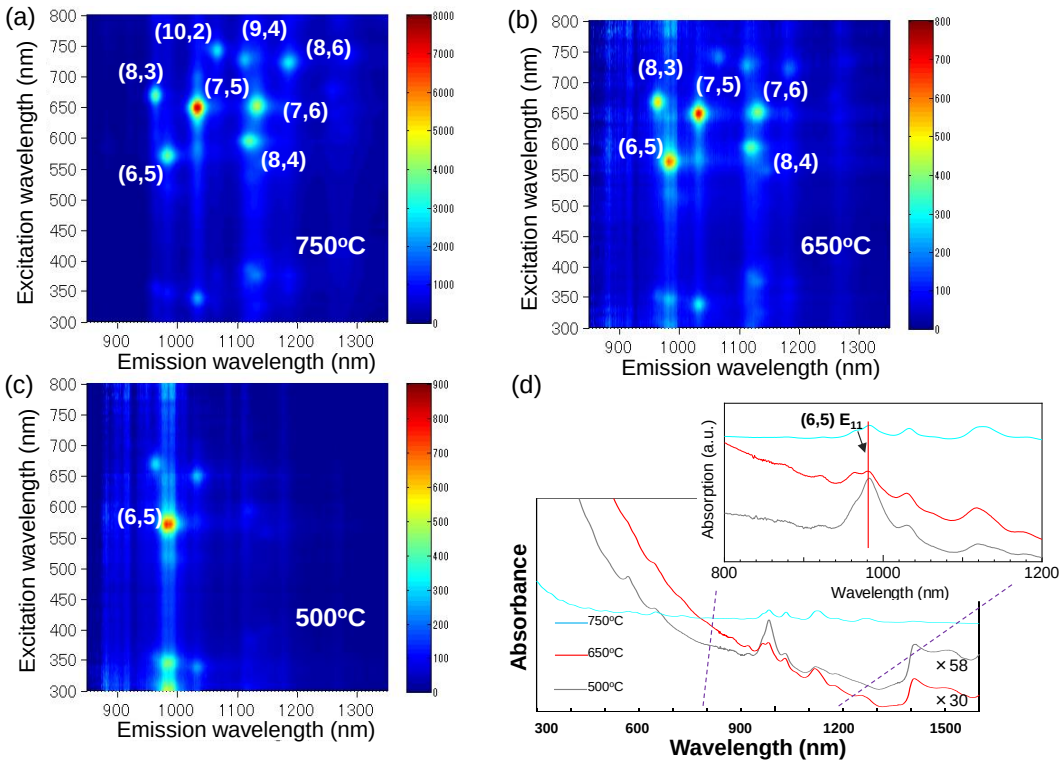

Figure 4-6 Absorption and PL map of SWNTs synthesized by Cu-Co at different temperature and at 5 Pa, present (6,5) is predominant at 500 °C.

4.4.2 Comparison between Fe-Co and Cu-Co in low temperature and pressure CVD

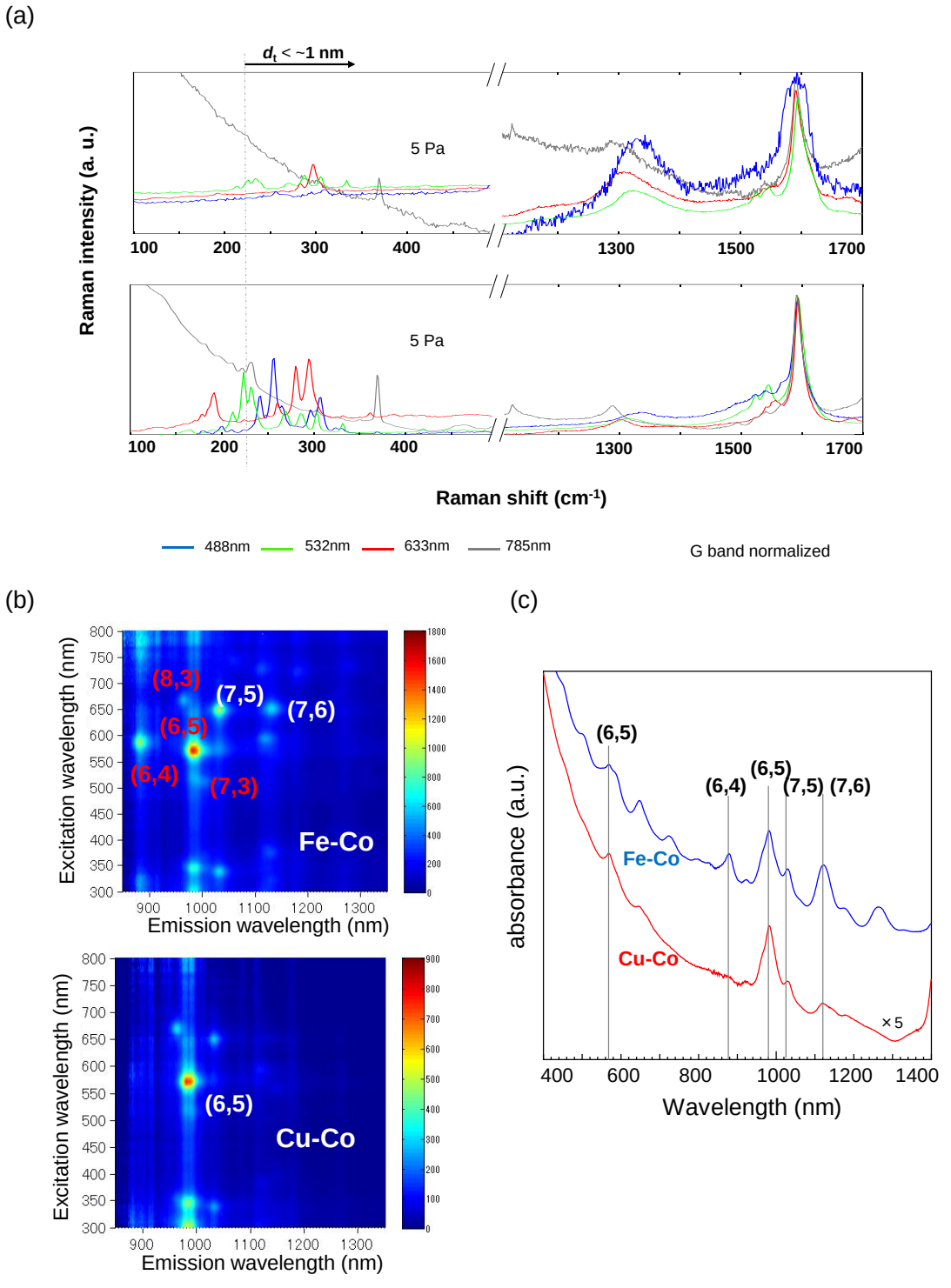

Figure 4-7 Comparison of results of using Fe-Co and Cu-Co at 500 ºC, 5 Pa observed by (a) Raman spectra, (b)PL map and (c) absorption spectra.

A clear difference between SWNTs growth by Fe-Co and Cu-Co can be observed in figure 4-7. In figure 4-7 (a), Cu-Co present benefit on narrow diameter distribution of SWNTs, most SWNTs obtained by Cu-Co are just smaller than 1 nm, comparing to Cu-Co, the SWNTs obtained by Fe-Co are broad, however, quality of SWNTs obtained by Fe-Co are better than that of Cu-Co from the G-band and D-band. It seems that Fe-Co is really an active catalyst that can be survived at extreme condition such as low temperature to grow SWNTs with high-quality more efficiently.

From figure 4-7 (b) and (c), Cu-Co and Fe-Co also demonstrate their each advantage on growth of super small diameter SWNTs. At low temperature 500 ^{o}C, super small diameter (6,4) was efficiently enhanced by Fe-Co while (6,5) is predominant in the case of Cu-Co by the observation both PLE map and absorption spectra, Fe-Co contributed to the growth of super-small diameter SWNTs which were hardly observed before, and (6,5) is definitely predominant with appearance of little amount of smaller diameter SWNTs by Cu-Co.

4.4.3 W-Co for charity controlled growth of SWNTs

Different concentration of W cooperated with Co on zeolite were used in ethanol CVD as catalyst. As the introduction of W catalyst on selective growth of SWNTs in section 4.1, a significant selective growth was obtained by increasing concentration of W, which demonstrated the importance of W on the chirality selective growth. In figure 4-8, most features are disappeared rather than the peak around 194 cm^{-1} observed by 633 nm laser once the concentration of W increased from 0.5 wt% to 5 wt% at 750 ^{o}C and 1300 Pa. The peak around 194 cm^{-1} observed by 633 nm laser is assigned as metallic SWNTs (12,6), increasing concentration of W was an efficient way to selective synthesis this chirality of SWNTs. However, the amount of SWNTs obtained by W-Co catalyst was very small, it can be roughly identified by the weak peaks in absorption and hardly assigned by absorption spectra.

However, defects of SWNTs aroused by increasing concentration of W cannot be ignored. From the study of influence of pressure on the formation of SWNTs, usually decreased pressure was useful to enhance the quality of SWNTs, so the experiment of

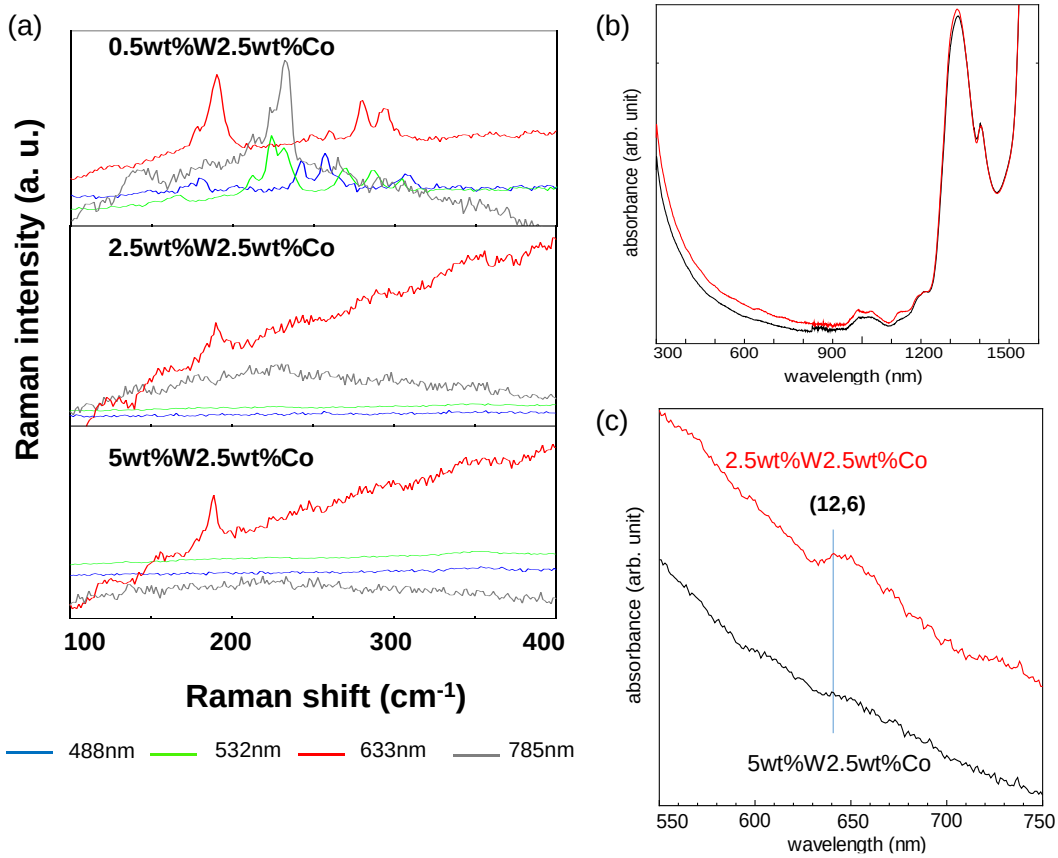

Figure 4-8 Raman spectra of SWNTs synthesized by W-Co in different concentration of W, 4 excitation energies lasers were used in Raman spectroscopy, where shows (12,6) is predominant at high concentration of W. Absorption spectra of SWNTs synthesized by 2 concentration of W is shown in (b) and enlarged absorption spectra is shown in (c).

lower pressure to pursue better quality of selective chirality growth of SWNTs. In figure 4-9, it cannot assist the better quality by decreasing CVD pressure from 1300 Pa to 300 Pa, which judged from the broaden G-band both appeared at 1300 Pa and 300 Pa, and unfortunately, more peaks raising in the RBM region are caused by more chirality SWNTs growth at 300 Pa. So how to enhance the quality of SWNTs while keeping the selective growth still need more efforts.

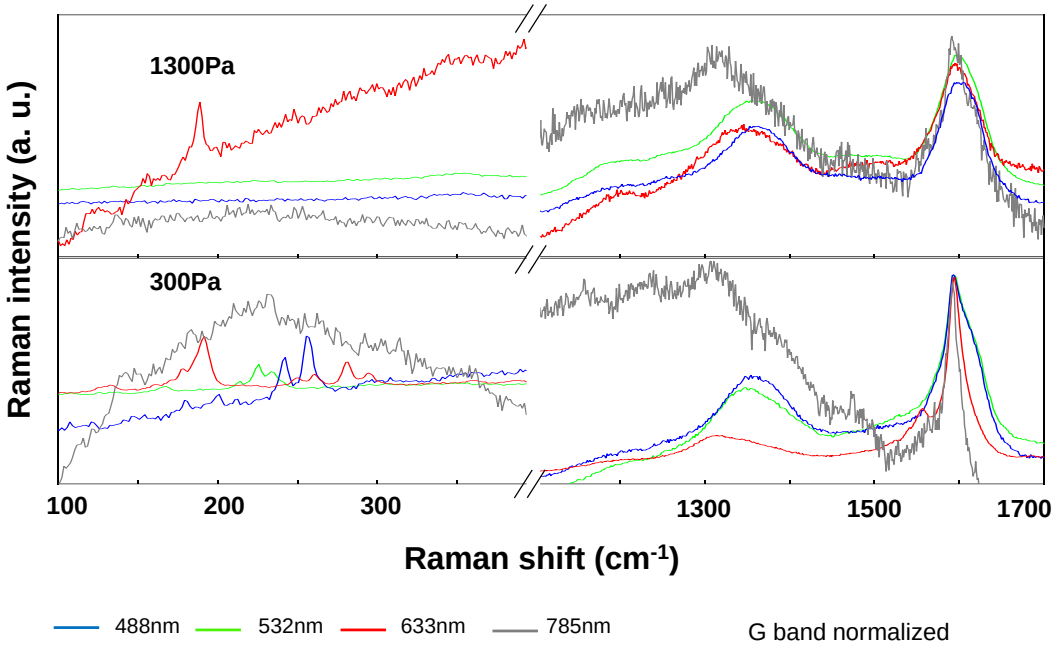

Figure 4-9 Raman spectra of SWNTs synthesized by W-Co at 750 ºC, 1300 Pa and 750 ºC, 300 Pa, 4 excitation energies lasers used in Raman spectroscopy.

4.5 Summary

In expanding CVD condition (low temperature and pressure), ethanol, DME and acetonitrile were almost directly arrived at the surface of catalysts without gas-phase decomposition, then participated into physical or chemical reaction on or with catalyst towards to growth steps of SWNTs. Difference of as-grown SWNTs obtained from ethanol, DME and acetonitrile were compared by Raman spectra. We can get the important information from the quality modulating of SWNTs by changing the feedstock, which is due to the different feedstock will participate very differently in the process of gas-phase, absorbing and dissociation on catalyst surface and so on.

Comparing the results of SWNTs obtained by different catalyst, effective catalyst Fe-Co catalyst assisted the exploration of CVD condition, and super-small diameter SWNTs were synthesized by it. Cu-Co and W-Co were useful and powerful to obtain specific SWNTs. By using Cu-Co catalysts, diameter distribution can be narrower. (6,5) SWNTs became predominant at 500 ºC. On the other hand, (12,6) became the predominant SWNTs when increasing the concentration of W in catalyst of W-Co. Growth of super-small diameter SWNTs and narrow chirality to a specific SWNT by adjusting catalysts are supposed to be promising toward application and understanding of CVD growth of SWNTs system.

Reference

[1] Z. W. Zhao, M. Chaos, A. Kazakov, and P. L. Dryer, "Thermal decomposition reaction and a comprehensive kinetic model of dimethyl ether," *Int. J. Chem. Kinet.* 40, 1 **(2008)**

[2] P. Ayala, A. Grüneis, C. Kramberger, M. H. Rümmeli, I. G. Solorzano, J. Freire, F. L., and T. Pichler, "Effects of the reaction atmosphere composition on the synthesis of single and multiwalled nitrogen-doped nanotubes," *J. Chem. Phys.* 127, 184709 **(2007)**

[3] E. Ibrahim, V. O. Khavrus, A. Leonhardt, S. Hampel, S. Oswald, M. H. Rümmeli, and B. Büchner, "Synthesis, characterization, and electrical properties of nitrogen-doped single-walled carbon nanotubes with different nitrogen content," *Diamond Relat. Mater.* 19, 1199 **(2010)**

[4] T. Thurakitseree, C. Kramberger, A. Kumamoto, S. Chiashi, E. Einarsson, and S. Maruyama, "Reversible diameter modulation of single-walled carbon nanotubes by acetonitrile-containing feedstock," *ACS nano*, 7, 2205 **(2013)**

[5] T. Thurakitseree, C. Kramberger, P. Zhao, S. Chiashi, E. Einarsson, and S. Maruyama, "Reduction of single-walled carbon nanotube diameter to sub-nm via feedstock," *Phys. Sat. Sol. (b)*, 249, 2404 **(2012)**

[6] M. He, C. Alexander I, P. V. Fedotoy, E.D. Obraztsova, J. Sainio, E. Rikkinen, H. Jiang, Z. Zhu, Y. Tian,E.I. kauppinen, M. Niemela, A. Q. I. Krause, "Predominant (6,5) single-walled carbon nanotube growth on a copper-promoted catalyst," *J. Am. Chem. Soc.*

132, 13994 **(2010)**

[7] M. He, A. I. Chernov, E. D. Obraztsova, H. Jiang, E. I. Kauppinen, and J. Lehtonen, "Synergistic effects in FeCu bimetallic catalyst for low temperature growth of single-walled carbon nanotubes," *Carbon* 52, 590 **(2013)**

[8] M.He, H. Jiang, B. Liu, P.l V. Fedotov, A.r I. Chernov, E. D. Obraztsova, F. Cavalca, J. B. Wagner, T. W. Hansen, I. V. Anoshkin, E. A. Obraztsova, A. V. Belkin, E. Sairanen, A. G. Nasibulin, J. Lehtonen and Es. I. Kauppinen, "Chiral-selective growth of single-walled carbon nanotubes on lattice-mismatched epitaxial cobalt nanoparticles," *Scientific report* 3, 1450 **(2013)**

[9] F. Yang, X. Wang, D. Zhang, J. Yang, D. Luo, Z. Xu, J. Wei, J.Wang, Zhi Xu, F. Peng, X. Li, R. Li, Y. Li, M. Li, X. Bai, F. Ding and Y. Li., "Chirality-specific growth of single-walled carbon nanotubes on solid alloy catalysts," *Nature* 510, 522 **(2014)**

[10] S. Maruyama, R. Kojima, Y. Miyauchi, S. Chiashi, and M. Kohno, "Low-temperature synthesis of high-purity single-walled carbon nanotubes from alcohol," *Chem. Phys. Lett.* 360, 229 **(2002)**

[11] Y. Murakami, Y. Miyauchi, S. Chiashi, and S. Maruyama, "Characterization of single-walled carbon nanotubes catalytically synthesized from alcohol," *Chem. Phys. Lett.* 374, 53 **(2003)**

[12] K. Mukhopadhyay, A. Koshio, N. Tanaka, and H. Shinohara, "A simple and novel way to synthesize aligned nanotube bundles at low temperature," *Jpn. J. Appl. Phys.* 37, L1257 **(1998)**

[13] K. Mukhopadhyay, A. Koshio, T. Sugai, N. Tanaka, H. Shinohara, Z. Konya, and J. B. Nagy, "Bulk production of quasi-aligned carbon nanotube bundles by the catalytic chemical vapour deposition (CCVD) method," *Chem. Phys. Lett.* 303, 117 **(1999)**

[14] B. Wang, C. H. P. Poa, L. Wei, L. J. Li, Y. Yang, and Y. Chen, "(*n,m*) Selectivity of single-walled carbon nanotubes by different carbon precursors on Co−Mo Catalysts," *J. Am. Chem. Soc.* 129 (29), 9014 **(2007)**

Chapter 5

Summary and conclusion

The growth of small diameter SWNTs with relatively large band gap is a challenge in the research of SWNTs and a variety of application is expected. Efficient growth of super-small diameter SWNTs was realized in this work. Sufficient number of systematic observation of the small diameter SWNTs, which was rarely reported before was also achieved in this work.

To understand the growth mechanism of SWNTs, variety of CVD parameters were studied in this work. The effect of feedstock compounds including heir decomposition in gas-phase, the effect of catalysts, and CVD operation conditions were systematically studied. How these factors affect the quality and chirality is the main interest and achievement of this study especially for low temperature and low pressure CVD.

The study of gas-phase decomposition of ethanol, DME and acetonitrile provided insights into the control of the formation of SWNTs from gas phase. The work on the extension of CVD condition from high to low temperature and pressure, contributed the systematic understanding on the key factors of the growth of super-small diameter SWNTs. The feedstock studies, suggested the potential quality modulation of SWNTs by feedstock. And finally, the effect of the catalysts was investigated and compared by using three typical catalysts Fe-Co, Cu-Co and W-Co on zeolite.

Appendix I

The G/D ratio presented in figure 3-19 were the average over the measurements with 4 excitation laser energies. Experimental conditions and each measurements are shown in table I-1.

	488nm	532 nm	633 nm	785 nm	Average
550 °C, 1300 Pa	2.6	2.4	3.5	3.5	3.0
460 °C, 5pa	2.0	3.0	3.0	6.0	3.5
750 °C, 0.2 Pa	2.1	5.4	3.0	5.0	3.9
380 °C, 0.1 Pa	6.0	3.0	4.0	3.0	4.0
850 °C, 1 Pa	5.0	4.0	5.2	2.0	4.1
550 °C, 150 Pa	7.5	3.3	3.0	6.0	5.0
650 °C, 0.02 Pa	4.0	6.0	6.0	10.0	6.5
430 °C, 0.02 Pa	9.2	11.0	13.8	7.9	10.5
700 °C, 1000 Pa	3.3	20.0	10.0	10.0	10.8
700 °C, 1300 Pa	6.3	15.8	9.5	15.8	11.9
500 °C, 1 Pa	13.3	20.0	13.3	8.0	13.7
700 °C, 0.1 Pa	10.0	19.6	15.0	12.2	14.2
500 °C, 5 Pa	8.0	20.0	20.0	10.0	14.5
600 °C, 0.02 Pa	18.8	8.5	15.5	21.0	16.0
550 °C, 5 Pa	17.5	17.5	17.5	11.7	16.1
700 °C, 350 Pa	5.0	20.0	20.0	20.0	16.3
500 °C, 0.1 Pa	17.5	17.5	17.5	14.0	16.6
700 °C, 150 Pa	14.0	22.0	22.0	22.0	20.0
650 °C, 5 Pa	20.3	20.3	20.3	20.3	20.3
700 °C, 50 Pa	12.0	23.0	23.0	23.0	20.3
550 °C, 0.1 Pa	29.4	15.5	15.1	21.9	20.5
800 °C, 1300 Pa	24.3	37.5	37.5	25.0	31.1
800 °C, 5 Pa	34.0	32.5	11.2	65.0	35.7
500 °C, 0.02 Pa	28.1	20.7	78.2	20.0	36.8
700 °C, 1 Pa	57.5	51.9	26.0	18.9	38.6
850 °C, 5 Pa	76.0	60.0	37.5	27.0	50.1

Table I-1 Details of the G/D ratio measurements for the samples with different CVD conditions.

Appendix II

TEM and SEM images of as-grown SWNTs on zeolite.

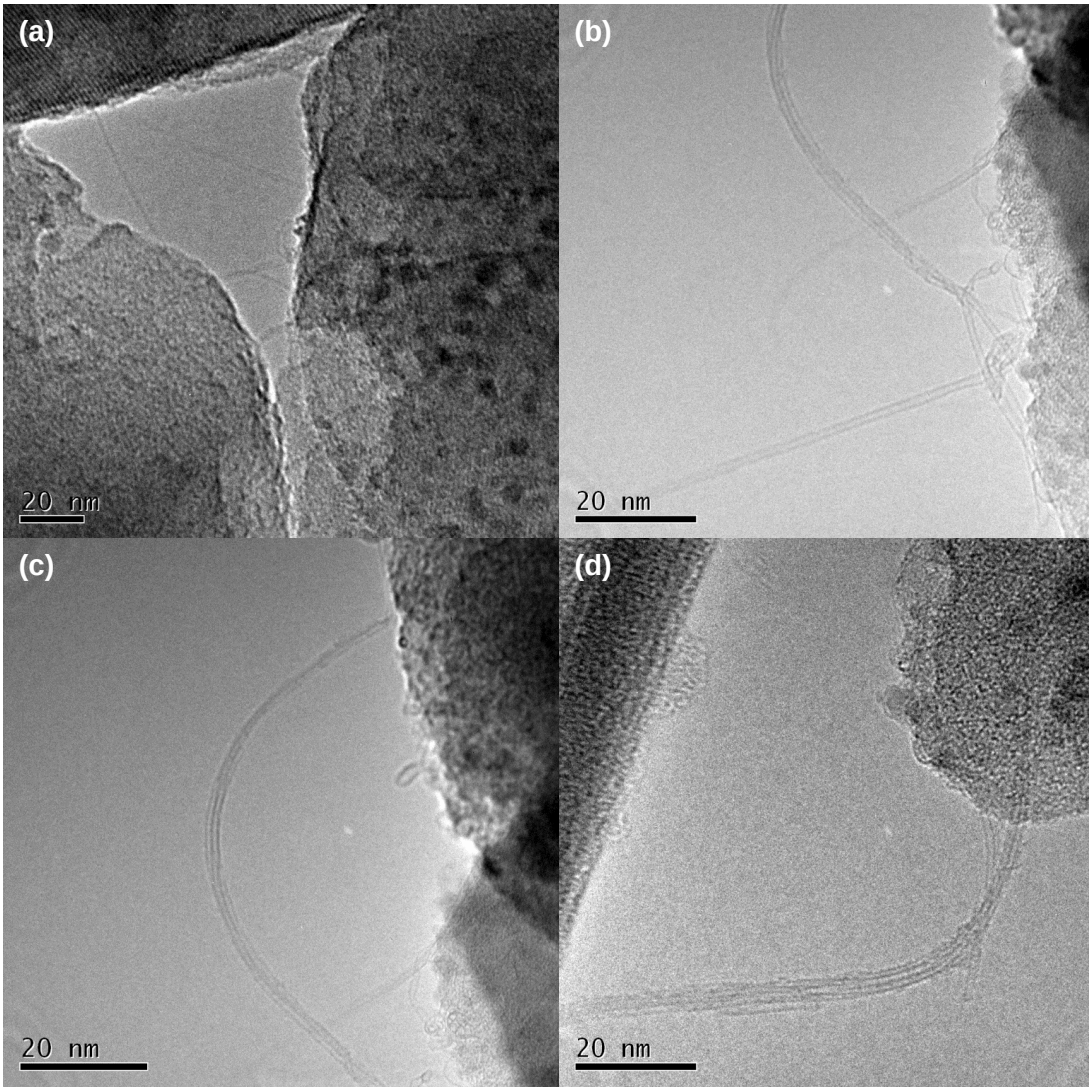

Figure II-1 TEM images of as-grown SWNTs sample obtained at 500 ºC, 5 Pa.

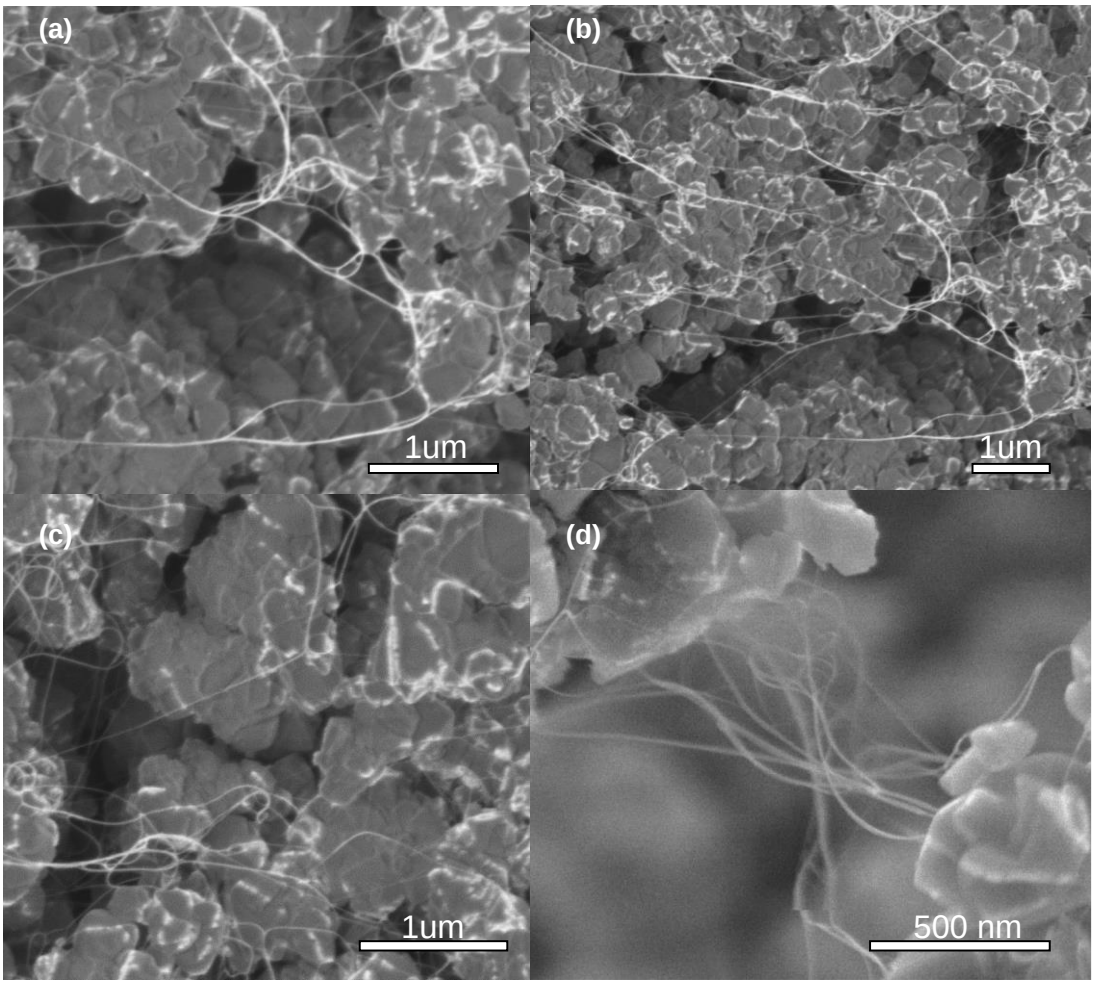

Figure II-2 SEM images of as-grown SWNTs sample obtained at 800 °C, 5 Pa.

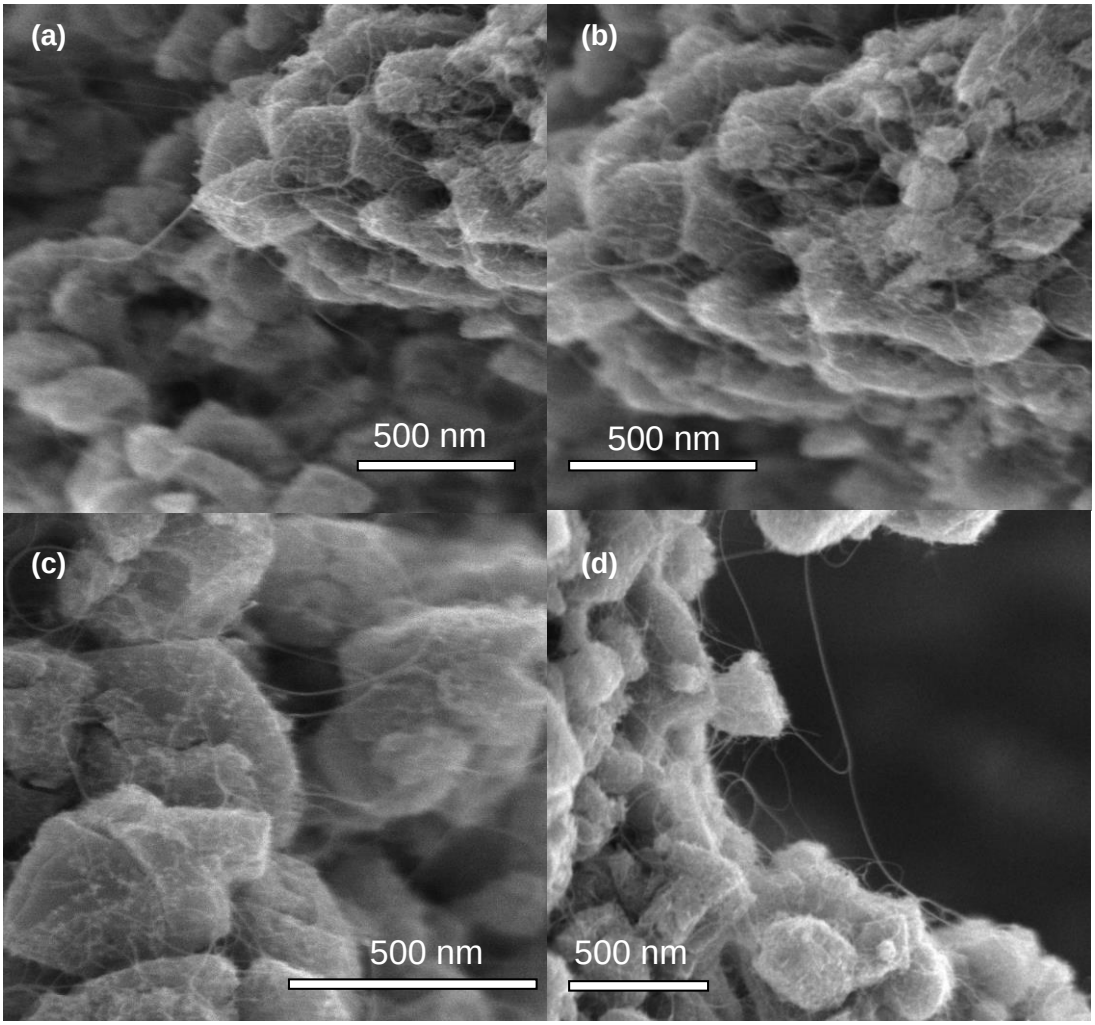

Figure II-2 SEM images of as-grown SWNTs sample obtained at 800 °C, 1300 Pa.

Appendix III

Thermal decomposition of ethanol, DME and acetonitrile at low temperature and low pressure.

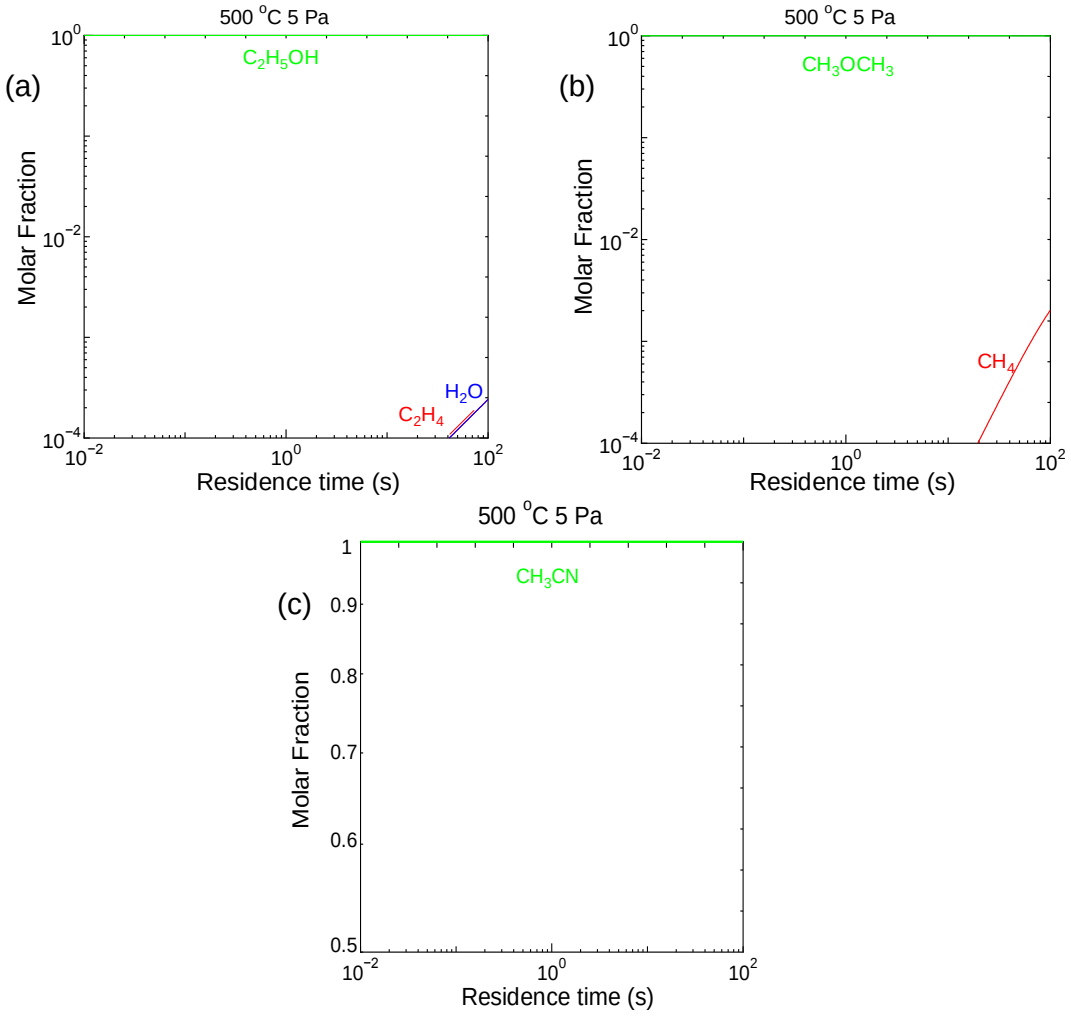

Figure III-1 Thermal decomposition of ethanol, DME and acetonitrile at 500 °C, 5Pa.

Table of figures

Acknowledgement

First of all, I am really appreciate my supervisor Professor Shigeo Maruyama. With Prof. Maruyama's great and constant support and encouragement, I can learn and achieve a lot during my doctoral course. I will always be inspired in the future by Prof. Maruyama's scientific sense.

I am grateful for Prof. Chiashi, Prof. Xiang and Prof. Inoue, they always help me a lot for my research. And I am also grateful for Prof. Akira Miyoshi's constant support during my academic life and helpful discussion on the decomposition study. I would like to thank Prof. Yuichiro Kato and Prof. Reo Kometani for their helpful suggestion and comments on my doctoral study. I also would like to thank technical staff Mr. Watanabe, Secretary Ms. Terao and Ms. Shimada, thanks a lot for their support during my study life.

Many thanks for Dr. Xiao Chen, Dr. Kehang Cui and Ms. Hua An for their discussion and help on experiments. I also would like to thank those people, who have already left our lab, now working around the world, Prof. Erik Einarsson, Dr. Pei Zhao, Dr. Shinya Aikawa, Dr. Theerapol Thurakitseree, Dr. Sivasankaran Harish, and Dr. Heeyuen Koh. I also would like to thank all the members in Maruyama-Chiashi lab.

Finally, I am appreciate all my families, my parents, parents in-law, my husband and my daughter, thanks a lot for your great support, understanding and love during my doctoral course time.

Publications and conference presentations:

Publications:

(1) **Bo Hou**, Rong Xiang, Taiki Inoue, Erik Einarsson, Shohei Chiashi, Junichiro Shiomi, Akira Miyoshi, and Shigeo Maruyama, "Decomposition of ethanol and dimethyl ether during chemical vapor deposition synthesis of single-walled carbon nanotubes," *Jpn. J. Appl. Phys. 50,* 065101 **(2011)**

(2) Rong Xiang, **Bo Hou**, Erik Einarsson, Zikang Tang, Shigeo Maruyama, "Carbon atoms in ethanol do not contribute equally to formation of single-walled carbon nanotubes during CVD synthesis," ACS *nano. 7*, 3095 **(2013)**

(3) Pei Zhao, **Bo Hou**, Xiao Chen, Sungjin Kim, Shohei Chiashi, Erik Einarsson, and Shigeo Maruyama, "Investigation of non-segregation graphnene growth on Ni via isotope-labeled alcohol catalytic chemical vapor deposition," *Nanoscale 5*, 6530 **(2013)**

(4) Pei Zhao, Akihito Kumamoto, Sungjin Kim, Xiao Chen, **Bo Hou**, Shohei Chiashi, Erik Einarsson, and Shigeo Maruyama, "Self-limiting chemical vapor deposition growth of monolayer graphene from ethanol," *J Phys Chem. C 117*, 10755 **(2013)**

(5) **Bo Hou**, Taiki Inoue, Rong Xiang, Shohei Chiashi and Shigeo Maruyama, "Efficient CVD growth of single-walled carbon nanotubes smaller than (6,5)" in preparation.

Conference presentations:

(1) **Bo Hou**, Rong Xiang, Taiki Inoue, Erik Einarsson, Junichiro Shiomi, Akira Miyoshi, and Shigeo Maruyama, "Experimental and numerical study on the effect of carbon feedstock decomposition on CVD synthesis of single-walled carbon nanotubes", XXIV INTERNATIONAL WINTERSCHOOL on ELECTRONIC PROPERTIES of NOVEL MATERIALS. Kirchberg in Tirol, Austria. (2010) *Poster*

(2) **Bo Hou**, Rong Xiang, Erik Einarsson, Junichiro Shiomi, Akira Miyoshi, and Shigeo Maruyama, "Decomposition of ethanol and dimethyl-ether during CVD synthesis of single-walled carbon nanotubes", The 38th Fullerenes Nanotubes General Symposium. Nagoya, Japan. (2010) *Poster*

(3) Rong Xiang, **Bo Hou**, Erik Einarsson, Junichiro Shiomi, and Shigeo Maruyama, "Gas-phase and on-surface decomposition of ethanol in alcohol CCVD", The 38th Fullerenes Nanotubes General Symposium. Nagoya, Japan. (2010) *Poster*

(4) Taiki Inoue, Hiroto Okabe, **Bo Hou**, Shohei Chiashi, Makoto Watanabe, Junichiro Shiomi, and Shigeo Maruyama, "CVD growth of vertically aligned SWNTs films using dimethyl ether as the carbon source", The 38th Fullerenes Nanotubes General Symposium. Nagoya, Japan. (2010)*Poster*

(5) **Bo Hou**, Rong Xiang, Erik Einasson, Junichiro Shiomi, and Shigeo Maruyama, "Controlled CVD synthesis of single-walled carbon nanotubes on zeolite", The 2nd GMSI international symposium. Tokyo, Japan. (2010) *Poster*

(6) Shigeo Maruyama, Rong Xiang, **Bo Hou**, Erik Einarsson, and Junichiro Shiomi, "Gas-phase and on-surface decomposition of ethanol in alcohol CVD", NT'10: The 11th International Conference on the Science and Application of Nanotubes. Montreal, Canada. (2010) *Talk*

(7) **Bo Hou**, and Shigeo Maruyama, "CVD synthesis of graphene from alcohol", The 2nd ZAO meeting for nano-carbon. Sendai, Japan. (2010) *Talk*

(8) Rong Xiang, **Bo Hou**, Pei Zhao, Erik Einarsson, and Shigeo Maruyama, "What determines on-surface decomposition of ethanol in ACCVD", The 39th Fullerenes-Nanotubes general symposium. Kyoto, Japan. (2010) *Talk*

(9) Xiao Chen, **Bo Hou**, Kevin Chu, Pei Zhao, Rong Xiang, Erik Einarsson, Shiohei Chiashi, and Shigeo Maruyama, "CVD synthesis of graphene from ethanol", The 39th Fullerenes-Nanotubes general symposium. Kyoto, Japan. (2010) *Poster*

(10) **Bo Hou**, Rong Xiang, Erik Einasson, Junchiro Shiomi, and Shigeo Maruyama, "The quality of produced SWNTs determined by decomposition condition of feedstock and catalyst treatment in CVD", PACIFICHEM 2010, Honululu, HI, U.S.A. (2010) "**Outstanding poster presentation award***" Poster*

(11) **Bo Hou**, Xiao Chen, Erik Einasson, Shohei Chiashi, and Shigeo Maruyama, "Chemical vapor deposition synthesis of graphene on Ni film using ethanol and dimethyl ether", The 3rd GMSI international symposium. Tokyo, Japan. (2011) *Poster*

(12) **Bo Hou**, Xiao Chen, Erik Einarsson, Shohei Chiashi, and Shigeo Maruyama, "Chemical Vapor Deposition Synthesis of Graphene on Metal Foil Using Ethanol and

Dimethyl Ether", GMSI-COSM-UT2 Workshop Toronto, Canada. (2011) *Talk*

(13) **Bo Hou**, Xiao Chen, Erik Einarsson, Shohei Chiashi, and Shigeo Maruyama, "CVD Synthesis Of Graphene Using Ethanol And Dimethyl Ether On Ni Foil", NT11, Cambridge, UK. (2011) *Poster*

(14) S.-J. Kim, Shinya Aikawa, **Bo Hou**, Erik Einarsson, Shohei Chiashi, and Shigeo Maruyama, "Fabrication of flexible thin film transistors using singlewalled carbon nanotubes and graphene," 24th International Microprocesses and Nanotechnology Conference（MNC 2011), Kyoto, Japan (2011) *Poster*

(15) Xiao Chen, Pei Zhao, **Bo Hou**, Erik Einarsso, Shohei Chiashi, and Shigeo Maruyama, "ACCVD growth of mono- and bi-layer graphene and mechanism study, "APS March Meeting, Boston, U.S.A (2012) *Poster*

(16) **Bo Hou**, Pei Zhao, Xiao Chen, Erik Einasson, Shohei Chiashi, and Shigeo Maruyama, "Chemical Vapor Deposition synthesis of grapheme on Ni foil with ethanol and DME", The 4th GMSI international symposium. Tokyo, Japan. (2012) *Poster*

(17) Pei Zhao, **Bo Hou**, Xiao Chen, Erik Einarsson, Shohei Chiashi, and Shigeo Maruyama, "Investigating Graphene Growth on Ni Surface Using Isotope-Labeled Alcohol Catalytic Chemical Vapor Deposition, "13th Int. Conf. Science Application Nanotubes (NT12), Brisbane, Australia (2012) *Poster*

(18) Xiao Chen, Pei Zhao, **Bo Hou**, Shohei Chiashi and Shigeo Maruyama, "CVD Growth of Mono- and Bi-layer Graphene from Ethanol", TeraNano 2012, Okinawa, Japan (2012) *Poster*

(19) Xiao Chen, Pei Zhao, **Bo Hou**, Erik Einarsson, Shohei Chiashi, and Shigeo Maruyama, "CVD Growth of Mono- and Bi-Layer Graphene from Ethanol", SSDM 2012, Kyoto, Japan (2012) *Poster*

(20) **Bo Hou**, Pei Zhao, Xiao Chen, Erik Einasson, Shohei Chiashi, and Shigeo Maruyama, "Chemical kinetics in CVD synthesis of graphene on Ni foil from ethanol and dimethyl ether", 2012 MRS Fall Meeting & Exhibit, Boston, U.S.A (2012) *Poster*

(21) Shigeo Maruyama, **Bo Hou**, Taiki Inoue, Rong Xiang, and Shohei Chiashi, "Efficient CVD growth of single-walled carbon nanotubes smaller than (6,5)", NT15, Nagoya, Japan. (2015) *Poster*